

# Infiltration and surface runoff dynamics on dryland hillslopes: a new method.

Joshua Matthew Wolstenholme

Submitted in accordance with the requirements  
for the degree of  
Master of Science by Research

The University of Leeds  
School of Geography

September 2018

The candidate confirms that the work submitted is his own and that appropriate credit has been given where reference has been made to the work of others.

This copy has been supplied on the understanding that it is copyright material and that no quotation from the thesis may be published without proper acknowledgement.

The right of Joshua Matthew Wolstenholme to be identified as Author of this work has been asserted by Joshua Matthew Wolstenholme in accordance with the Copyright, Designs and Patents Act 1988.

## Acknowledgements

I would like to thank my supervisors, Prof. Andy Baird and Dr. Mark Smith, for their assistance in the completion of this work. Thank you also to Tom Sim for assisting with fieldwork in Portugal. Finally, thank you to my girlfriend Lucy, as well as friends and family for supporting me through this qualification.

## Abstract

Drylands cover approximately 41% of the Earth's land surface (Middleton and Thomas, 1997); a habitat for over 38% of the planet's population (Huang *et al.*, 2017). Understanding the interaction between ground surface characteristics, infiltration and overland flow in this environment is paramount to identifying areas vulnerable to erosion and flash flooding.

Currently, infiltration is measured in drylands using techniques which are often not suited to the environment. Existing measurement methods typically cannot be used on steep slopes, and slopes with stone or vegetation cover, without disturbing the natural soil. As well as this, the impact of overland flow is often neglected from measurements.

Here, a new method for quantifying infiltration and overland flow is presented: 'the infiltrator'. The device outputs a pulse of water to the surface, allowing the measurement of runoff dimensions. Soil surface and slope characteristics are also measured with the use of field and GIS based techniques. The methods enable two main research questions to be assessed: (i) the impact of surface cover on surface runoff, and (ii) the influence of surface characteristics on flow concentration.

The infiltrator was used successfully on rangeland slopes in a semi-arid environment (Salema, Western Algarve, Portugal), allowing for assessment of infiltration and overland flow, without disturbing the natural soil. Using regression modelling, the results from experimentation using the infiltrator indicated that: (i) infiltration and the nature of surface runoff are strongly related to stone and vegetation cover, and (ii) flow concentration controls include those identified in (i), as well as surface roughness and slope angle.

The new method effectively enables the quantification of infiltration and overland flow, whilst remaining representative of the surface. It can be used on slopes up to 40°, and is an inexpensive, quick solution to characterising the vulnerability of dryland slopes to surface runoff and erosion.

## Table of Contents

Acknowledgements .....	iii
Abstract.....	iv
List of Illustrative Material.....	vii
List of Tables .....	viii
Abbreviations.....	ix
Symbols.....	x
1. Introduction .....	1
1.1. Rationale .....	1
1.2. Research Aims.....	2
1.3. Thesis Aims .....	3
2. Issues surrounding the measurement of infiltration in drylands.....	4
2.1. The Dryland Environment.....	4
2.2. Identification of Literature .....	9
2.3. Synthesis of Reviewed Studies .....	10
2.4. Rainfall Simulators .....	14
2.5. Infiltrometers.....	18
2.5.1. Single Ring.....	19
2.5.2. Double Ring.....	22
2.5.3. Tension Infiltrometers .....	23
2.5.4. Mini Disk Infiltrometers .....	25
2.5.5. Hydraulic Conductivity.....	26
2.6. Indirect monitoring of water content.....	27
2.6.1. Electrical Tomography .....	28
2.6.2. Discharge Analysis .....	29
2.7. Summary of Methods .....	30
2.8. Discussion .....	32
2.8.1. Are current infiltration measurement methods suitable for drylands?.....	32
2.8.2. Ideal properties of a dryland infiltration measurement method.....	34
2.9. Chapter Summary .....	34
3. A New Methodology .....	36
3.1. The Infiltrator.....	36
3.1.1. Experimental Design .....	38
3.2. Field Area .....	39
3.2.1. Catchment Characteristics.....	40

3.2.2. Experimental Locations .....	42
3.2.3. Summary of Experiments .....	45
3.3. Data Capture .....	45
3.3.1. Field Variables .....	46
3.3.2. Spatial Analyses .....	47
3.4. Data Processing.....	50
3.4.1. Surface Cover .....	50
3.4.2. Roughness.....	51
3.5. Chapter Summary .....	53
4. Results.....	55
4.1. Using the infiltrator in the dryland environment .....	55
4.2. The influence of surface cover on runoff .....	57
4.3. Soil surface controls on flow concentration .....	61
5. Discussion .....	64
5.1. The effectiveness of the infiltrator .....	64
5.2. The relationship between surface cover and runoff .....	65
5.3. Flow concentration and soil surface controls.....	66
5.4. An aggregate measure for infiltration and overland flow conveyance.....	67
5.5. Suggestions for further research .....	68
5.6. Wider Implications.....	69
6. Conclusion.....	70
7. References .....	71
Appendix .....	I
Appendix i: Prototype One 3D model.....	I
Appendix ii: Prototype Two 3D model.....	I
Appendix iii: ArcPy Automation Script (Setup).....	II
Appendix iv: ArcPy Automation Script (Area Calculation).....	III
Appendix v: CloudCompare Automation Script.....	IV

## List of Illustrative Material

<i>Figure</i>	<i>Caption</i>	<i>Page</i>
2.1	The range of dryland surfaces	6
2.2	Hydrological processes on topsoil rock schematic	8
2.3	World map (Mercator projection) of drylands	12
2.4	Frequency of case studies and associated countries	13
2.5	Infiltration methods identified alongside their associated primary application	14
2.6	Measurement of infiltration via captured runoff	15
2.7	Portable rainfall simulator prior to experimentation without curtain	16
2.8	Disturbance to soil structure due to SRI insertion	19
2.9	SRI showing wetting front	20
2.10	SRI pressure differentials	21
2.11	DRI schematic	22
2.12	TI schematic	24
2.13	MDI schematic	26
2.14	Interpretations of a seismic profile combined with an electrical profile	28
3.1	The infiltrator (annotated)	37
3.2	Distribution experiment results	38
3.3	Salema location with respect to Western Europe map	39
3.4	Images of the Salema area	40
3.5	Weather station data from Faro and Sagres	41
3.6	Precipitation data from Sagres	42
3.7	Topographic map of Salema	43
3.8	Images of surfaces 1-3	44
3.9	Images of surfaces 4-5	44
3.10	Polar histogram of slope aspect	45
3.11	Schematic diagram of runoff variables	47
3.12	SfM workflow	50
3.13	Classified orthophotograph (experiment 25)	51
3.14	Wetted area of point cloud visualised in CloudCompare	53
4.1	Sample of classified orthophotographs	56

4.2	Multiple linear regression model for $Lmax$	58
4.3	Multiple linear regression model for $Wmax$	60
4.4	Multiple linear regression model for $tLmax$	61
4.5	Multiple linear regression model for $Wmin$	62

## List of Tables

<i>Table</i>	<i>Caption</i>	<i>Page</i>
2.1	PICO search terms	9
2.2	Number of articles located during research and filtering	10
2.3	Distribution of case studies by continent	11
2.4	Summary of methods	30-32
3.1	Average descriptive characteristics for experimental locations 1 - 5	43
4.1	Multiple linear regression model estimated coefficients for $Lmax$	59
4.2	Multiple linear regression model estimated coefficients for $Wmax$	59
4.3	Multiple linear regression model estimated coefficients for $tLmax$	61
4.4	Multiple linear regression model estimated coefficients for $Wmin$	62

## Abbreviations

<i>Abbreviation</i>	<i>Term</i>
<i>APS-C</i>	Advanced Photo System type-C
<i>Csa</i>	Hot Summer Mediterranean Climate
<i>DEM</i>	Digital Elevation Model
<i>dGPS</i>	Differential Global Positioning System
<i>DRI</i>	Double Ring Infiltrometer
<i>f/</i>	Aperture (f stop)
<i>GPS</i>	Global Positioning System
<i>LiDAR</i>	Light Detection and Ranging
<i>MDI</i>	Mini Disk Infiltrometer
<i>MP</i>	Megapixel
<i>MVS</i>	Multi View Stereo
<i>OSB</i>	Oriented Strand Board
<i>p</i>	Probability
<i>RFS</i>	Rainfall Simulator
<i>SfM</i>	Structure from Motion
<i>SRI</i>	Single Ring Infiltrometer
<i>TDR</i>	Time-Domain Reflectometry
<i>TI</i>	Tension Infiltrometer
<i>TLS</i>	Terrestrial Laser Scanner
<i>UTM</i>	Universal Transverse Mercator (coordinate system)

## Symbols

<i>Symbol</i>	<i>Name</i>	<i>Units</i>
$A$	Area	$m^2$
$b_0$	Value of regression variable when all independent variables are equal to zero	Various
$b_n$	Estimated regression coefficients	Various
$d$	Depth	m
$\varepsilon$	Regression error	No units
$f$	Infiltration rate	$m \text{ min}^{-1}$
$L_{max}$	Maximum runoff extent downslope	m
$N$	Frequency	No units
$P_{smax}$	Highest monthly precipitation values for summer half-years on the hemisphere considered	$mm \text{ yr}^{-1}$
$P_{smin}$	Lowest monthly precipitation values for summer half-years on the hemisphere considered	$mm \text{ yr}^{-1}$
$P_{wmax}$	Highest monthly precipitation values for winter half-years on the hemisphere considered	$mm \text{ yr}^{-1}$
$P_{wmin}$	Lowest monthly precipitation values for winter half-years on the hemisphere considered	$mm \text{ yr}^{-1}$
$Q_{in}$	Inflow	$m^3 \text{ min}^{-1}$
$Q_{out}$	Outflow	$m^3 \text{ min}^{-1}$
$t_{add}$	Elapsed time between water additions	minutes
$tL_{max}$	Time to maximum runoff extent downslope	seconds
$T_{max}$	Monthly mean temperatures of the warmest months	$^{\circ}C$
$V$	Water volume	$m^3$
$W_{max}$	Maximum runoff width	cm
$W_{min}$	Minimum runoff width	cm
$X$	Combination of independent variables ( $X_n$ )	No units
$x_n$	Independent variables where n is a number (1-4)	Various
$y$	y axis variable	Various

# 1. Introduction

## 1.1. Rationale

Approximately 41% of the Earth's land surface is covered by drylands (Middleton and Thomas, 1997), of which 25% is dedicated to agriculture, 65% to rangelands, 8% urban and 2% other land use (Safriel *et al.*, 2005). Drylands are also home to over 38% of the global population (Huang *et al.*, 2017), distributed over all continents with the exception of Antarctica (Kottek *et al.*, 2006). Due to dryland soils having low fertility, they are extremely sensitive to degradation induced by climate warming and human activity (Huang *et al.*, 2017). Land degradation by surface runoff is influenced by high intensity rainfall; in Chinese Loess drylands over 60% of annual rainfall occurs within three months (Shangguan *et al.*, 2002). Runoff following high intensity rainfall often leads to flash flooding (e.g. Yang *et al.* (2017)) which can be detrimental to those living in vulnerable areas with little preparation. Despite this, there is little understanding of the hydrological coupling between hillslopes and rivers (Michaelides *et al.*, 2018). Hillslopes in drylands are spatially highly variable in terms of their hydraulic and hydrological properties. Their often steep gradients, thin, stony soils and inconsistent, but mostly sparse, vegetation cover (Michaelides and Wilson, 2007) make measuring infiltration and quantifying overland flow particularly challenging.

Techniques utilised to measure infiltration in drylands have not been developed with dryland soil surfaces in mind. Many methods (e.g. single and double ring infiltrometers, tension and mini disk infiltrometers) require soft, flat soils for effective use, with little to no stone or vegetation cover. Using techniques such as these in agricultural areas is acceptable due to typically deep soils that are low-angled and well-maintained for crop production. Agricultural land, however, represents only 25% of drylands (Safriel *et al.*, 2005). On natural dryland surfaces, the existing devices can only be used by disturbing the soil, resulting in less representative results. As well as this, runoff dynamics on the hillslope scale and their influences on flood generation and connectivity are rarely studied, presenting a gap in knowledge that could inform flood management techniques if investigated.

Evidently, there is a need for the devising of a more dryland specific infiltration and runoff measurement device that can be used more effectively across the entirety of the dryland environment, whilst remaining representative of the area. The device should also successfully incorporate soil surface characteristics (cover, slope, roughness) without disturbing natural conditions. This thesis presents such a method, after identifying key issues surrounding the methods currently used.

Infiltration is currently quantified using single point methods such as ring or tension infiltrometers (Angulo-Jaramillo *et al.*, 2000). The methods provide data for one specific point, typically without considering the influence of overland flow hydraulics in routing any locally generated runoff downslope. Previous studies have assessed the influence on surface runoff due to vegetation patterns (Abrahams *et al.*, 1995), connectivity (Reaney *et al.*, 2014), as well as the surface topography (Dunkerley, 2004a; Kirkby *et al.*, 2002). Studies have not, however, quantified the combination of infiltration whilst also considering the influence of surface hydrology. The methodology and workflow described in this thesis aggregates both local effects of runoff generation (i.e. vertical exchange processes) with the propensity of a surface to transfer any excess rainfall through the landscape as overland flow (i.e. horizontal fluxes). This simple yet novel workflow yields data that better reflects the emerging concept of hydrological connectivity, typically invoked to explain non-linear runoff response observed in the dryland mosaic. As the workflow can be used in almost any dryland environment, this will enable a single technique to be used globally, allowing for the direct comparison of different localities. Numerical models can also be parameterised with data that covers a greater surface area (per experiment) from across in the catchment, rather than specific point localities chosen based on the suitability of the instrument (Clark *et al.*, 2015). Models could then be used for better understanding of catchment scale erosional or flood vulnerability, whilst enabling risk mapping.

## 1.2. Research Aims

The aim of this research is to develop a new method for characterising infiltration and surface runoff dynamics in drylands, which will enable experiments to be performed on soil surfaces that are more representative of the dryland environment. The spatial-distribution approach of this workflow provides data which is inclusive of any variability across the hillslope, including changes of topography, cover and slope angle; representing flow hydraulics and infiltration more effectively than previous methodologies.

In addition to this primary aim, two research questions have been developed in response to gaps in the literature arising from the limitations of current infiltration measurement methods, as well as the need to understand controls on overland flow hydraulics. These questions are specifically related to soil surface characteristics at the hillslope scale; mainly assessing how different surface properties influence both infiltration and overland flow.

- ❖ **RQ1: How does surface vegetation, stone cover and the position of stones with respect to the soil influence surface runoff?**

Poesen *et al.* (1994) noted that rock fragments and their position in the soil, whether resting on the surface or embedded, are key controls for infiltration. Incorporating this into the experimental design of the new method, alongside vegetation, allows the importance of surface cover to be recognised. Currently, only rainfall simulators can effectively quantify the influence of cover, due to their design (i.e. simulating natural rainfall). The disadvantage (explored in Chapter 2), however, is that they cannot be used on steep slopes. This question allows for the exploration of cover on both shallow and steep slopes.

❖ **RQ2: What are the main soil surface controls on flow concentration?**

Geomorphology varies across landscapes in drylands, including stone pavements with a high proportion of stone cover, rills on steeper slopes and more vegetated, flatter surfaces. Establishing the controls on flow concentration, by adopting a method more representative of the soil surface, will permit further understanding of how these various surface types develop and stabilise.

### 1.3. Thesis Aims

This thesis assesses current methods used to measure infiltration in dryland environments and evaluates their suitability (Chapter 2). Following this review, a new methodology is proposed (Chapter 3) that utilises a controlled release of water onto the hillslope to assess the soil surface characteristics, and how these characteristics influence both infiltration and overland flow hydraulics. The method is applied in a sub-humid environment in southern Portugal to both assess its performance in the field and to understand the influence of surface properties on runoff generation and hydraulics by addressing the two research questions identified in section 1.2 (Chapter 4). Chapter 5 discusses the usefulness of the new method, making suggestions for improvements and further research. Finally, Chapter 6 presents brief conclusions relating to topics discussed throughout the thesis, including the applicability of the new method to the dryland environment and the proposed research questions.

## 2. Issues surrounding the measurement of infiltration in drylands

Infiltration is the hydrological process of water entering the soil. The rate can determine how flora and fauna develop, as well as alter the stability of a slope. Infiltration can also govern how overland flow is generated and maintained, including increasing or decreasing flood risk in any given area. The central premise of this thesis is that existing methods of measuring infiltration in the field are not well suited to natural dryland environments. Typical properties of dryland surfaces (e.g. stoniness, enhanced local variability of soil properties) complicate attempts to apply existing infiltration measurement methods that were initially designed for more temperate or agricultural environments. This chapter reviews the current application of field infiltration measurement methods to dryland environments through a systematic literature review. These methods mainly involve the vertical application of water to the surface, rather than considering the influence of surface properties spatially. Firstly, surface properties of dryland soils that influence the choice of infiltration measurement are summarised (section 2.1). The criteria used to select studies for the systematic review is detailed in section 2.2. A synthesis of these studies is provided in section 2.3. Sections 2.4 and 2.5 describe direct infiltration measurement methods used in these studies, noting their advantages and limitations when applied to natural dryland surfaces. Section 2.6 is similar, but focuses on indirect infiltration measurement methods. Section 2.7 summarises the advantages and disadvantages of infiltration methods that should be considered when choosing a dryland-specific infiltration method. Finally, section 2.8 discusses the suitability of the current infiltration measurement methods for dryland environments, and identifies the ideal variables and properties required for infiltration measurements. This chapter is then summarised in section 2.9.

### 2.1. The Dryland Environment

A dryland environment is one which is, as a result of low rainfall and high evaporation rates, has limited soil moisture. Included in this environment are woodland, grassland and desert sub-zones (Safriel, 2006), including dry sub-humid, semi-arid, arid as well as hyper-arid zones (Kottek *et al.*, 2006). The Aridity Index (AI) is calculated as the ratio of precipitation to potential evapotranspiration where an AI value of  $<1.0$  indicates an annual deficit of moisture. Semi-arid areas are defined as having an AI of  $<0.65$  (Middleton and Thomas, 1997). Images representative of surfaces within a semi-arid environment (Salema, Portugal) are shown in Figure 2.1.

Surfaces can influence overland flow in multiple ways. Surface variables include the macro- and microtopography of the surface; where the depth, size and distribution of depressions can result in a higher volume of overland flow reaching a channel, as well as reduced infiltration rates (or vice versa). Also, the connectivity of possible channels and vegetation patterns influence how water flows over the surface and its path (Bracken *et al.*, 2013; Reaney *et al.*, 2014). Surface cracking is another contributor to the movement of water; if there is a larger surface area for water to infiltrate directly into the soil, infiltration rates can be higher. However, larger crack sizes can result in flow concentration, leading to channelization, further erosion and faster land degradation (Nicholson, 2011).

Surfaces can have varying levels of plant and stone cover. In the Mediterranean, stone fragment rich soils cover over 60% of the land, impacting how precipitation interacts with the surface (Poesen, 1990). High surface cover can influence the aeolian erodibility by sheltering the soil surface immediately below the rock fragments. This could reduce deflation of the particles. On the other hand, roughness of the rock fragments can influence wind resulting in increased turbulence, and leading to higher rates of aeolian erosion (Poesen and Lavee, 1994); a particular issue in the Mediterranean due to low rates of soil formation (Borrelli *et al.*, 2014; Masri *et al.*, 2003; Middleton and Thomas, 1997). The influence of rock fragments is complex and is dependent upon a multitude of factors: roughness, height and surface cover.

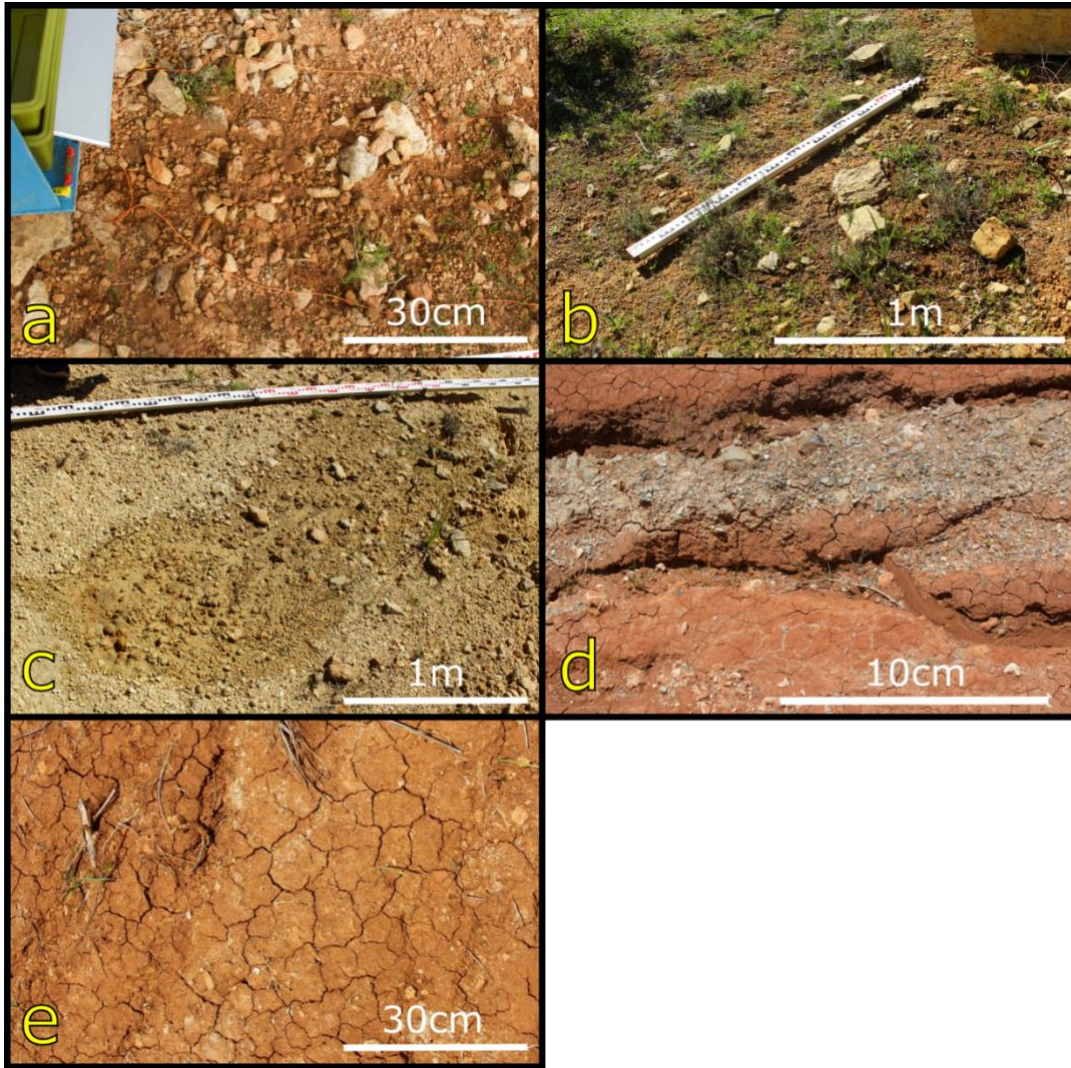


**Figure 2.1:** The range of dryland surfaces in the area surrounding Salema, Western Algarve, Portugal. Images captured March 2018. Where:

- a Low vegetation, moderate cover of both surface and embedded stones
- b Highly vegetated, moderate surface stone cover
- c No vegetation, high surface stone cover, little embedded stone cover
- d No vegetation, little surface and embedded stone cover
- e Bare slope, no cover

Little is known about the influence of lithology and soil properties during the early stages of erosion, indicating for uncertainties and knowledge gaps within such environments (Martínez-Hernández *et al.*, 2017).

Rock fragments can be found on top of the surface, partially embedded or fully embedded within the topsoil. Depending on their location, the surface hydrology can be drastically

altered; if a stone is fully embedded, surface seals can be formed resulting in an decrease of time to runoff concentration and decreased water intake rates (Poesen *et al.*, 1990; Poesen and Ingelmo-Sanchez, 1992; Poesen *et al.*, 1994). This has a positive relationship, as a greater proportion of stones are fully embedded, the time to runoff concentration increases. If the stone fragments are partially embedded or resting on the surface, this can have a negative relationship impact on the hydrology, where there are increased infiltration rates. This is a result of structured porosity, where the rock fragments create pore space (Poesen *et al.*, 1990; Poesen and Ingelmo-Sanchez, 1992).

Rock fragments within the soil surface also have an impact on the physical degradation of the top soil. This occurs via sealing, crusting and compaction. Fragments that exist at the surface protect against bulk aggregate breakdown. Due to compaction and sealing, runoff is less concentrated and therefore less sediment is eroded. Fragments can also exist below the surface. The sub-surface fragments support the existing porosity structure, reduce the impact of compaction and, as previously stated, create structural pore spaces which increase infiltration (Poesen and Lavee, 1994).

Rock fragments can move within the soil profile. This is a result of factors including fauna, flora, swelling of clays, wind, overland flow and freeze thaw weathering (Abrahams and Parsons, 1994). Minor influences (those occurring less often than the aforementioned) also include earthquakes and human disturbance (e.g. cultivation) (Poesen and Lavee, 1994). As rock fragments migrate within the soil, surface hydrology alters, increasing the underlying complexity of quantifying infiltration and overland flow.

Local weather has a significant role in developing variability on a surface. Areas exposed to high levels of precipitation over a short duration results in land that is increasingly vulnerable to erosive action from overland flow, producing bare soils (Langbein and Schumm, 1958). Increased rainfall can also lead to plant growth and an increase in vegetation cover, stabilising slopes. Temperature is another contributor to surface characteristics. The thermal diffusivity, thermal conductivity and heat storage capacity can vary from surface to surface due to local geology, percentage of stone and plant cover and the local climate (Poesen and Lavee, 1994). Thermal characteristics of the surface can produce moisture migration, increasing the susceptibility to erosion, thus reducing the likelihood of colonisation by vegetation for stability (Schwarz *et al.*, 2010).

Understanding and appreciating the variability of the surfaces within drylands, and the processes that act upon them, is pertinent to any experimental design. Attempting to

develop experiments that are truly representative of such variability is increasingly complex. A summary schematic of these processes acting on a theoretical surface during rainfall is presented in Figure 2.2.

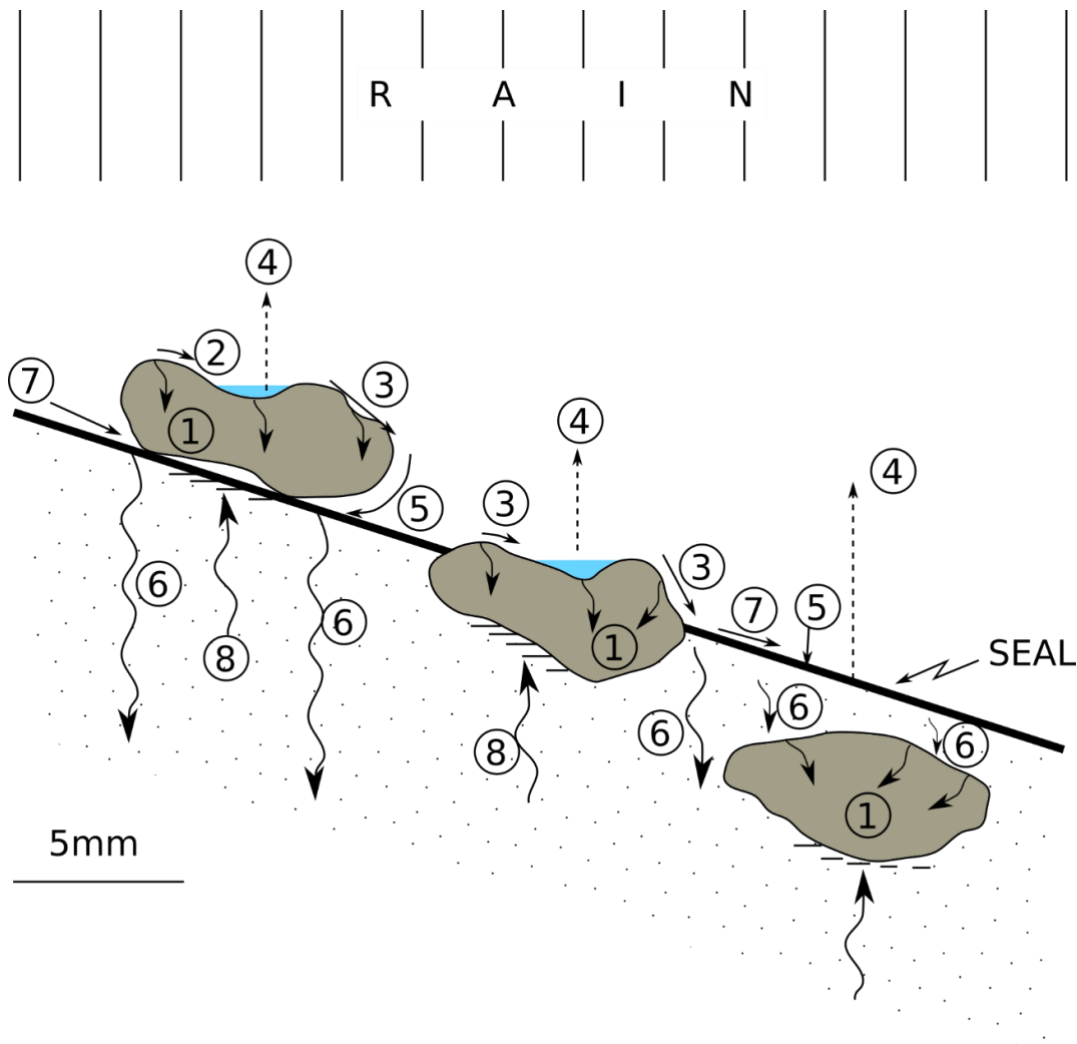


**Figure 2.2:** Schematic illustration showing different hydrological processes on topsoil rock fragments in varied positions, adapted from Poesen and Lavee (1994). **Key:** 1 = water absorption, 2 = interception and depression storage, 3 = rockflow, 4 = evaporation, 5 = infiltration, 6 = percolation, 7 = overland flow, 8 = capillary rise.

Vegetation in the dryland environment ranges from none (i.e. bare soils) to fully vegetated surfaces. This is a highly variable characteristic dependent upon land use, local climate, soil type, geology and precipitation. Surface vegetation can influence soil characteristics, increasing the competency of the soil and reducing the risk of erosion. Vegetation can also

intercept rainfall and reduce overland flow via friction. This causes some wetter climates to experience less soil degradation in comparison to those that are more arid (Middleton and Thomas, 1997). Comprehending how surface variability influences both infiltration and overland flow enables the ability to better characterise areas which are vulnerable to periods of prolonged or intense rainfall.

## 2.2. Identification of Literature

Dryland locations are highly complex with various characteristics that influence infiltration, as identified in section 2.1. The purpose for this and following sections is to systematically identify current methods used to measure infiltration, and to determine their effectiveness within the dryland environment.

This literature review was conducted in accordance with the protocols identified by Siddaway (2014), which were designed to assist postgraduate students conducting and producing a systematic literature review.

Key terms were extracted from the following question (based on the research aims stated in Chapter 1): *are existing infiltration methods suitable for use in the dryland environment?* This allowed for the identification of relevant literature using the PICO (Population, Indicator, Comparison and Outcome) method as suggested by Liberati *et al.* (2009)<sup>1</sup>. These terms can be found in Table 2.1.

Search terms were combined using Boolean operators ('AND' and 'OR'). These were used to perform a topic search, which includes the title, abstract, as well as author identified key words, with the use of the Web of Science database. This resulted in the following combination: ((dryland\* OR semi arid OR semi-arid OR desert OR arid) AND (infiltration OR permeation) AND (method\* OR technique\* OR process\*) AND (effective OR ineffective OR suitable\* OR use\*))<sup>2</sup>.

<i>Population</i>	<i>Indicator</i>	<i>Comparison</i>	<i>Outcome</i>
Dryland*	Infiltration	Method*	Suitable*
Semi arid	Permeation	Technique*	Effective
Semi-arid		Process*	Ineffective
Desert			Use*
Dryland			

**Table 2.1:** Search terms using the PICO technique (Liberati *et al.*, 2009)

<sup>1</sup> This study was designed for use in healthcare and has been adapted for this review.

<sup>2</sup> Asterisk denotes wildcard, where the suffix or prefix of a word can be searched automatically.

Unpublished works were also identified, using the above search terms stated in Table 2.1. Databases were searched in order to locate any relevant theses or other work. Sites used included WorldCat.org; opengrey.eu; and opendoar.org.

Articles were eliminated from the review based on their relevance to the research question; if any articles collected during the data capture did not show relevance upon inspection of either the abstract or full text, they were removed from the sourced literature. The stages of data collection and number of identified articles are represented in Table 2.2.

<i>Stage</i>	<i>Number of articles (prior to removal)</i>
<i>1: Initial Web of Science</i>	462
<i>2: Filtering</i>	164
<i>3: Location</i>	103
<i>4: Abstract analysis</i>	92
<i>5: Full text analysis</i>	57
<i>Final</i>	57

**Table 2.2:** Articles located during research and filtering.

### 2.3. Synthesis of Reviewed Studies

Articles can contain multiple case studies. Within the 57 articles found, 71 case studies were identified, including three in a laboratory setting. However, 11 of the case studies were not associated with a specific area.

Several studies were removed from the review, either due to being unable to obtain the article, or the language not being English. These were: Bridge and Bell (1994); Hanson *et al.* (1999); Loch (1994a); Loch (1994b); Moameni and Farshad (1998), Mohamed (2012) and Sharma *et al.* (2009).

A map of the global coverage of these studies within the context of the global extent of drylands is provided in Figure 2.3, with the frequency of studies in each country indicated in Figure 2.4). Case studies (see Table 2.3) are located within all continents (with the exception of Antarctica), covering Asia (22), Africa (16), North America (11), Europe (11), Oceania (7), and South America (4); highlighting that issues surrounding infiltration measurement are global.

Continent	Proportion of studies	Order of Studies	Continent Dryland Land Cover (DLC)	Order of DLC
Asia	31%	1	41%	1
Africa	23%	2	31%	2
North America	15%	3	9%	4
Europe	15%	3	3%	6
Oceania	10%	5	11%	3
South America	6%	6	6%	5

**Table 2.3:** Distribution of case studies by continent, compared to the total dryland area in that continent (calculated from Figure 2.3)

Table 2.3 highlights that the two largest continents, Asia and Africa, are correctly represented upon comparison of the proportion of studies to the dryland cover distribution. North America and Europe are both over-represented (indicated in red in Table 2.3) as their proportion of studies are greater, relative to their dryland land cover distribution. This may be due to accessibility and the researcher's location. In comparison, Oceania and South America are both under-represented; having a greater percentage of dryland cover but fewer studies.

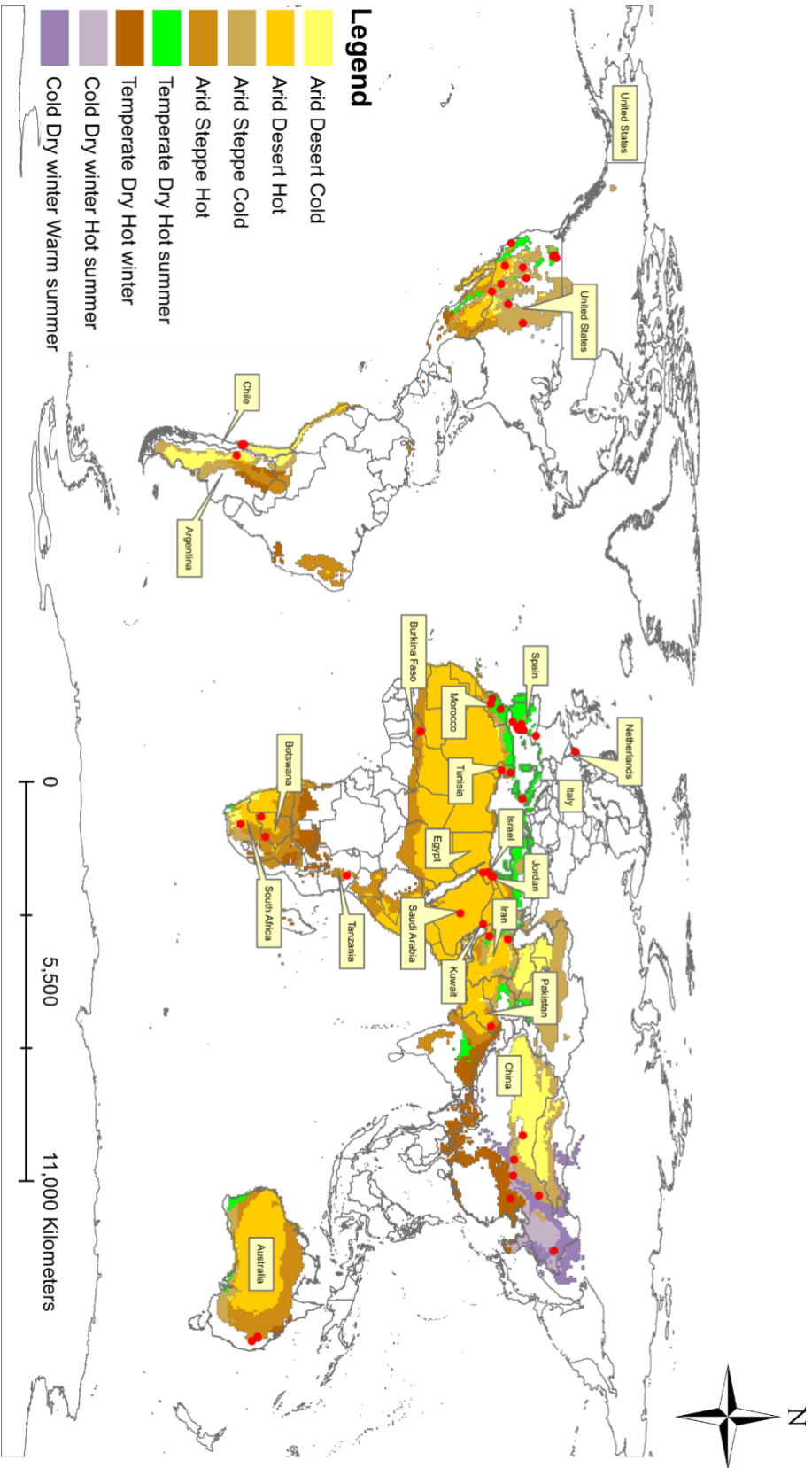


**Figure 2.3:** World Map (Mercator Projection) adapted from Lewis (1992) and Kottek *et al.* (2006) highlighting countries where research has been conducted, and where possible, case studies within those countries in red.

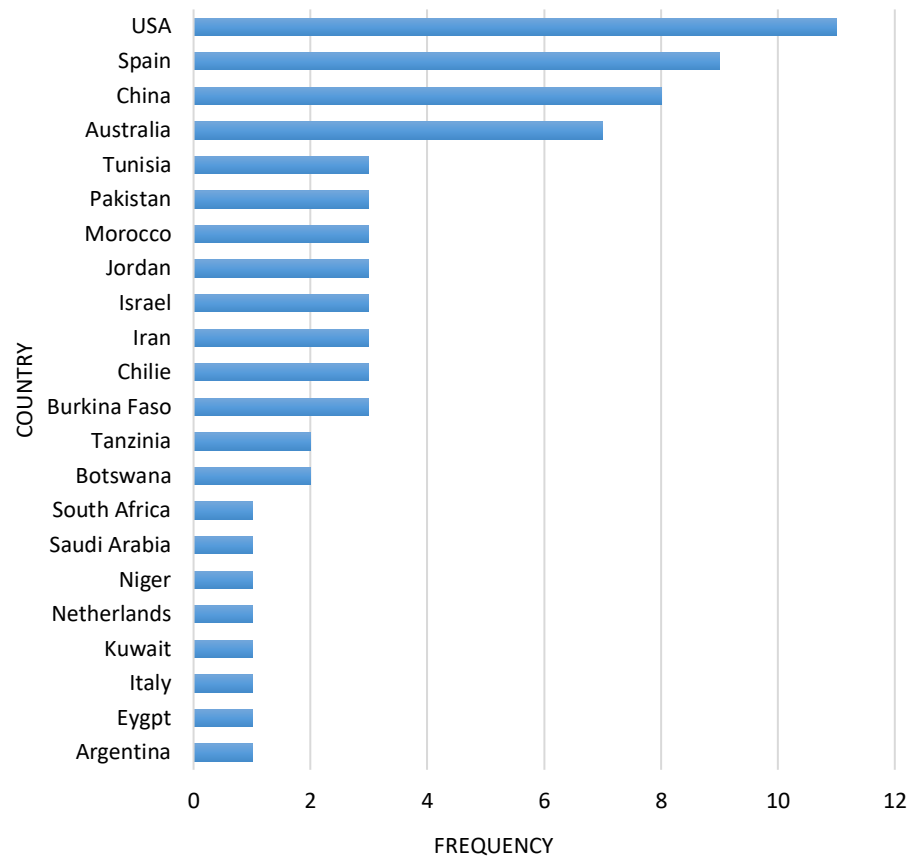


**Figure 2.4:** Frequency of case studies and associated countries. N = 71

Throughout the literature, eight methods were referenced on multiple occasions by up to 18 different groups of authors, and with use in many different fields such as agriculture or research (see Figure 2.5). Note that there is a focus on the agricultural field (14 studies, 23%), although these soils are typically well maintained, low angle, with soft soil, and typically have less stones and vegetation. Using data from these studies alone would be unrepresentative of the dryland environment and its complexities.

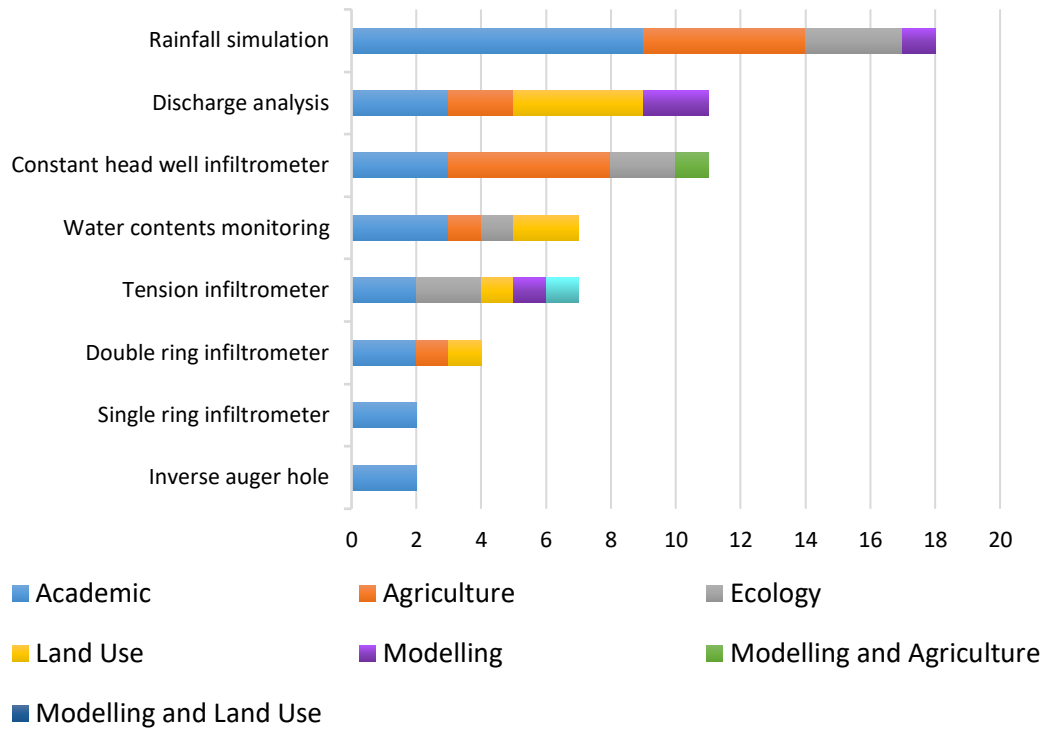


**Figure 2.5:** Infiltration methods identified in the literature, alongside their associated primary application (N = 62)

The following sections review each of the identified methods shown in Figure 2.5, assessing their relevance to application in the dryland environment and its complexities (identified in section 2.1). Assessments are extracted from the literature where possible with some interpretation of the presented issues.

#### 2.4. Rainfall Simulators

Rainfall simulators (RFS) enable the indirect calculation (e.g. Dimanche and Hoogmoed (2002); Figure 2.6) of infiltration rate, or infiltration capacity, by measuring applied rainfall and runoff whilst simulating typical rain and/or storm conditions of the location. Infiltration is calculated with the use of equation 1.

$$f = \frac{Q_{in} - Q_{out}}{A} \quad (1)$$

Where  $f$  = infiltration rate ( $\text{m min}^{-1}$ ),  $Q_{in}$  = inflow (added rainfall;  $\text{m}^3 \text{min}^{-1}$ ),  $Q_{out}$  = outflow ( $\text{m}^3 \text{min}^{-1}$ ) and  $A$  = plot area ( $\text{m}^2$ ) (Walker, 1989).

Rainfall simulators can be installed in both the field (Arnau-Rosalen *et al.*, 2008; Bergkamp *et al.*, 1999; Dimanche and Hoogmoed, 2002; Heilweil *et al.*, 2007; Hikel *et al.*, 2013; Pierson

*et al.*, 2010; Seeger, 2007; Simonneaux *et al.*, 2015; Williams *et al.*, 2006) and a laboratory setting (Abrol *et al.*, 2016; Alemu *et al.*, 1997; Ismail and Depeweg, 2005; Van Wie *et al.*, 2013; Verbist *et al.*, 2013).

Lavee and Poesen (1991) describe the main characteristics required for a rainfall simulator experiment: to include the median size of raindrops; rainfall intensity and variability; the determination of fall height; the kinetic energy required; and the duration of the experiment.

There are multiple methods for the application of water from the simulator which include, but are not limited to, the drip method and the sprinkler method. The drip method involves a casing, such as described by Bryan and Deploey (1983), used with a constant influx of water to form drops which impact the soil surface from a height (from cm to m). This can be adapted and constructed without the aid of manufacturing professionals (DIY) as shown by Salmon and Schick (1980), where surgical needles were used alongside a moving net to create droplets. However, this cannot guarantee uniform rainfall and therefore is not as reliable as using a sprinkler. The sprinkler method uses pressurised water and either a stationary or oscillating nozzle to distribute water over a given area. This enables more customisability over water characteristics (representative of the area) in comparison to the drip method; however, it requires much more equipment as shown by a multitude of authors (Hikel *et al.*, 2013; Pierson *et al.*, 2010; Stone and Paige, 2003; Williams *et al.*, 2006).

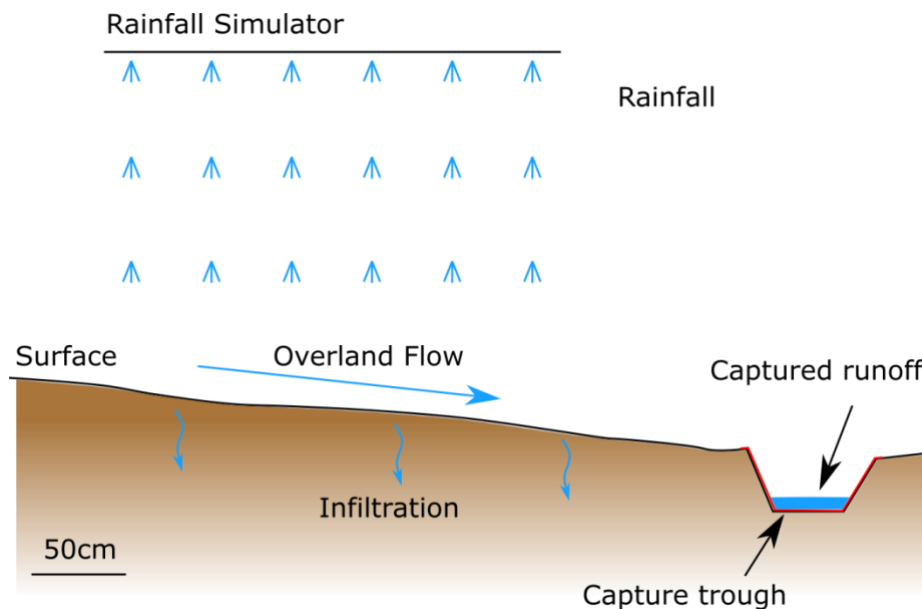


**Figure 2.6:** Measurement of infiltration via captured runoff diagram. Infiltration calculated using eq. 1 (Ismail and Depeweg, 2005; Walker, 1989).

Regardless of the type of method used, variables such as surface runoff and infiltration are typically measured in a similar way. The time between rainfall and the start of ponding is recorded to determine time until infiltration capacity is achieved. Soil samples are also weighed gravimetrically upon completion of an experiment to determine the percentage (by weight) of runoff (Pierson *et al.*, 2010; Williams *et al.*, 2016). This is then used to calculate infiltration, by determining the difference between applied precipitation and runoff. Alternatively, any captured runoff can be compared to applied fluid, with the amount of infiltration being the difference. As well as this, the plot used can be any size; as long as the chosen rainfall method can effectively distribute water over the area, analysis can be conducted. Rainfall simulators can be adapted to a variety of sizes (from 0.25 m<sup>2</sup> up to 20 m<sup>2</sup>) to suit the needs of the user (for example, Figure 2.7). However, during experimentation in the field, rainfall simulators typically cover a range of 1 m<sup>2</sup> to 10 m<sup>2</sup>, resulting in increasing complexity and limitations for transportation (Williams *et al.*, 2006).



**Figure 2.7:** Portable rainfall simulator prior to experimentation without curtain.

Taken in April 1992 in central Spain (Quenca Province). *Images: A. Baird*

Field parameters (Heilweil *et al.*, 2007) can also be identified to determine potential controls for infiltration (e.g. soil thickness, texture, topographic slope). Measurable surface

parameters are not damaged or altered due to there being no direct contact with the rainfall simulator and the soil surface. This is due to its capabilities in replicating natural rainfall, rather than the necessity to insert a device directly into the soil surface; a clear advantage of this method. Runoff results in ponding, if it is natural, alongside the development of crusts by kinetic energy.

However, there are also drawbacks to the method; dependent upon datasets available (e.g. historic rainfall and temperatures), it is questionable whether collected data prior to the experiment is representative of the typical weather characteristics in a region. For example, a weather station can be positioned 10s of km away from the study location, which is unlikely to represent conditions at the site. Renard (1979) also proposed that there are multiple factors not emulated by rainfall simulators, including wind, temperature and humidity. The importance of factors such as humidity and surface temperature are unknown when rainfall simulation is considered, and whether it is necessary that they are incorporated into the experimental design is unclear. Beyond this, depending on the size of the area analysis plot, and the required rainfall intensity and rainfall duration, the method can require significant volumes of water. Apparatus setup and experimentation duration can be time consuming, and with larger sites presents a higher cost and need for mandatory resources. Also, there is not a specific direct method for calculating infiltration rate or capacity; it is dependent upon the volume of runoff captured (e.g. Figure 2.6) and the accuracy of soil samples for moisture content, which further increases the margin for error.

Laboratory experimentation involves, but is not limited to, use of the rainfall simulator on soil samples within a highly controlled environment. This can typically reduce time constraints, enabling further testing of hypotheses. Soil samples can be sieved prior to rainfall to determine grain size distribution. However, this destroys any natural structure within the soil. Vegetation must also be removed to eliminate the distribution of rainfall via precipitation interception of the outer surface layer (the canopy effect) (Alemu *et al.*, 1997). Soils can then be air dried and crushed to the desired size. Water is generally readily available and transportation to a field location is not required. Weather and temperature can also be regulated to reduce any unwanted variability, and the analysis plot can be constructed in a way that infiltrated water can seep out of the base into storage cylinders for analysis. Nonetheless, this is not always practical due to the large amount of space and resources required (Abrol *et al.*, 2016).

Laboratory experiments, however, do not always completely represent the complexity of an environment; including sunlight exposure, surface temperatures, humidity, as well as scale variations. For example, Abrol *et al.* (2016) conducted experiments on relatively small plots  $0.3 \times 0.5$  m to assess the effects of biochar on infiltration. These small plots may not reflect important surface variables of infiltration and overland flow, such as hillslope-channel connections due to their small area (Reaney *et al.* (2014)).

When using a rainfall simulator, an experimental area can only be used once in any given location without having to return several days later. This is to allow for the soil to fully dry before further experiments can be conducted. Alternatively, the simulator must be relocated to allow for repeated experiments, which can often be both time consuming and impractical.

Also, the number of experiments that can be conducted is limited due to time constraints previously mentioned, as well as being able to repeat experiments on similar surfaces. Rainfall simulators enable experiments to cover a more representative area, without the need to omit perennial vegetation, large stones or steep slopes. However, with highly variable data comes highly variable processes. Seeger (2007), after conducting over 100 rainfall simulations in seven different locations (four in the Ebro Basin, Pyrenees, Spain [semi-arid], and three in two different basins in SE-Spain) concluded that most investigated surface parameters had no influence on runoff and erosion due to plot scale quantitative data not being statistically significant. It is clear that another view of the parameters controlling runoff generation is required for rainfall simulation experiments, along with a knowledge-based classification of roughness and vegetation cover.

Although this technique is highly useful, and most likely the most representative of actual rainfall, due to the practical aspects of transportation and water supply, this is not the most effective method for quantifying the hydrological response of the soil surface. With minimal resources, this technique is not simple to reproduce and the lack of repeat measurements can result in less reliable data, not truly representative of the environment.

## 2.5. Infiltrimeters

Infiltrimeters are one of the most used methods in drylands (44% total) and are divided into four categories: single ring, double ring, tension and mini disk. Infiltrimeters have been used in 24 different articles and for a variety of applications (see Figure 2.5).

### 2.5.1. Single Ring

One of the least favoured methods (3% of identified studies), the single ring infiltrometer comprises a cylinder composed of metal or plastic which is inserted vertically into the ground, whilst causing as minimal disturbance to the soil as possible (see Figure 2.8).

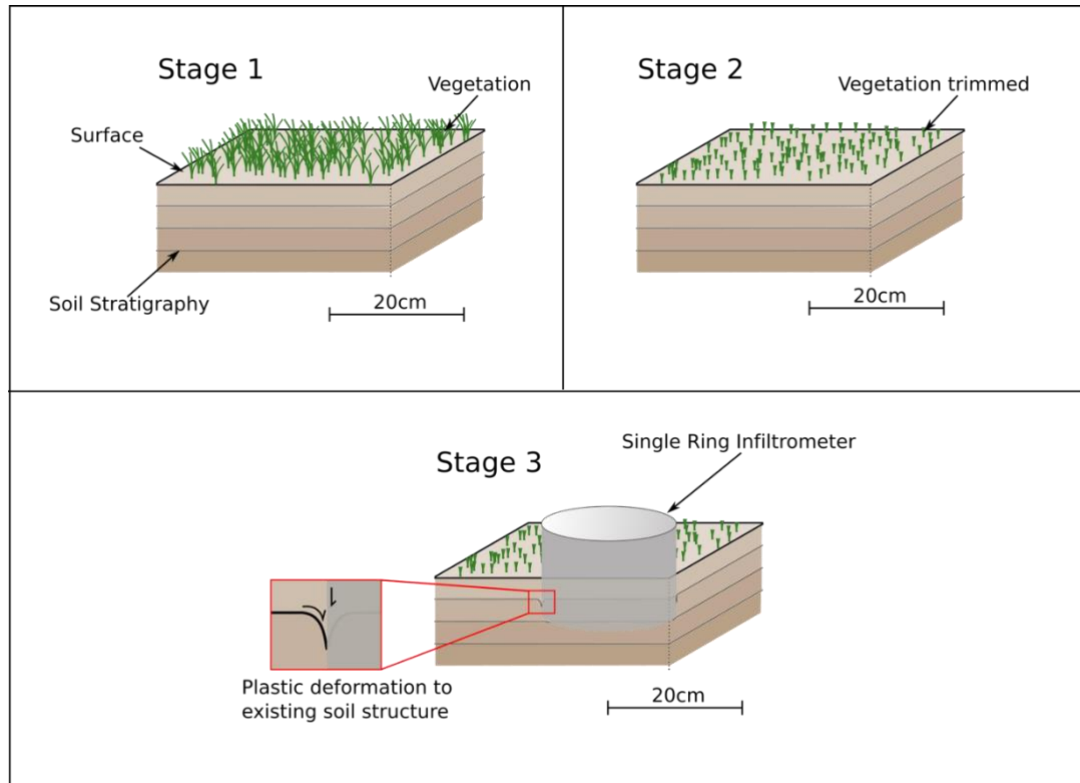


**Figure 2.8:** Disturbance to soil structure as a result of insertion of an SRI. Stage 1 highlights soil conditions prior to preparation. Stage 2 represents the initial preparation of reducing vegetation before insertion of the SRI (stage 3). Stage 3 represents deformation of the subsoil structure which may influence infiltration rate. Cracking can also occur if the soil is dry upon insertion.

Operating either on the principle of a falling or constant head (the latter often maintained by a Mariotte regulator), single ring infiltrometers (SRIs) typically range from 13–20 cm in diameter (Xu *et al.*, 2012). A hollow cylinder is inserted approximately 6 cm into the ground, taking care not to disturb any soil layering and to prevent the formation of cracks (see Figure 2.8). This can be successful in softer or less resistive soils such as those in agricultural areas; however, dryland soils are often hard with desiccation cracks and the insertion of the ring can be challenging. This can require a sledgehammer for successful insertion, destroying soil layering around the perimeter of the ring. The ring must be level to enable an even distribution of pressure from the water, meaning that this device cannot be used on sloping

ground without the possibility of distortion to results. If the device is not level, hydraulic head would vary across the area of the device, resulting in a pressure gradient on the surface, which may increase infiltration in one area of the soil contained within the ring.

Any perennial vegetation is mostly removed to prevent distortion to the results. This generates bias towards greater infiltration, as the removal of vegetation does not provide a representative area for analysis since the experimental surface is being altered from its natural state. A pre-determined maximum and minimum head is marked on the side of the cylinder to enable volume calculations. Water is then added to the inside of the cylinder, whilst attempting to not to create surface seals. This can be performed with use of a mesh or other 'cushion' to reduce the impact of the force of the water on the soil which reduces the creation of unnatural microtopography (see Figure 2.9).

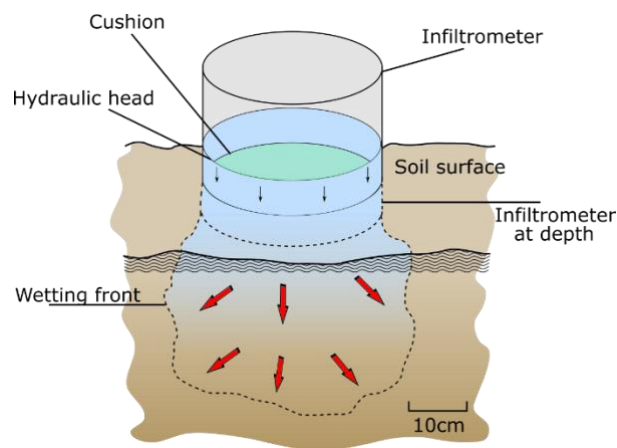


**Figure 2.9:** Single ring infiltrometer showing wetting front (adapted from Sanders (1998)).

Wetting front represents the movement of water through the sub-surface.

Once the equipment is set up, recording using a stopwatch, or similar device, can begin. When the hydraulic head of the cylinder reaches the minimum marking, the device is refilled to the maximum point (if using the constant head method). If using a falling head, the device is not refilled. This results in minor variations in applied pressure to the experimental surface which has been represented in Figure 2.10. The time at which this occurred is recorded, alongside the volume added. When steady state is reached (time between refills is constant), or after a predetermined time, the experiment is concluded.

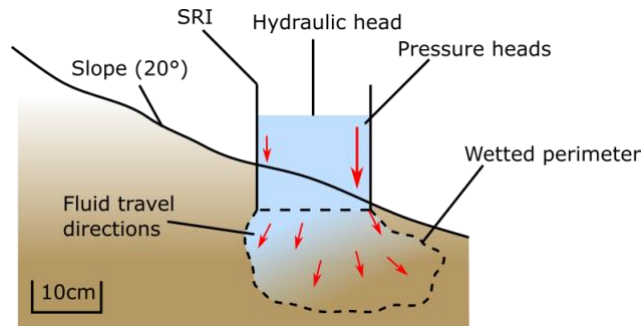


**Figure 2.10:** SRI pressure differentials visualised on a 20° slope

Measurements taken include insertion depth, water start level and water refill level. Timing begins when water reaches water start level, and measurements of water input are taken with a set time increment. From this (alongside total volume of added water), infiltration rate can be calculated using equations (2) and (3) adapted from Sanders (1998):

$$d = \frac{V}{A} \quad (2)$$

$$f = \frac{d}{t_{add}} \quad (3)$$

Where  $d$  (m) is depth of added water;  $V$  (m<sup>3</sup>) represents volume of water;  $A$  is area (m<sup>2</sup>);  $f$  is infiltration rate (m min<sup>-1</sup>); and  $t_{add}$  (min) is the elapsed time between additions of water. This technique is adapted and deployed by Abu-Taleb (1999); utilising infiltration ponds to calculate infiltration rate, and further analysed by Verbist *et al.* (2013).

The single ring method uses the ponding of water to allow infiltration; however ponding can result in unrepresentative infiltration rates, as water does not always pond on any given surface. When precipitation strikes bare soil, the kinetic energy imparted can result in soil surface sealing. This is the process of forming a more compact and less permeable layer which results in the reduction of infiltration (Chen *et al.*, 2013). Ponded water does not have the same kinetic energy as rainfall does, resulting in the absence of surface sealing, and therefore can result in an infiltration rate being measured higher than it truly would be.

In addition to this, with the use of a single ring setup, movement of water in the vertical direction cannot be guaranteed due to the lateral spreading and movement of wetting fronts (Sanders, 1998). This is crucial for 1D modelling (e.g. flood modelling) as the reaction of a single dimension ( $x$ ,  $y$  or  $z$ ) can be analysed to determine the response to change within the system. The error source can result in unexpectedly high rates of infiltration, also due to any

stone content in the surface. As well as this, infiltration can be very variable, and is unlikely always vertical. The best uses of this technique are likely agriculturally oriented as soils are typically stone and vegetation free.

Due to the varied nature of dryland surfaces in terms of slope angle, vegetation and stone cover, this device is not suitable for use on the majority of dryland surfaces.

### 2.5.2. Double Ring

Comparable to a single ring infiltrometer, the double ring infiltrometer (DRI) comprises of two open ended cylinders which are driven into the soil surface. The outer ring is inserted approximately three times deeper than the inner. Within these rings, fluid is placed to measure infiltration rates (see Figure 2.11). Both rings are filled with water to approximately the same level (the outer ring is filled first), and refilled when the minimum head is reached. The data for the two rings is recorded separately, and the experiment is concluded when infiltration is at steady state, or, a scheduled time stop is reached.

The purpose of the outer ring is to reduce lateral spreading of fluid from the central ring, providing more accurate data collection as infiltration is assumed to be largely 1D under natural conditions (Sanders, 1998) as previously discussed in section 2.5.1.

The double ring method is utilised by multiple authors (Al-Awadhi, 2013; Guzha, 2004; Perrolf and Sandstrom, 1995; Verbist *et al.*, 2013), typically in conjunction with another method (e.g. tension infiltrometer) to provide more accurate and reliable data sets by limiting error and constraining results.

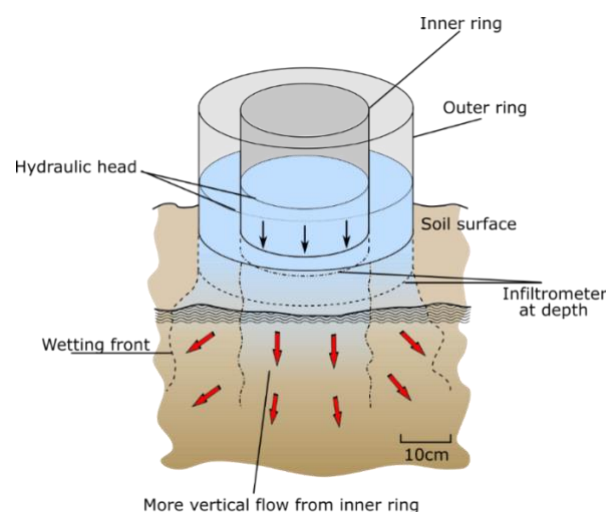


**Figure 2.11:** Double ring infiltrometer schematic adapted from Sanders (1998)

Perrolf and Sandstrom (1995) indicate the ring infiltrometers high dependency on topography and soil texture, resulting in variances of up to 20 times infiltration capacity (when considering different soil crusts). Perrolf and Sandstrom (1995) also identify the issue of double ring infiltrometers partially destroying surface crusts, resulting in infiltration data describing the subsurface conditions more than the soil surface.

The double ring method is thought to be both more reliable and accurate than the SRI due to its dual rings and increased control over the direction of flow. The double ring infiltrometer also has the same, if not greater, impact on disturbance to the soil due to insertion of the dual rings into the ground, consequently damaging existing structures. It is also essential that vegetation is trimmed to ensure that data can be effectively collected.

For both the SRI and DRI, it is suggested by Reynolds *et al.* (2002) that physical sources of measurement errors include soil compaction (during installation); siltation of the soil surface (due to a lack of overland flow); and gradual plugging of soil pores resulting from deflocculated silts and clays (when using a major cation water e.g. Na, Mg, Ca and K). Another source error results from 'short circuit flow' which is concentrated along the cylinder walls. These errors can be reduced with the use of a 'cushion' to lessen the impact of the water to the surface to mitigate against siltation. The impact of soil flocculation can also be reduced by using local tap water. The use of tap water, however, is not always practical, particularly in areas experiencing drought.

Due to the aforementioned features, as with SRIs, this method is deemed unsuitable for the majority of dryland surfaces. Verbist *et al.* (2010) compares SRIs with DRI methods on stony soils. The authors focus on the various techniques for calculating infiltration rather than the errors identified via using the device. It is noted, however, that upon insertion of the DRI stone fragments surfaced, damaging any existing textural porosity, and the device required a larger volume of water than the SRI. In terms of calculating infiltration, it was concluded that there was no clear variance between the methods. It is apparent that the key issue with the devices is actually size of the inner ring, as stated in Verbist *et al.* (2010). Presented by Wu and Pan (1997) and confirmed by Lai and Ren (2007), when the inner ring diameter is greater than 20 cm, measurement errors as a result of lateral flow decrease.

### 2.5.3. Tension Infiltrometers

A tension infiltrometer (TI) is likely one of the most versatile methods for calculating infiltration rates and hydraulic conductivity within soils (Verbist *et al.*, 2013), due to its adaptability for targeting specific capillary sizes within compacted soils. A tension

infiltrometer works by adjusting the tension of the water supply reservoir, excluding pores of varying sizes from conducting water into the soil (Brady and Weil, 2008). This can be adjusted by varying the inlet pressure and adjusting the aperture of the contact mesh (outlet), as shown in Figure 2.12. Adjusting these parameters enables the direct comparison of data for different soil capillary sizes (Kelishadi *et al.*, 2014; Verbist *et al.*, 2013; Young *et al.*, 2004; Zhou *et al.*, 2011).

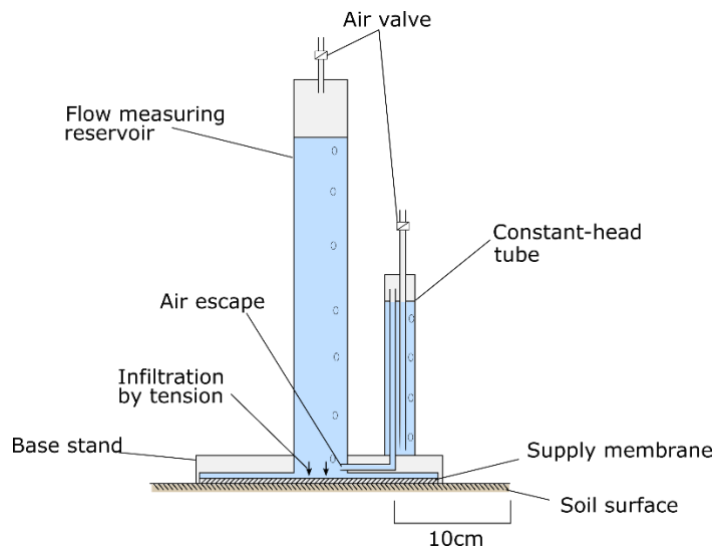


**Figure 2.12:** Tension infiltrometer schematic diagram adapted from Amoozegar and Wilson (1999)

As shown in Figure 2.12, the TI contains a water reservoir; water is stored prior to contact with the ground, as well as an area to create a negative pressure head. The devices also have a ground contact disk, which is connected to the ground via a thin (max. 3 mm) semi-permeable membrane (e.g. fine silica sand). This improves the hydraulic connection between the device and the surface (Kelishadi *et al.*, 2014; Perroux and White, 1988). As with the ring infiltrometers, it is essential that vegetation is trimmed to surface height prior to commencing experimentation, and the soil should be levelled (if undulating) to ensure a good hydraulic connection (Perroux and White, 1988). The influence of the negative hydraulic head can be adjusted enabling infiltration into different pore sizes. This allows a thorough analysis of how the soil behaves. The TI can also be automated; recording measurements over time and so multiple devices can be left in different locations (Ankeny *et al.*, 1988), making their use efficient.

A major disadvantage of this technique is that TIs cannot be used on sloped surfaces, nor where there is rock cover or thick vegetation. The surface must be disrupted to ensure it is level; altering its hydraulic properties. Also, using a wet layer of sand to ensure an effective hydraulic connection could omit larger pore sizes due to the smaller grain size. Another identified issue is that like ring infiltrometers, adjusting the soil surface results in their use being less representative of the area, reducing their effectiveness for use in the dryland environment.

#### 2.5.4. Mini Disk Infiltrimeters

Mini disk infiltrimeters (MDIs) are smaller and more transportable versions of tension infiltrimeters (see Figure 2.13). These work in the same way as TIs, though they assess a smaller surface area and generally require a lower volume of water (Li *et al.*, 2005; Smith, 2009).

These devices house a reservoir for water and an adjustable pressure head. Vegetation still should be reduced or removed, and the device cannot be used on a sloping surface without disruption to the soil; a major issue similar to the TI (section 2.5.3). The advantage of the MDI is that the device can be used whilst altering less of the soils hydraulic properties. A wet layer of contact media must also be added to ensure an effective hydraulic connection.

An advantage of using an MDI over the TI is the smaller size and lower water usage. This allows for experiments to be conducted over a shorter period, and infiltration experiments are also more accessible (as the need for the transportation of large volumes of water is reduced); making the MDI easier to use in the dryland environment in comparison to the TI. However, issues, such as vegetation removal and disturbance of the soil, still exist and therefore reduce the reliability of measurements.

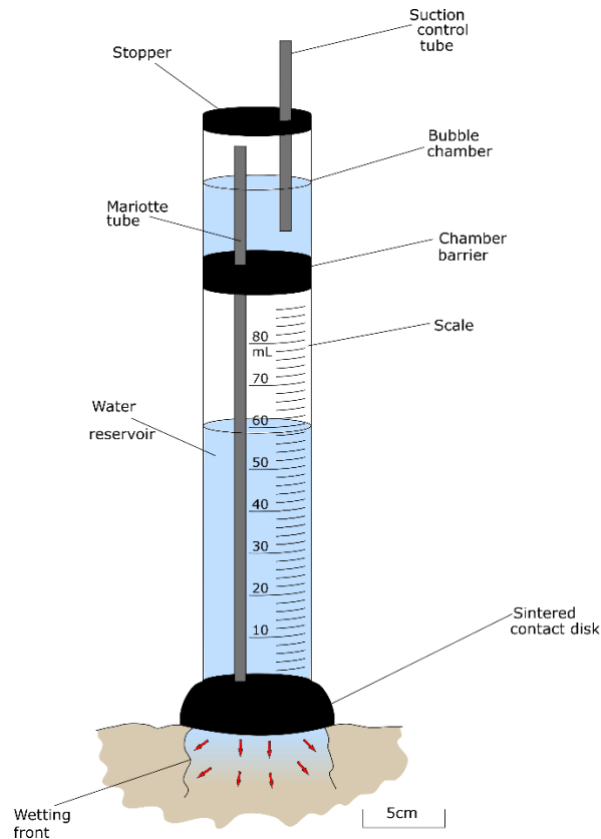


**Figure 2.13:** Mini disk infiltrometer adapted from Decagon Devices (2016)

### 2.5.5. Hydraulic Conductivity

Infiltration can be indirectly calculated by measuring hydraulic conductivity. Although this is an indirect measure of infiltration, hydraulic conductivity can provide an insight into the infiltration capacity as infiltration rate is dependent on the hydraulic conductivity of the soil. This is due to hydraulic conductivity being dependent on the soil moisture content. However, this changes during infiltration. When the soil is fully saturated, the hydraulic conductivity becomes constant.

Zhou *et al.* (2016) note that a wide range of hydraulic conductivities can be measured by adjusting hydraulic head gradients between 0.5 cm and 30 cm. Experiments are conducted on soil core samples obtained from the field. However, this method poses risk to causing disturbance to the soil core and requires more equipment than most methods. The disturbance error is reduced by removing any compacted soil from the collected core. This reduces the degree of representation of the sample obtained from the soil column, which in turn reduces its effectiveness for measuring infiltration in the environment (Reynolds and Elrick, 2002).

The literature rarely discusses issues surrounding methods of measuring infiltration but describes issues with manipulating the obtained data when attempting to calculate infiltration rate or hydraulic conductivity. An example of this is presented by Verbist *et al.* (2013), where multiple methods are compared for the effectiveness of determining hydraulic conductivity. The issue of how the data capture device introduces inaccuracies is typically overlooked.

Auger holes (boreholes) can also be used to measure hydraulic conductivity. They are drilled and then filled with water which is then measured as it infiltrates into the soil. The amount of water the auger hole is filled with is dependent on the type of soil (i.e. loam soils will need to be filled 1-3 times, sandy soils 3-6 times). Van Hoorn (1979) identified that data obtained from auger holes is comparable to that of ring infiltrometers. As well as this, auger holes enable the insertion of equipment (such as neutron probes or TDIs) into the ground at varying depths. This provides the ability to generate 2-dimensional or 3-dimensional plots which can be used to form time series maps, allowing for highly detailed monitoring of groundwater (Clement *et al.*, 2009).

Auger holes, although useful, are not always practical. Due to the high stone content found in some soils identified by Poesen and Lavee (1994), it may not be possible to bore a hole into the soil. As well as this, soils in drylands can be very hard, and when a drill is applied this may deform the structure of the soil and introduce fractures. This would most likely alter the actual infiltration rate to be faster than under natural conditions. The location for drilling must also be considered, where some areas are avoided, i.e. those with outcrop and densely vegetated zones. This results in the method not being truly representative of that dryland surface. The impact of precipitation onto the soil surface is also negated (alongside interception of precipitation by vegetation or stones resting on the surface) due to the measurements occurring in the sub-surface. Alongside this, auger holes enable the measurement of hydraulic conductivity below the surface, which may not accurately reflect surface conditions at all.

## 2.6. Indirect monitoring of water content

Soil water monitoring can provide information on rates and amounts of infiltration via tracking rainfall volume, temperature fluctuations changes in resistivity and soil moisture content. Data collected then is incorporated into numerical models to assess infiltration rates indirectly in response to a stimulus; irrigation for example Feki *et al.* (2018). There are many methods of monitoring within the hydrological cycle. Techniques can be deployed at multiple

scales, from palaeo-watershed [km<sup>2</sup>] (Oster *et al.*, 2017) to micro-drainage [cm<sup>2</sup>] (e.g. (Menon *et al.*, 2011)).

### 2.6.1. Electrical Tomography

Electrical tomography was the focus of four of the identified articles (Clement *et al.*, 2009; Lghoul *et al.*, 2012; Martinez-Pagan *et al.*, 2009; Wubda *et al.*, 2017). Geophysical methods, combined with the implantation of electrodes (into the soil), enables resistivity to be measured to allow for a better characterisation of hydrological processes, such as infiltration. Changes in resistivity highlight differences in the lithology, water content or texture, and can be used to monitor and track water movement, as well as infer infiltration depth with the use of time-lapse. This is an advanced geophysical method, but is open to individual interpretation and errors, as explored by Clement *et al.* (2009). Despite this, it produces results which can be used to highlight where the preferential direction of infiltration is most likely (e.g. Figure 2.14).

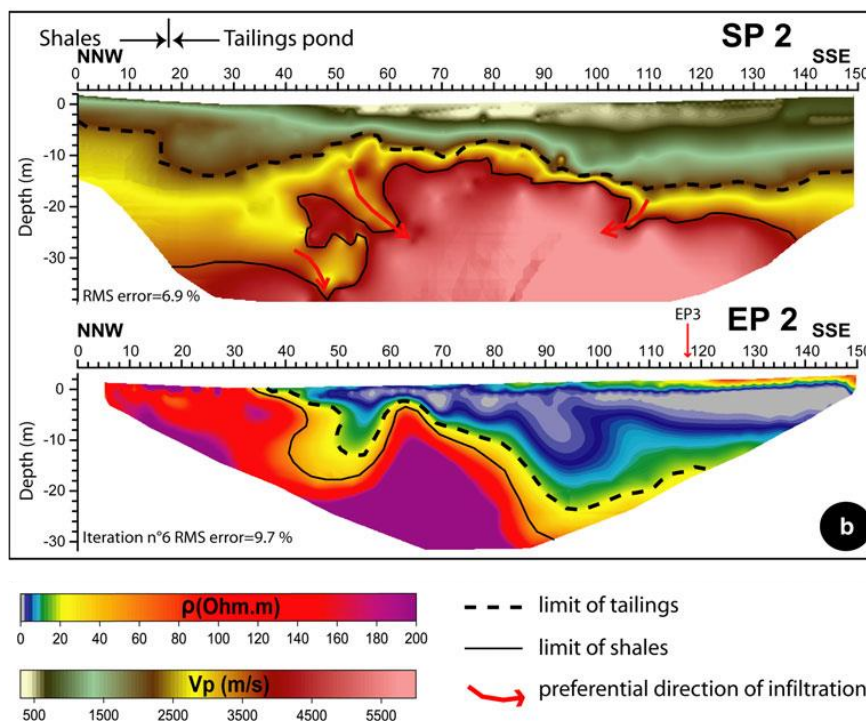


**Figure 2.14:** Interpretations of the seismic profile combined with the electrical profile to provide continuous cover of the tailings pond at the abandoned Kettara Mine, Morocco (Lghoul *et al.*, 2012)

Gravimetrically, soil moisture can be measured with the use of neutron probes or time-domain reflectometry (TDR). After determining the volumetric soil water content prior to

experimentation, the probes can be calibrated to assess change soil moisture (neutron probes are represented by a linear relationship (Fan *et al.*, 2016)) or the apparent dielectric constant for TDRs (Skierucha *et al.*, 2012). By revisiting sites, the changes can be measured and related to infiltration events, enabling the infiltration extent and capacity to be determined with respect to rainfall or artificial recharge (Ibn Ali *et al.*, 2017). These studies, however, focus on recharge of the groundwater and not surface infiltration, so are generally not applicable to the short-term measuring of surface infiltration.

#### 2.6.2. Discharge Analysis

Water balance models can be applied to multiple scales, from river system discharge at the watershed scale (de Laat and Nonner, 2012; Gargouri-Ellouze and Bargaoui, 2009; Li *et al.*, 2016; Qiu *et al.*, 2011; Sun *et al.*, 2013; Tabeni *et al.*, 2016; Zema *et al.*, 2017) to discharge in urban environments and steppe scale (Koob *et al.*, 1999; Maestre and Puche, 2009). By utilising measurable parameters, such as rainfall, runoff, evaporation, land use, surface cover, local climate and assuming conservation of mass, residual factors, such as infiltration, can be determined.

Local scale discharge analysis is also conducted utilising GIS and water balance models. On this scale, however, experiments can be conducted at different sites to provide an average for the micro-catchment to determine soil function in relation to diverting urban storm water runoff (Koob *et al.*, 1999) and land use possibilities (Maestre and Puche, 2009). This technique works in a similar way to rainfall simulation, although on a much larger scale (watershed), combined with monitoring data to establish the amount of water lost to soil. This data can then be compared to the geology of a catchment basin and in turn to other basins to assess the overall level of infiltration, relative to precipitation.

## 2.7. Summary of Methods

Table 2.4 summarises methods identified in sections 2.4 - 2.6, key advantages and disadvantages are identified for each method. These have either been stated by authors in the literature, or interpreted considering the limitations of the dryland environment.

METHOD	ADVANTAGES	DISADVANTAGES
Rainfall Simulator  Captures: Infiltration  Influence of topography; vegetation/stone cover; surface roughness; soil moisture	<ul style="list-style-type: none"> <li>• Simulate rainfall specific to an area</li> <li>• Work on most surfaces</li> <li>• Incorporates all aspects of the dryland surface</li> <li>• Replicate the kinetic energy imparted onto a surface by natural precipitation</li> </ul>	<ul style="list-style-type: none"> <li>• Can be highly expensive</li> <li>• Experiments cannot be repeated readily</li> <li>• Large volume of water required</li> <li>• Difficult to use on steep slopes</li> <li>• Impractical to move long distances</li> </ul>
Single Ring Infiltrometer  Captures: Infiltration	<ul style="list-style-type: none"> <li>• Relatively small size</li> <li>• Directly measures infiltration</li> </ul>	<ul style="list-style-type: none"> <li>• Alters surface and subsurface structure</li> <li>• Cannot be used in areas with a high stone content</li> <li>• Vegetation requires trimming</li> <li>• Assumes constant ponding</li> <li>• Cannot be used on sloping surfaces</li> <li>• Possible overestimation of vertical infiltration due to lateral flow</li> <li>• Moderate volume of water required</li> <li>• Must be forced into the surface (with hands or sledgehammer)</li> </ul>

METHOD	ADVANTAGES	DISADVANTAGES
Double Ring Infiltrometer  Captures: Infiltration	<ul style="list-style-type: none"> <li>• Relatively small size</li> <li>• Directly measures infiltration</li> <li>• The second ring is thought to mitigate against lateral flow</li> </ul>	<ul style="list-style-type: none"> <li>• Unrepresentative of the area</li> <li>• See single ring infiltrrometer (without lateral flow issue)</li> </ul>
Tension Infiltrometer  Captures: Infiltration	<ul style="list-style-type: none"> <li>• Focuses on pore size in soil</li> <li>• Can be automated</li> <li>• Moderate volume of water required</li> </ul>	<ul style="list-style-type: none"> <li>• Cannot be used on sloping surfaces</li> <li>• Relatively large size</li> <li>• Vegetation has to be trimmed/removed</li> <li>• Cannot be used in high stone content areas</li> <li>• Contact medium required</li> </ul>
Mini Disk Infiltrometer  Captures: Infiltration	<ul style="list-style-type: none"> <li>• Low volume of water required</li> <li>• Small size</li> <li>• Rapid experiment turnaround</li> </ul>	<ul style="list-style-type: none"> <li>• Cannot be used on sloping surfaces</li> <li>• Only gives an inter-stone infiltration rate</li> <li>• Vegetation has to be trimmed/removed</li> <li>• Not representative of all areas</li> <li>• Contact medium required</li> </ul>
Discharge Analysis  Captures: Aggregate infiltration  Surface runoff	<ul style="list-style-type: none"> <li>• Used in conjunction with rainfall measurements to estimate aggregate infiltration</li> <li>• Used to assess multiple variables at once</li> </ul>	<ul style="list-style-type: none"> <li>• Resource intensive</li> <li>• Time intensive</li> <li>• Typically utilised on catchment scales</li> </ul>

METHOD	ADVANTAGES	DISADVANTAGES
Soil Moisture Measurement	<ul style="list-style-type: none"> <li>Useful at large scales</li> <li>Highlights changes in response to seasonal changes or weather changes</li> <li>Can be used in conjunction with other methods (e.g. ring infiltrometer)</li> </ul>	<ul style="list-style-type: none"> <li>Time intensive</li> <li>Equipment intensive</li> <li>Not practical at all scales</li> <li>Focuses on groundwater rather than infiltration over the short term</li> </ul>
Inverse Auger Holes	<ul style="list-style-type: none"> <li>Comparable to infiltrometers</li> <li>Enable insertion of equipment for long term monitoring</li> </ul>	<ul style="list-style-type: none"> <li>Destroys natural soil structure</li> <li>Cannot be used in areas with high stone content</li> <li>Does not incorporate the influence of vegetation</li> <li>Water intensive</li> </ul>

**Table 2.4:** Summary of methods

## 2.8. Discussion

### 2.8.1. Are current infiltration measurement methods suitable for drylands?

The current methods used to measure infiltration use both direct measurement of the flow of water into soil and indirect measurements. Three of these methods, ring infiltrometers (single and double) and inverse auger holes, involved inserting apparatus into the soil surface; which is not always practical due to vegetation, stone cover and rock outcrop. This leads to over-representation of the percentage of land which does not contain rock fragments, and the overall data is less representative of the dryland environment. As well as this, the insertion of equipment into the soil destroys (or damages) any structure already developed.

Four of the identified methods (ring infiltrometers, tension infiltrometer and mini disk infiltrometer) require the trimming or removal of vegetation to ensure good contact between the soil and the device. Again, this leads to less representation of vegetated areas, which are not uncommon in drylands (especially those which are semi-arid).

Most methods (six out of nine) are impractical to use on shallow slopes (eight out of nine on steep slopes). Those which are practical are rainfall simulators (shallow slopes only), indirect monitoring and discharge analysis. This is mainly due to the mobility of equipment used, practicality and differences in hydraulic head across the apparatus (e.g. Figure 2.10).

Volume of water required varies across the devices. However, some methods (rainfall simulator, constant-head, inverse auger holes and discharge analysis) require a large amount of water, whilst others (ring infiltrometers, tension infiltrometer) require a moderate volume of water. In an arid environment, this is a major limitation due to possible drought and lack of available natural water. The most effective method considering this is the mini disk infiltrometer, due to its relatively low levels of water consumption.

Time intensive experiments also exist (rainfall simulators, discharge analysis and auger holes), although these are typically time intensive due to the composition of the soil. Setup time, however, can be lengthy and increases with the scale of the experiment. More practical equipment, such as ring infiltrometers, or the tension and mini disk infiltrometers, are more applicable in this case due to the short setup time, and short experiment time (depending on the soil type).

The only experiment to incorporate overland flow and downstream infiltration is the rainfall simulator. Overland flow is generally overlooked or excluded in other methods, despite it being common in the dryland environment due to the high erodibility of soils. Downslope infiltration of the overland flow is also overlooked, with infiltration measurement techniques not accounting for how the water interacts with the surface.

Rainfall simulators are also the only technique able to be used on vegetated and/or stony soils. As rainfall is simulated, this enables the precipitation (and overland flow) to interact with the surface in the most natural way possible. However, the position of the rock fragments within the soil (i.e. embedded or resting on the surface) are not always reported, as identified by Poesen and Lavee (1994); a key control for infiltration and surface runoff.

On the premise of the identified factors, there is no one optimum method for measuring infiltration in a dryland environment; only mitigations for the use of each method. For ease of use, practicality, time, cost and low water requirements, the mini disk infiltrometer appears to be the most applicable infiltration measuring method, despite not replicating rainfall. This is reflected by its position as the most common field method used for measuring

infiltration with an infiltrometer; 50% of measurements taken in the field with an infiltrometer used a tension or mini disk infiltrometer (Smith, 2009).

As shown above all existing methods have issues. A particular problem for nearly all of the direct methods is that they do not take proper account of the effect of stones, whether they be resting on the surface or are embedded. Direct methods also require disturbance to the soil surface, changing the hydrological characteristics. Indirect methods such as the rainfall simulator incorporate cover more effectively, however cannot be used on steeper slopes, and are also resource intensive in terms of water and time. Furthermore, all methods with the exception of the rainfall simulator do not consider the influence of overland flow on the surface, assuming that infiltration only occurs vertically. Therefore, there is a need for a new method which can successfully integrate surface characteristics whilst remaining representative of the surface; by not avoiding rock fragments, removing vegetation, dismissing steep slopes and incorporating overland flow.

#### 2.8.2. Ideal properties of a dryland infiltration measurement method

It is evident that an infiltration measurement method for use in the dryland environment should be able to measure a multitude of factors and variables in order to be effective. Rock fragments and their position within the soil can alter the relationship between runoff and infiltration to have a positive or negative correlation (Poesen and Lavee, 1994), and therefore it is vital to quantify this. Vegetation cover also provides a canopy which can increase infiltration rates in the soil located beneath them. Removing the vegetation results in an unrepresentative view on the hydrological characteristics of the soil, which is otherwise crucial.

The water volume of a device used should be as low as practically possible. This enables increased mobility, decreases cost and weight, as well as use in times of drought. The device should also have effective use on as steep a slope as possible, as this is a proportion of the land that is currently neglected. It is crucial that infiltration from overland flow is considered, as without this, data collected is not fully representing surface hydrological processes in drylands. By making a measuring technique simple, the true response of a complex environment becomes more unclear as increasing uncertainties are introduced.

#### 2.9. Chapter Summary

To conclude, nine distinctly different methods were identified by the review process, two of which (inverse auger and discharge analysis) have been deemed the least suitable for deployment within a dryland environment, due to being inappropriate for the complexity of

the environment. The most suitable method for fieldwork application is therefore the tension and mini disk infiltrometers due to their minimal water consumption, small size, and ability for multiple use in the same location, providing increasingly reliable data. However, if possible, this method should be used in conjunction with others, such as rainfall simulation (digital or in the field) or monitoring. This would provide a wider array of information for future analysis. Overland flow is also barely considered when discussing infiltration, despite having a large role in the erosivity of soil, due to flow concentrations in microtopographic hollows. Overland flow needs to be integrated into a new infiltration measure to enable a better quantification of infiltration, erosivity and assessing the vulnerability of a semi-arid hillslope.

A new measuring technique is required, one which incorporates stone fragments and their position as well as roughness, vegetation cover and infiltration from overland flow, whilst being able to be used on any slope and keeping water consumption to a minimum.

### 3. A New Methodology

As identified in Chapter 2, devising a new method for measuring infiltration and overland flow in the dryland environment is required. This technique must be able to quantify soil surface properties (cover of stone fragments and vegetation, roughness, texture), and information surrounding the slope as a whole (e.g. dip and aspect), whilst creating overland flow. It is also necessary that this method be both affordable, and as lightweight as possible, whilst using a small volume of water. By using an aggregate measure of infiltration and overland flow dynamics, rather than the traditional measuring of infiltration alone, a more natural hydrological response can be witnessed and analysed.

This chapter details the proposed new method for quantifying infiltration and overland flow in dryland environments (section 3.1). The methodology identifies multiple measurable variables; recognising both the influence of surface characteristics on overland flow and infiltration. Section 3.2 introduces and describes the field area where experimentation was performed, alongside experimental design and a summary of the experiments conducted. The workflow used in the field to capture data, combining both high- and low-tech techniques, is described in section 3.3. How this data was processed and prepared for analysis is then discussed in section 3.4, with a detailed workflow.

#### 3.1. The Infiltrator

The primary aim (alongside those identified in Chapter 1) of the new method is to produce data which is more representative of a dryland surface with as little surface damage as possible. This includes steeper slopes; something that most of the infiltration measurement methods identified in Chapter 2 omitted. Due to this, direct application of water vertically (e.g. a ring infiltrometer) was not suitable. The only infiltration measurement method which successfully incorporated the effect of stone cover was the rainfall simulator. The new method (referred to as 'the infiltrator' herein) uses a similar approach of applying water to the surface from a water reservoir, however, as overland flow rather than precipitation.

The infiltrator uses a set volume of water, which is introduced to the slope as overland flow to quantify runoff characteristics, and produce a proxy for infiltration via three-dimensional analysis of the runoff pattern and maximum flow length. Through analysis of produced runoff and variables on the slope such as cover, topography and angle, an estimation for infiltration can be established. The indirect method was chosen to prevent damage to the soil surface, and to ensure that more representative data is produced.

A planting trough with a capacity of six litres was used as a reservoir (Figure 3.1). This enables a variety of water volumes to be used as and where required. A trough was chosen over a bucket due to its width and the ability to effectively produce flow. This was favourable as a larger, and wider, surface area would be exposed to water, enabling the generation of more data for collection. A slit was cut into the reservoir trough to allow water to evenly flow out of the reservoir and distribute onto the ground. Consistent flow was ensured by a thin aluminium sheet, which was attached to the displacement gap. The aluminium also reduced the height between the displacement output and the soil surface to 10 cm, reducing any error that could result from a plunge pool effect. This was attained by evenly bending the aluminium sheet to a 45° angle, so that the angle of flow would remain equal.

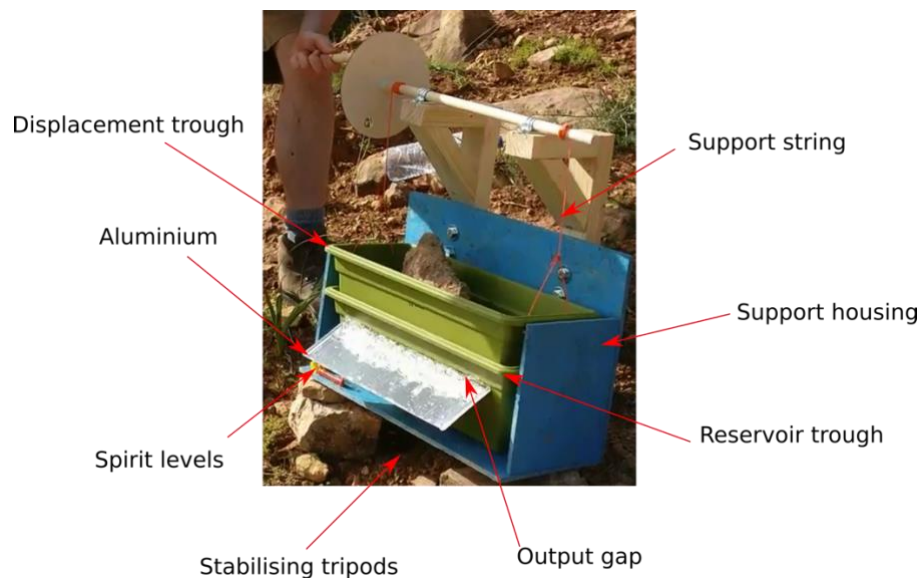


**Figure 3.1:** Annotated image of the infiltrator in the field

Displacement was achieved by inserting a second, identical trough into the first trough, which was forced at a constant rate into the reservoir for a set duration. The displacement flow rate can be adjusted based on experimental design, by either increasing or decreasing the displacement rate, to ensure displacement is accurately representative of a location's rainfall history.

To measure the distribution of the flow over the length of the output slit, five consecutive experiments were conducted by displacing 3,500 ml of water over a 10 second duration. The output was captured using four beakers and the volume of water was measured to account for discrepancies. The result of this experiment is shown in Figure 3.2. Experimentation reveals that output is typically  $\pm 5$  ml indicating a reliability of 1.5%.

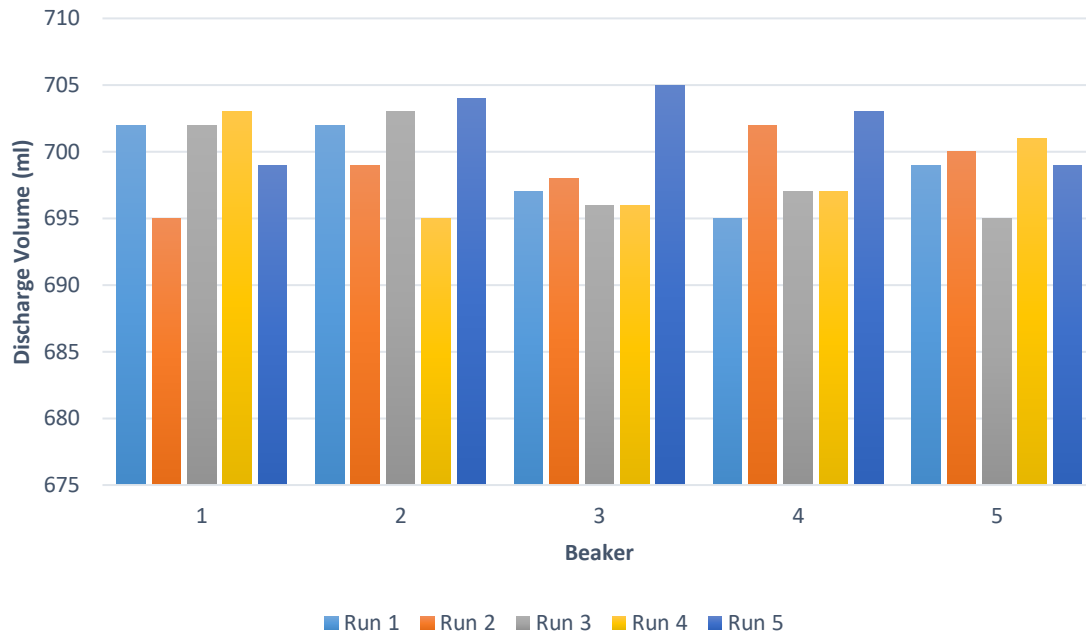


**Figure 3.2:** Results of distribution experiment

To ensure the infiltrator could remain horizontal on almost any surface, and provide even displacement, three flexible tripods were attached to the base of the device. Spirit levels in the X and Y directions were also affixed to the infiltrator, so that they could be used in conjunction with the tripods to ensure a stable level.

The housing for the reservoir is constructed from oriented strand board (OSB) due to its tensile strength, low weight and low cost. Combined with the planter trough, this device is low in weight and therefore can be carried in one hand with relative ease. Water used can be acquired from a nearby water source if available, reducing weight. The device can also be dismantled and reassembled for transportation making it highly flexible.

Prior to the creation of the infiltrator, 3D model prototypes were generated using Blender. These are illustrated in appendices i and ii.

### 3.1.1. Experimental Design

After locating an area representative of the slope profile, the device is positioned perpendicular to the steepest angle of slope. This was then stabilised with the use of the attached tripods and rocks sourced from the immediate vicinity ensuring that the device would remain horizontal throughout the duration of discharge. Discharge was achieved by displacing a set volume of water 2.5 L from the reservoir trough at a set rate ( $0.25 \text{ L s}^{-1}$ ) over a predefined duration (10 seconds). This is lower than as measured in the distribution experiment in section 3.1 to reduce water consumption. This enabled consistency

throughout each experiment and permits more reliable data analysis of measurements taken.

### 3.2. Field Area

To evaluate the effectiveness of the infiltrator and answer the research questions identified in Chapter 1, fieldwork was conducted in the area surrounding Salema, Portugal (Figures 3.3 and 3.4). Salema is located within the municipality of Vila do Bispo (Algarve district) where the recorded population in 2011 was 5,258 (Instituto Nacional de, 2012). The landscape is generally hilly, with bare slopes to fully vegetated ones. Towns are clustered close to the coast, with modern infrastructure connecting them.



**Figure 3.3:** Field site location with respect to Western Europe (1:10 000 000)



**Figure 3.4:** Images surrounding the Salema area

### 3.2.1. Catchment Characteristics

As described by Kottek *et al.* (2006), Salema and its surrounding areas are classified by a hot-summer Mediterranean climate (*Csa*). The criterion states that to be classed as *Csa* (warm temperate climate [C], steppe precipitation [s] and with dry summer [a]), the following:  $P_{smin} < P_{wmin}$ ,  $P_{wmax} > 3 P_{smin}$  and  $P_{smin} < 40 \text{ mm}$ ,  $T_{max} \geq 22^{\circ}\text{C}$ . Where  $P_{smin}$ ,  $P_{smax}$ ,  $P_{wmin}$  and  $P_{wmax}$  are the lowest and highest monthly precipitation values for summer and winter half-years for the given hemisphere (all in mm).  $T_{max}$  represents the maximum average temperatures in the warmest months.

Annual and monthly temperatures show that the maximum annual temperature in the area reaches  $\geq 22^{\circ}\text{C}$  (however temperatures can exceed this during the summer), as illustrated in Figure 3.5; weather station data from Faro and Sagres (nearby cities to the field site, within 80 km and 12 km respectively).

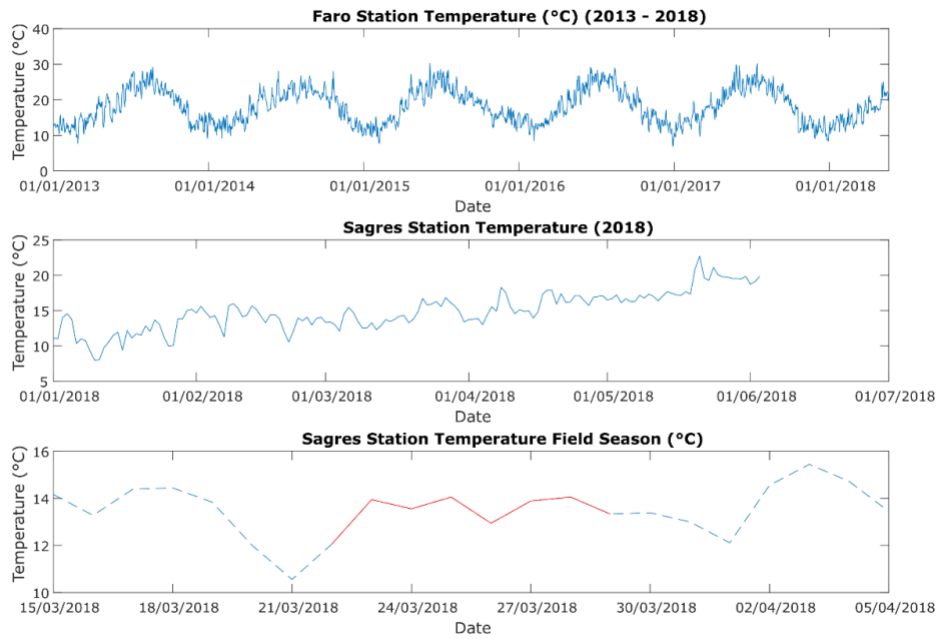


**Figure 3.5:** Weather station data from Faro and Sagres: a) Daily temperature variations in Faro since 2013, b) Temperature increase in Sagres every other day since January 2018, and c) Daily temperature values close to the field season (dashed = not season, red = in the field) (NOAA, 2018)

Rainfall data collected in Sagres since 1973, with the exception of some years due to missing data, indicates that rainfall is highly variable and has averaged 479.36 mm over the past 45 years. It can be seen, in Figure 3.6, that some years such as 1985, 1987, 1988 and 1989 experienced double the depth of precipitation when compared to other years. This places the environment at risk for high intensity flooding and land degradation if not appropriately managed.

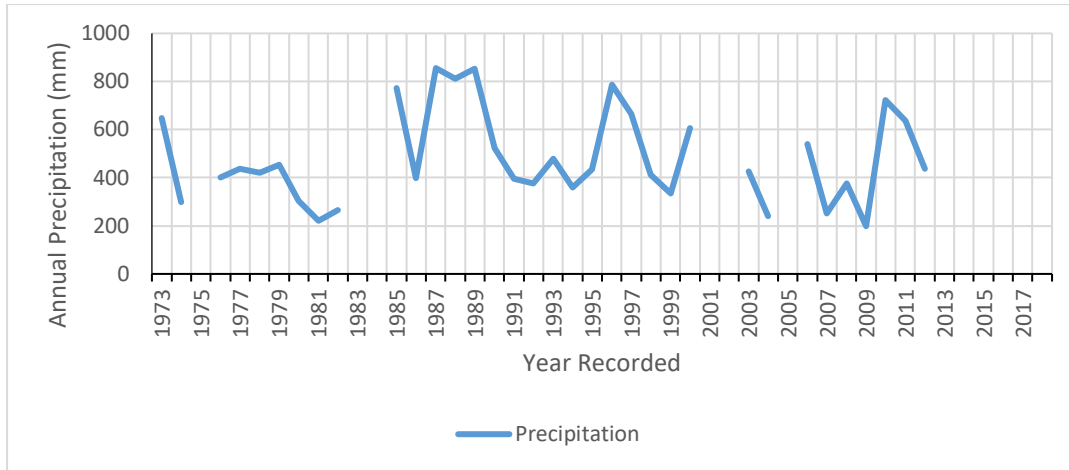


**Figure 3.6:** Precipitation data recorded in Sagres, Portugal (TuTiempo, 2018a; b). N.B. Gaps represent missing data.

### 3.2.2. Experimental Locations

Five main locations were identified for experimentation; their relative locations are displayed in Figure 3.7. Representative images of these locations can also be viewed in Figures 3.8 and 3.9. The locations were chosen based on representing multiple types of surfaces; including rilled landscapes to more vegetated ones, with varying gradients and percentages of surface cover.

To ensure consistency across every experiment in different locations, the requirements for experimental area were stringent. Firstly, slopes were required to be consistent cross-slope and downslope to enable multiple experiments in the same location and so experiments could be reproduced without having to wait for the infiltrated soil to dry, improving efficiency. The infiltrator needed to remain stable throughout the duration of the experiment, and there needed to be sufficient downslope runoff distance to ensure runoff would not reach the base of the slope. Following this, the measurement protocol identified in section 3.1.1 was utilised.

The majority of slopes experimented upon have a southerly aspect, represented in Figure 3.10 and had different degrees of roughness identified by eye in the field (see section 3.3.1). Ensuring a range of surface roughness conditions were sampled enables slope characteristics to be further investigated in Chapter 4 for research question 2.

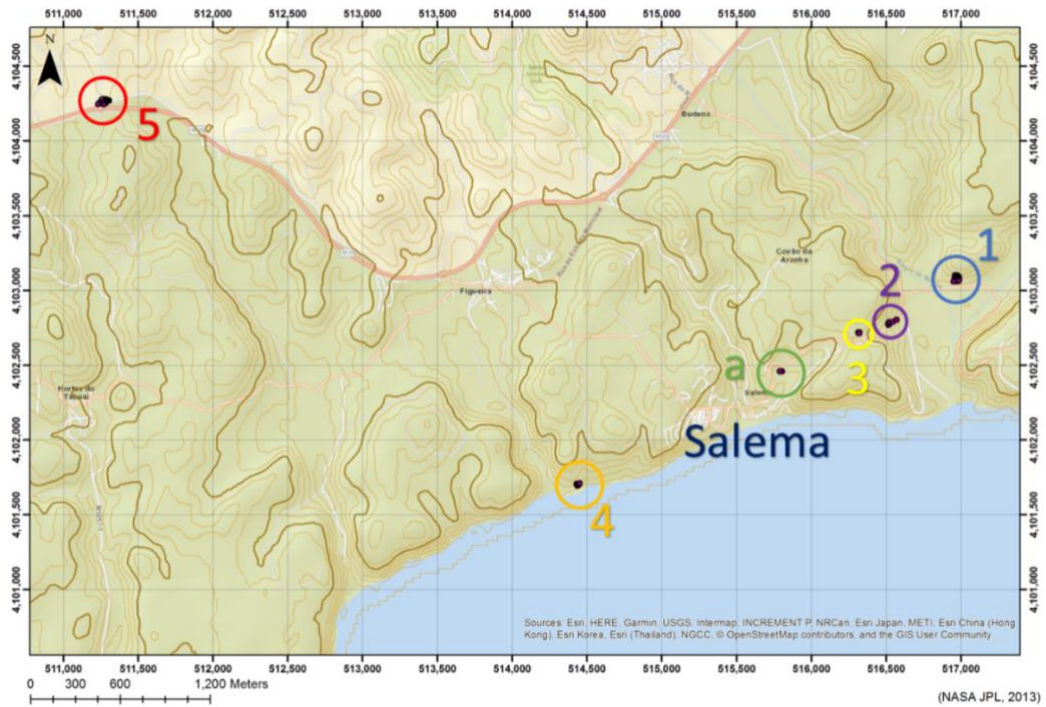


**Figure 3.7:** Topographic map of Salema, Portugal (1:24 000). Experimental locations with respect to Salema, Portugal. Locations have distinct characteristics: a) Test location to assess device effectiveness – no data collected. Characteristics are described in Table 3.1.

Location	Mean Gradient (°)	Mean Aspect (°)	Vegetation Cover	Embedded Stones	Stones Ontop	Estimated Roughness (1-10)
1	24	181	14%	14%	12%	4
2	20	123	10%	26%	19%	4
3	22	128	35%	8%	11%	4
4	11	123	9%	49%	20%	3.5
5	28	208	18%	1%	0.2%	1.5
(5a)	34	182	21%	16%	0.8%	1.5
(5b)	20	257	10%	1.5%	0.4%	1.7
(5c)	35	145	36%	0.35%	0%	1.2

**Table 3.1:** Average descriptive characteristics for experimental locations 1-5. N.B. Location 5 is split into sub-locations due to cover and slope differences in the same location.

Slopes were selected based on the continuous nature of cover and surface characteristics (e.g. roughness). This enabled experiments to be repeated with little variation between characteristics at each location. The locations are different however, allowing various slope and cover properties to be examined and analysed.

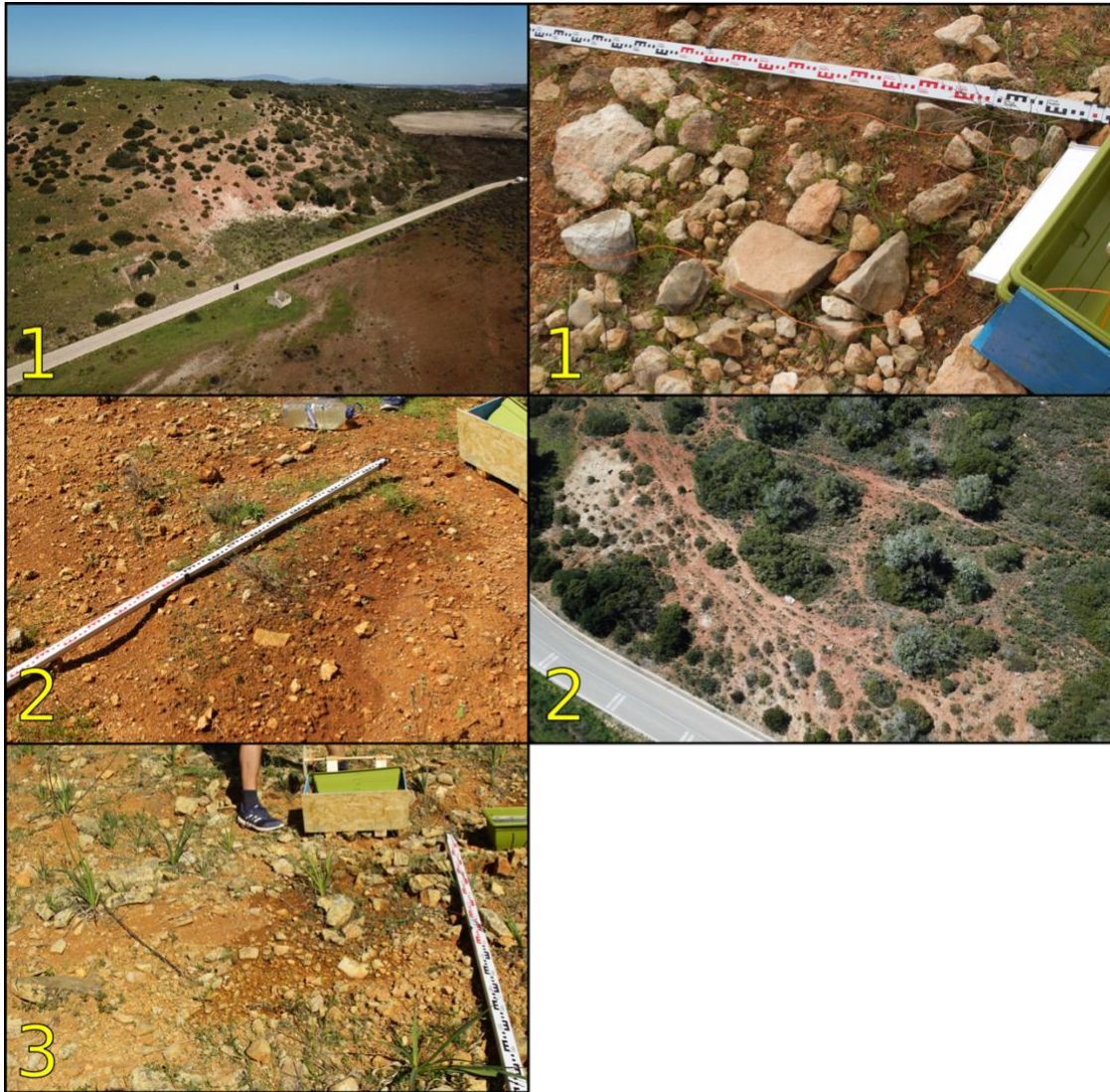


**Figure 3.8:** Images of surfaces 1 – 3 including two aerial images of slopes 1 and 2. Location references refer back to Figure 3.7 and Table 3.1.

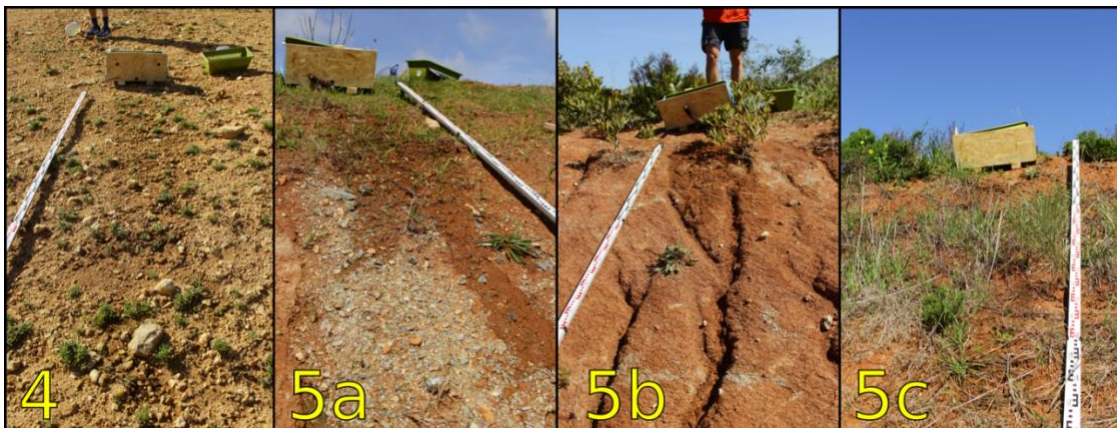


**Figure 3.9:** Surfaces 4 – 5c, location references refer back to Figure 3.7 and Table 3.1

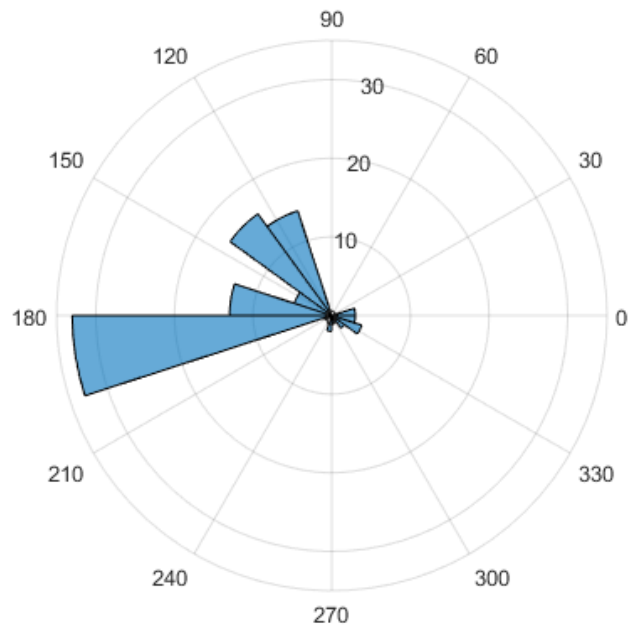


**Figure 3.10:** Polar Histogram of aspect data of experimental slopes in Salema, Portugal. N = 98

The aspect of experimental slopes (Figure 3.10) highlights that they are fairly constant with slopes mainly facing 175° (south).

### 3.2.3. Summary of Experiments

100 experimental runs were conducted over six days (23/03/18 – 28/03/18) between the hours of 8:00 and 18:00. Time taken for set up and experimentation per run was dependent on the stability of the slope (a function of the slope texture, particle content and slope gradient) for measuring variables and capturing images. This resulted in the total experimental time including set up, measuring variables and transportation along the slope ranging between 10 and 30 minutes. Actual time to maximum runoff took a minimum of 17 seconds, a maximum of 105 seconds, and an average time of 38.5 seconds.

### 3.3. Data Capture

This section describes exactly how each variable was measured and is divided into two sections; section 3.3.1 (field variables) includes everything that could be measured or estimated in the field, whilst section 3.3.2 (GIS-based data capture) explains how advanced techniques were used to capture more accurate data which were digitised and analysed after the field season.

### 3.3.1. Field Variables

There are four key groups of variables of continuous data which can be measured in the field. The infiltrator enables flow that can spread over a wide area, allowing the measurement of the following concomitantly over a meaningful representative area. Firstly, **slope properties**: dip, dip direction, placement of the device on the slope and a short slope description (e.g. a concave rilled slope). Dip and dip direction provide data for analysis towards establishing flow concentration controls (RQ2).

**Soil characteristics** were also obtained prior to experimentation. This includes a description of the soil texture and particle distribution to identify how changes in these can influence runoff (RQ2). Grain size distribution of the soil was identified using a hand lens and recorded according to the Phi grain size chart (Wentworth, 1922). Dip and aspect were obtained by eye using a compass clinometer with the correctly adjusted declination ( $-2^\circ$ ), accounting for the variation between true north and magnetic north in the field site (Magnetic-Declination, 2018). Moisture was also estimated on a scale (0-10, where 0 is devoid of moisture and 10 is fully saturated) to account for any variation in weather across field days. Finally, **stone and vegetation cover** was calculated digitally from orthophotographs as a percentage of the wetted area to gain a better understanding of their influences on runoff, concentration and slopes where the different covers are more abundant (RQs 1 and 2).

**Runoff properties** were captured following experimentation by measuring the wetted perimeter of the area, as well as maximum runoff length and time to reach this length (see Figure 3.11). The wetted perimeter was outlined with the use of brightly coloured string; facilitating the later digitisation of the runoff pattern by making the wetted perimeter easier to identify due to the bright colour. Wetted area was calculated via digitisation, similarly to cover. The maximum and minimum widths were also measured, alongside widths across the entire length of runoff over 25 cm intervals. This enables quantified concentration (based on length to maximum runoff,  $L_{max}$ , and minimum runoff width,  $W_{min}$ ) to be extracted. Measuring runoff provides data required for RQ1 and RQ2.

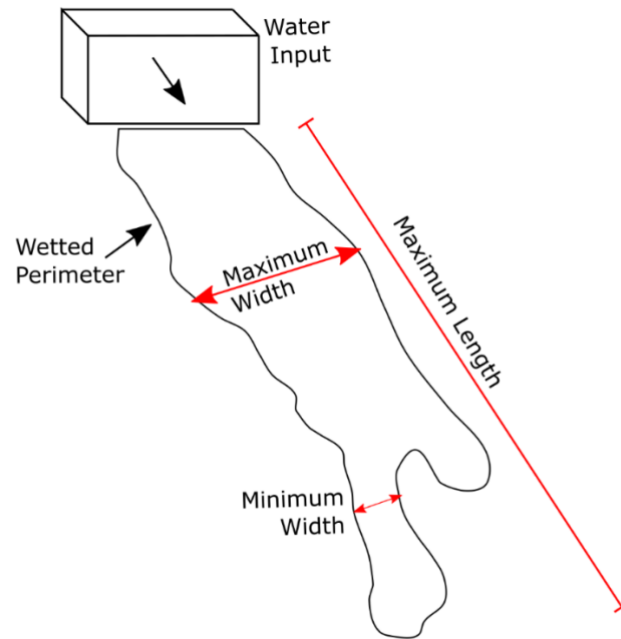


**Figure 3.11:** Schematic diagram of runoff variables to measure (not to scale)

The only variable not measured in the field was wetted area, due to the impracticality of calculating the area of complex irregular shapes that would form following runoff.

### 3.3.2. Spatial Analyses

To obtain more accurate data, spatial analysis for certain variables vital to the research questions is required. These variables are specifically stone cover, vegetation cover, wetted perimeter, wetted area, roughness and maximum runoff length.

There are different techniques for capturing the shape and/or topographic form of a subject (in this case a soil surface). This can include single image photography, satellite (or aerial) imagery, photogrammetry and terrestrial laser scanning (TLS). Single image photography is unsuitable due to the difficulty of raising a high-resolution camera above unstable slopes and taking a perpendicular image. This image also would not be evenly scaled across the extents of the image due to lens distortion. Satellite (or aerial) imagery is also unsuitable due to the infiltrator operating on the hillslope scale; image quality and cost does not justify using this method.

Terrestrial lasers scanners are LiDAR systems mounted on a static tripod which can generate a 3D point cloud of an area. This is done by a rotating scanner emitting light whilst a sensor measured the time taken for light to be reflected off a surface (Smith, 2015). TLS can also be used in conjunction with a digital camera to colour the point cloud. They can operate on

areas of varying scales from 1 – 1000 m (depending on model). TLS can achieve mm-scale precision; however TLS is limited in terms of movement and mobility. They can weigh in excess of 10 kg alongside auxiliary equipment (e.g. batteries, dGPS) and are also expensive (>£30,000). If an area is excluded from view due to topography or other features, the TLS must be moved to a different position to capture this, as well as to generate a navigable 3D point cloud (Smith and Vericat, 2015). This is a disadvantage, especially if time is a limitation.

Structure from Motion (SfM) is similar to TLS, where points are acquired from different viewpoints to construct a 3D model and minimise occlusions. Numerous authors have discussed the benefits and drawbacks of using SfM (Carrivick *et al.*, 2016; Chandler and Buckley, 2016; Westoby *et al.*, 2012), and its use versus terrestrial laser scanning. However, SfM with Multi-View Stereo (MVS) enables points to be extracted and point density increased (using photogrammetry algorithms) from camera imagery. SfM-MVS can be used on the  $10^2 \text{ m}^2$  to  $10^6 \text{ m}^2$  scales (Smith and Vericat, 2015) with mm scale accuracy. To implement SfM in the field, a high-resolution digital camera is required to capture images (normally at least 10) surrounding the subject. This results in a highly portable, quick method, which has comparable accuracy to that of the TLS. These images can then be processed post field season.

The advantages of using SfM in a dryland environment are that it is quick, effective and easier to use than a more traditional method (e.g. TLS) of capturing data. Using SfM is appropriate due to recording the infiltration overland flow measurements as simply and quickly as possible, without compromising on data quality. On the other hand, harsh sunlight and steep slopes make data capture more taxing as image quality is highly dependent on the weather. Overcast is ideal, however this is not a guarantee in a dryland environment.

Multiple high-resolution images (minimum 23, maximum 168 during experimentation, based on the size of the experimental plot) were captured at each experiment using a Canon 60D (18MP resolution) DSLR camera with a Canon EF 28-135 mm *f*/3.5-5.6 mm lens. Images were captured at a 28 mm focal length, which was set to remain constant throughout the field season. Normally, due to the wide focal length this would result in lens distortion; however, as the Canon 60D has a 1.6x APS-C crop sensor, lens distortion is mitigated (March, 2018). The crop sensor results in effective focal length (focal length multiplied by crop factor) being 44.8mm (O'Connor *et al.*, 2017). Images were captured from different perspectives surrounding the experimental plot, enabling a 3D point cloud to be created with minimal occlusions. An adjustable 5 m measuring staff was placed next to the runoff plot which was

then scaled in a local coordinate system within Agisoft PhotoScan (see Figure 3.12 for workflow).

After images were imported into Agisoft PhotoScan, they underwent pairwise matching at the highest accuracy to ensure as many matches as possible were identified. This generated a sparse point cloud which was assessed visually to identify if any errors (such as mismatched points) had occurred. Following this, a dense point cloud was generated on medium accuracy; increasing processing time substantially. If the dense cloud generation was successful, images were georeferenced to a local coordinate system. Images were not fully georeferenced to a projected coordinated system (e.g. UTM Zone 29N) due to the small scale of the plots, the lack of high resolution dGPS, and the requirement of a rapid field technique that can be replicated multiple times. A local co-ordinate system was sufficient for the purposes of these experiments.

Following the manual georeferencing, the dense point cloud was exported as an XYZ file (.txt) for roughness analysis. The dense cloud underwent mesh surface generation to enable the building of an orthorectified mosaic image for use in ArcGIS (section 3.4).

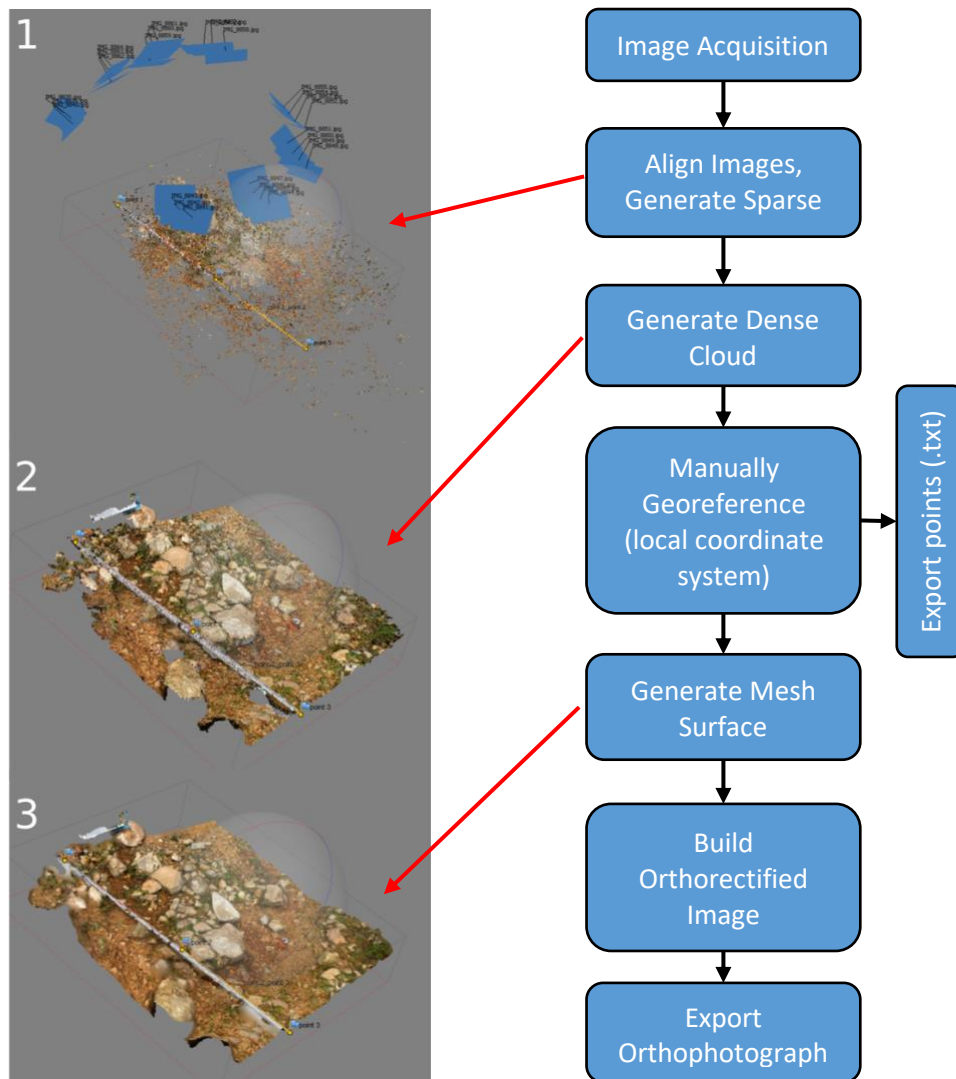


**Figure 3.12:** SfM workflow including examples of main stages (experiment 25)

### 3.4. Data Processing

Following the SfM workflow and detrending the surface, the orthophotograph produced for each experiment was then digitised manually in ArcMap (10.4) and analysed using the Spatial Analysis toolbox. This is detailed in section 3.4.1. For roughness, XYZ point clouds were imported into CloudCompare for analysis (section 3.4.2).

#### 3.4.1. Surface Cover

Following importing each experimental orthophotograph into ArcMap (after an automated environment setup Python script, see appendix iii); the wetted perimeter was first digitised using the create features polygon tool. This established the area where vegetation and stones could be identified. Vegetation was identified and outlined using the same method as the wetted area. Determining whether stones were resting on the surface or embedded was

conducted based on field notes, the 3D model and individual images used in the generation of the 3D model. Maximum runoff length was calculated using the 'measure' tool and recorded to identify any differences between the field measurements and digital measurements. After the classification of surface cover, a second Python script (appendix iv) was implemented to automatically eliminate any identified cover that was outside of the wetted area. The polygons in their classes were then merged, and the total area was calculated in m<sup>2</sup>. The area of each class was then calculated as a percentage of the total runoff area. Each of the three classes were calculated independently of one another, as vegetation can cover stones resting on the surface, and embedded stones can be covered by other stones. Figure 3.13 shows an example of a classified orthophotograph.

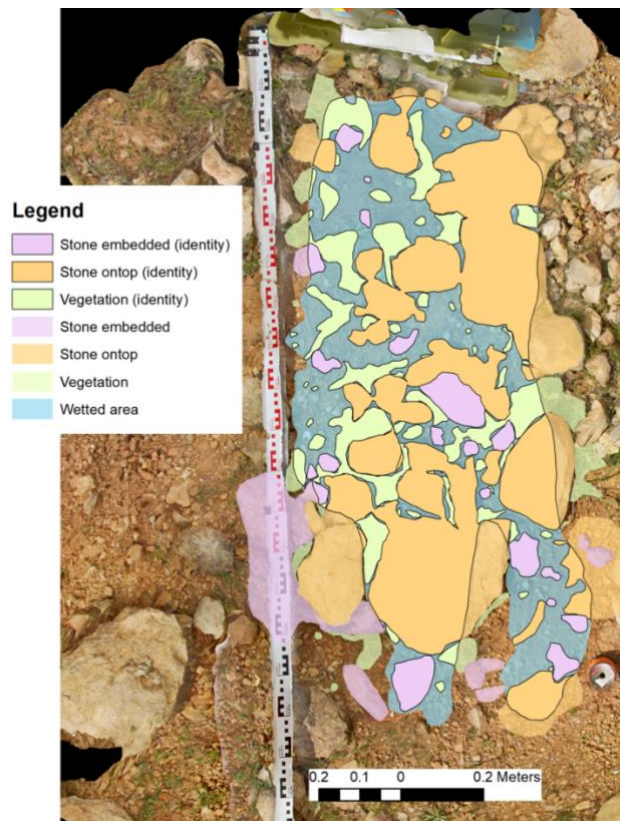


**Figure 3.13:** Experimental run 25 classified orthophotograph

#### 3.4.2. Roughness

CloudCompare was used to obtain roughness measurements from the dense point cloud generated via SfM-MVS. As the point clouds are quite large (between  $\sim 2.7 \times 10^6$  and  $\sim 1.2 \times 10^7$  points), the clouds were first cropped to only include the wetted area. Prior to roughness calculations, the point cloud was detrended by removing errors (detached points) as a result of vegetation or poor reconstruction.

Following detrending, the point cloud underwent level eight octree resampling to remove bias and distribute the points more evenly across the extent of the point cloud, as well as reducing the total processing time by 1,200%. This resampling reduced the influence of areas which had a higher or lower point density and reduced error as a result of occluded areas. Any anomalous data points generated by vegetation or alignment errors were then removed from the point cloud manually; preventing incorrect roughness interpretations by the software.

Figure 3.14 shows the point cloud within CloudCompare. Images 1a and 1b show the full colour point cloud (side and plan view respectively) prior to octree sampling. 2a and 2b show the same full colour point cloud after octree sampling.

Roughness was calculated within CloudCompare with a 50 mm kernel size to encompass any larger rock fragments and is computed by calculating the distance of a point to a plane fitted to its nearest neighbours within the kernel. This distance is represented by colour in Figure 3.14 (3a, 3b – prior to octree sampling, and 4a and 4b – after octree sampling), where red represents a greater distance and blue a shorter distance.

This process was fully automated with the use of the command line interface found within CloudCompare (see appendix v).

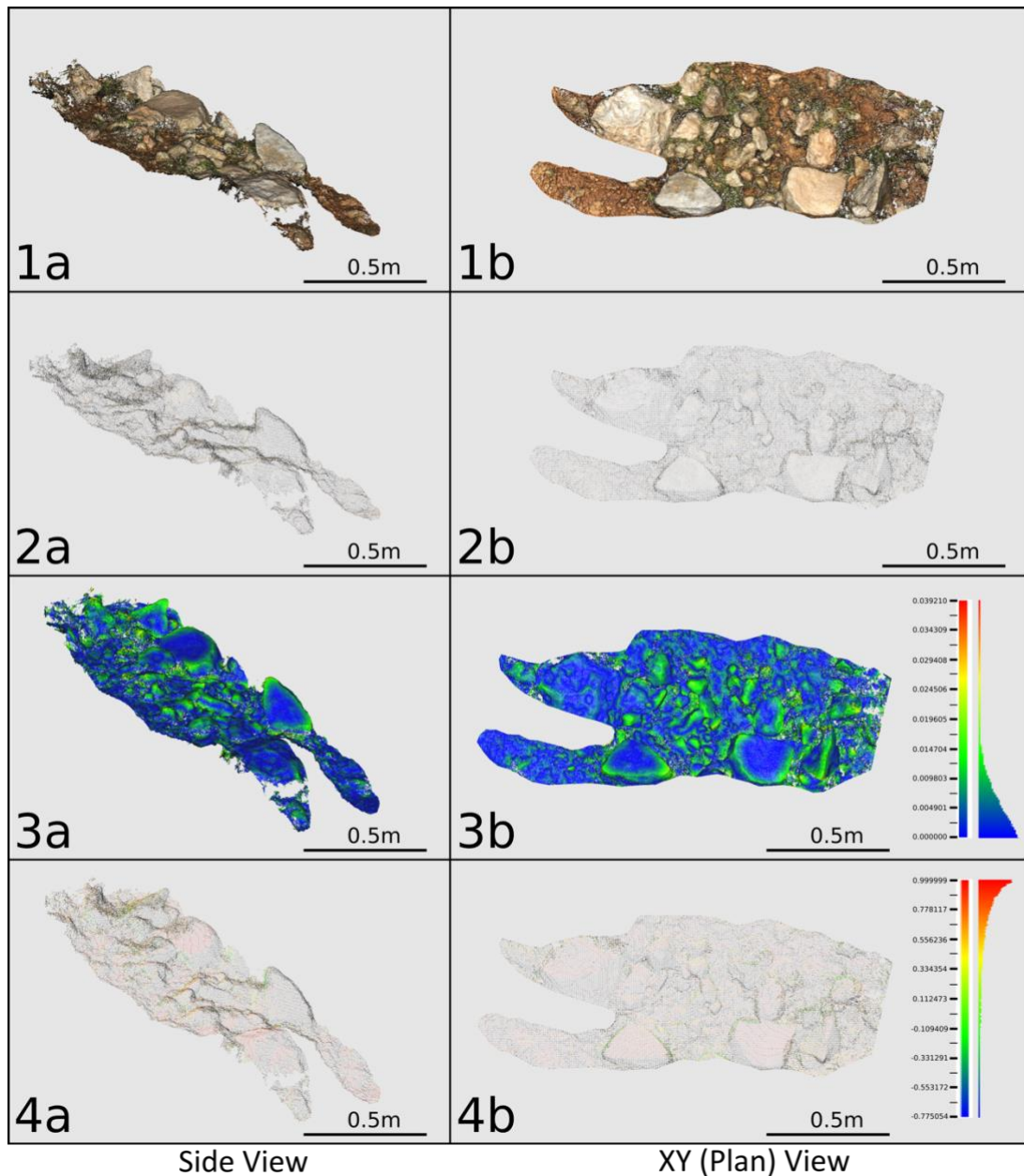


**Figure 3.14:** Wetted area of point cloud visualised in CloudCompare. 1 and 2 represent the point cloud in RGB before and after octree sampling. N.B. panel 2 appears monochrome due to the low point density following octree sampling. 3 and 4 represent the point cloud in the roughness scalar field before and after octree sampling. Experiment used: 25.

### 3.5. Chapter Summary

It had been identified in Chapter 2 that there is a need for a different method for obtaining data regarding overland flow and infiltration to combat the variability of the dryland environment. By conducting a critical analysis of existing methods, it was identified that none were truly suitable for the dryland environment when there are stony soils and high percentages of vegetative cover, unless mobility, cost and water availability were no issue.

The new suggested method can be used on all slopes with the exception of those which are remarkably steep ( $>40^\circ$ ), and accounts for the variability present in the surfaces. The method also allows for 'quick-fire' data collection with the ability to collect data from many variables following one experiment and hence can be repeated over a variety of surfaces and be more representative. This device was used in the field in the area surrounding Salema, Portugal, where surface characteristics were analysed and recorded for further analysis.

## 4. Results

This chapter presents the results of field experimentation described in chapter 3, in relation to both the use of the infiltrometer, and the research questions proposed in chapter 1:

- ❖ **RQ1: How does surface vegetation, stone cover and the position of stones with respect to the soil influence surface runoff?**
- ❖ **RQ2: What are the main soil surface controls on flow concentration?**

Research questions are addressed using the measurements of four different dimensions of surface runoff (flow metrics); maximum extent of runoff downstream ( $L_{max}$ ), minimum runoff width ( $W_{min}$ ), maximum runoff width ( $W_{max}$ ) and time to  $L_{max}$  ( $tL_{max}$ ). There is no single parameter that can solely quantify runoff or flow concentration, as  $L_{max}$  (for example) will be affected by both infiltration and flow hydraulics. By combining  $L_{max}$  and  $W_{min}$  flow concentration can be quantified; with the additions of  $W_{max}$  and  $tL_{max}$ , runoff is represented more thoroughly.

### 4.1. Using the infiltrator in the dryland environment

A total of 100 experimental runs were conducted across five different slopes, with experimentation time varying between 10 and 30 minutes. The average experiment time (time for water to reach the furthest extent downslope) was 38 seconds. The infiltrator was successfully used on slopes from 10° to 39° (average slope 14°). Experimentation was conducted on slopes which were bare (no surface cover) to slopes with up to 79% vegetation cover, 93% stones embedded in the surface, and 83% with surface resting stones. However, cover was much lower across all slopes, with vegetation, embedded stones and surface stones averaging 15%, 14% and 10% respectively.

Of the 100 experiments conducted, 64 were successfully reconstructed in 3D and digitised from an orthophotograph (Figure 4.1). Reconstruction failures were due to poor alignment on some surfaces due to harsh shadows and rapidly changing weather conditions.

In using the device, there were no restrictions on where experiments could occur; however, it proved difficult locating slopes that were completely bare (no cover). Overall, the infiltrator was used on all available surfaces, enabling better representation of the environment.

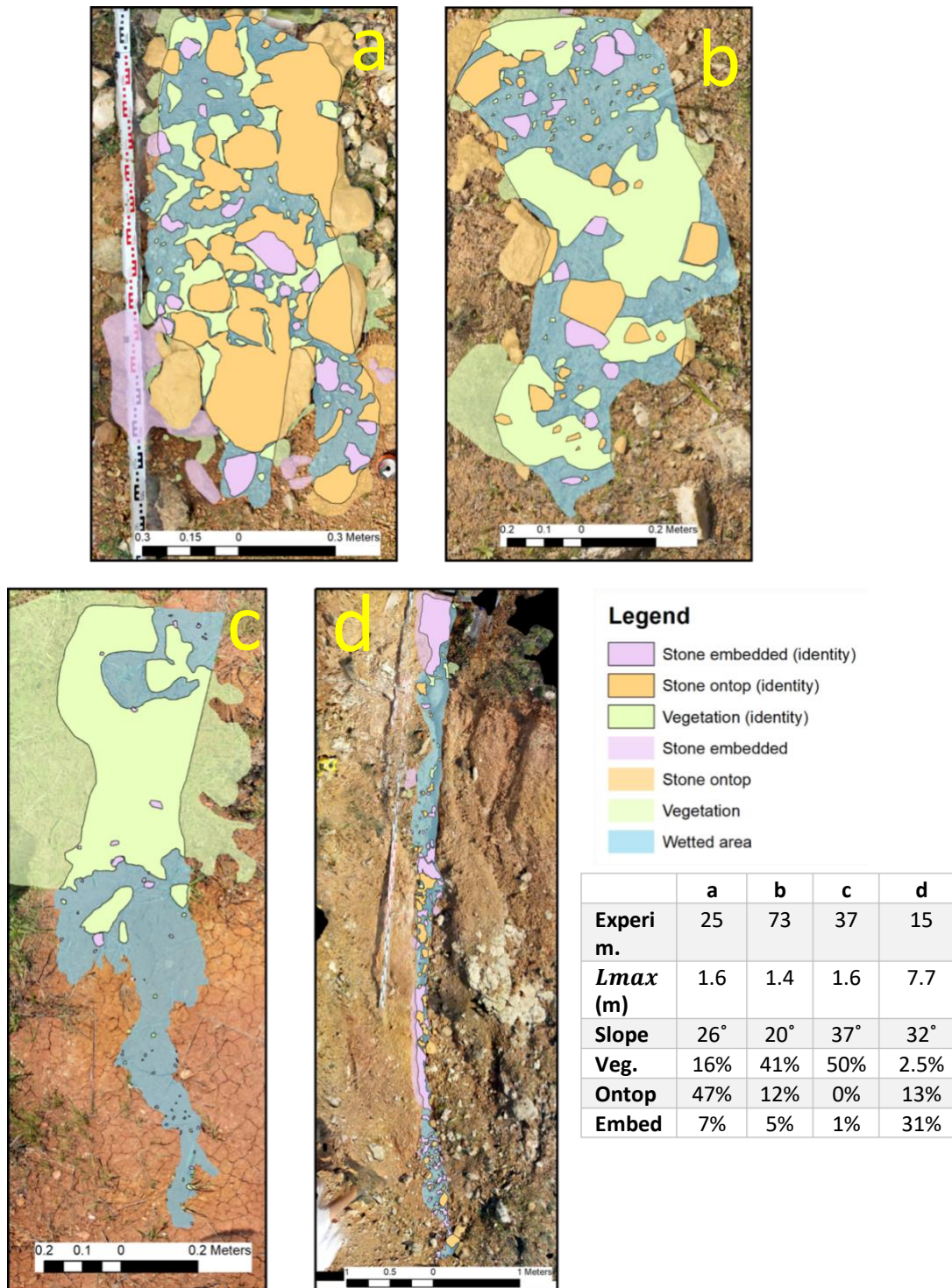


**Figure 4.1:** Sample of classified orthophotographs. Wetted area represents the runoff extents, stone embedded, stone ontop and vegetation are the different classifications of surface cover. Identity represents the cover that has been identified (by an automated script, appendix iv) as being within the wetted area.

- a Experiment 25 on a 26° surface with 16% vegetation cover, 47% surface stone cover and 7% embedded stone cover. Wetted area is dispersed with a maximum width of 63 cm and maximum length of 1.6 m.
- b Experiment 73 on a 20° slope with vegetation covering 41% of the surface, surface stones 12% and embedded stones 5%. The wetted area is disperse (58 cm) and  $L_{max}$  is shorter than experiment 25 at 1.4 m.
- c Experiment 37 on a slope of 37°, where 50% is covered by vegetation and 1% by embedded stone cover. At the top of the experiment the wetted area is consistent and disperse (46 cm) before concentrating towards the base.  $L_{max}$  is 1.6 m.
- d Experiment 15 on a 32° slope. Vegetation cover is minimal (2.5%), surface stones represent 13% of cover, and embedded stones 31%. The wetted area is concentrated ( $W_{max}$  37.5 cm) and elongate with an  $L_{max}$  of 7.7 m.

#### 4.2. The influence of surface cover on runoff

Runoff was characterised as described in Chapter 3 (section 3.3.1). Cover has also been defined as the percentage of wetted area covered by either embedded stones, stones resting on the surface or vegetation. By performing multiple linear regression on the different aspects of cover, the significance of soil surface cover can be identified. All linear regression equations are provided in the notation shown in equation 4.

$$y = b_0 + b_1x_1 + b_2x_2 + \dots + b_nx_n + \varepsilon \quad (4)$$

Where  $y$  is the dependent variable;  $b_0$  is the value when all independent variables ( $x_1$  to  $x_n$ ) are equal to zero.  $b_1$  to  $b_n$  are the estimated regression coefficients, and  $\varepsilon$  represents the error. Prior to statistical analysis, experiments 15, 72 and 98 were removed due to not being able to reconstruct roughness in CloudCompare following octree resampling.

To ensure assumptions (linearity, homoscedasticity, independence and normality) of linear regression are met, regression diagnostics were performed to remove outliers prior to the interpretation of results. To identify outliers, four plots were created to assess the aforementioned assumptions. Any outliers were then removed, and the plots regenerated to assess the influence (if any) outliers had on the data. In the case of  $L_{max}$  (maximum extent of runoff downslope), stone and vegetative cover, removing residuals greater than two increased normality, linearity and homoscedasticity. Independence was tested by

plotting residuals against time recorded and recognising a lack of correlation ensuring that there is no clustering.

$L_{max}$  is significantly ( $p < 0.05$ ) influenced by vegetation ( $x_1$ ) and also by surface stone cover ( $x_2$ ) (Table 4.1). Increasing surface stone cover by  $\sim 53\%$  results in a decrease of approximately 1.8 m in maximum runoff length. This is also applicable to vegetation; where an 80% increase results in a  $\sim 3.4$  m decrease in runoff length (Figure 4.2). Stones embedded ( $p = 0.162$ ) did not have a statistically significant impact on the maximum runoff length.

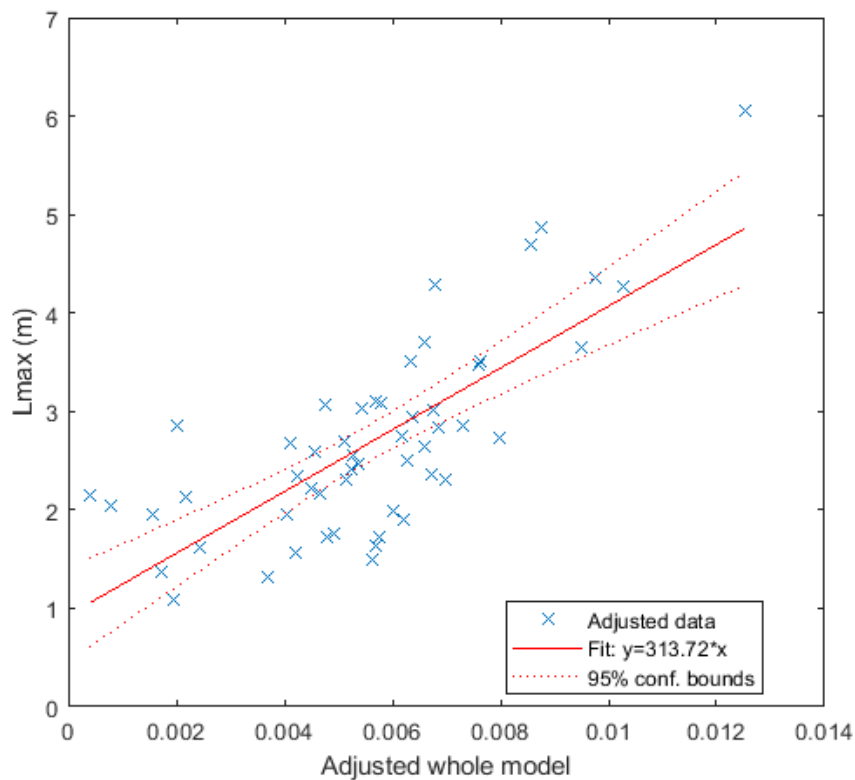


**Figure 4.2:** Multiple linear regression model for  $L_{max}$ , with the x axis variables being cover (vegetation and surface stones), average roughness and slope angle. Dashed line represents the 95% confidence limits.  $N = 53$ .

The multiple linear regression (Figure 4.2) equation (5):

$$L_{max} = 0.93114 - 4.2295 \times x_1 - 2.5941 \times x_2 + 313.68 \times x_3 + 0.047859 \times x_4 + 0.675 \quad (5)$$

This model produces a  $p$  value of  $2.19e-08$ ,  $r^2$  0.571 with 48 degrees of freedom. Correlation coefficients are listed in Table 4.1. Outliers were residuals greater than one (experiments 2, 10, 27, 28, 38, 41, 56 and 58) which were removed.

	Estimate	SE	tStat	pValue
<b>(Intercept)</b>	0.93114	0.39919	2.3326	0.024
<b>Vegetation (<math>x_1</math>)</b>	-4.2295	0.66971	-6.3154	<0.001
<b>Surface Stones (<math>x_2</math>)</b>	-2.5941	0.76029	-3.4119	0.001
<b>Average Roughness (<math>x_3</math>)</b>	313.68	87.528	3.5838	<0.001
<b>Angle of Slope (<math>x_4</math>)</b>	0.047859	0.015248	3.1387	0.003

**Table 4.1:** Linear regression model estimated coefficients for  $Lmax$ ,  $x_1$  through to  $x_4$  presented in Figure 4.2.

$Wmax$  (maximum runoff width) was also analysed. When  $Wmax$  is plotted on the  $y$  axis, regression diagnostics resulted in residuals greater than 13 being removed to ensure normality and remove outliers. Outliers removed include experiments 5, 10, 13, 14, 19, 21, 23, 29, 30, 51 and 79.

When analysing runoff with respect to  $Wmax$  (Figure 4.3), it is also significantly ( $p < 0.05$ ) controlled by cover. Specifically, stones resting on the surface and embedded stones ( $x_1$  and  $x_2$  respectively) increase the maximum width when more cover is present. This is shown by a 35 cm increase in  $Wmax$  when surface stone cover is increased from 0% to 83.2%. An 18 cm  $Wmax$  increase also occurs if embedded stone cover is increased from 0% to 93.5%. Vegetation is statistically insignificant ( $p = 0.142$ ) in terms of maximum width according to the collected data.

The multiple linear regression produced the follow equation (6):

$$Wmax = 54.352 + 42.2 \times x_1 + 18.791 \times x_2 + 8.71 \quad (6)$$

to quantify  $Wmax$ . The model produces a  $p$  value of 4.64e-08,  $r^2$  0.513 with 47 degrees of freedom. Correlation coefficients are listed in Table 4.2.

	Estimate	SE	tStat	pValue
<b>(Intercept)</b>	54.352	1.6026	33.915	<0.001
<b>Surface Stones (<math>x_1</math>)</b>	42.2	7.6066	5.5478	<0.001
<b>Embedded Stones (<math>x_2</math>)</b>	18.791	3.5573	3.5573	<0.001

**Table 4.2:** Linear regression model estimated coefficients for  $Wmax$ ,  $x_1$  and  $x_2$ .

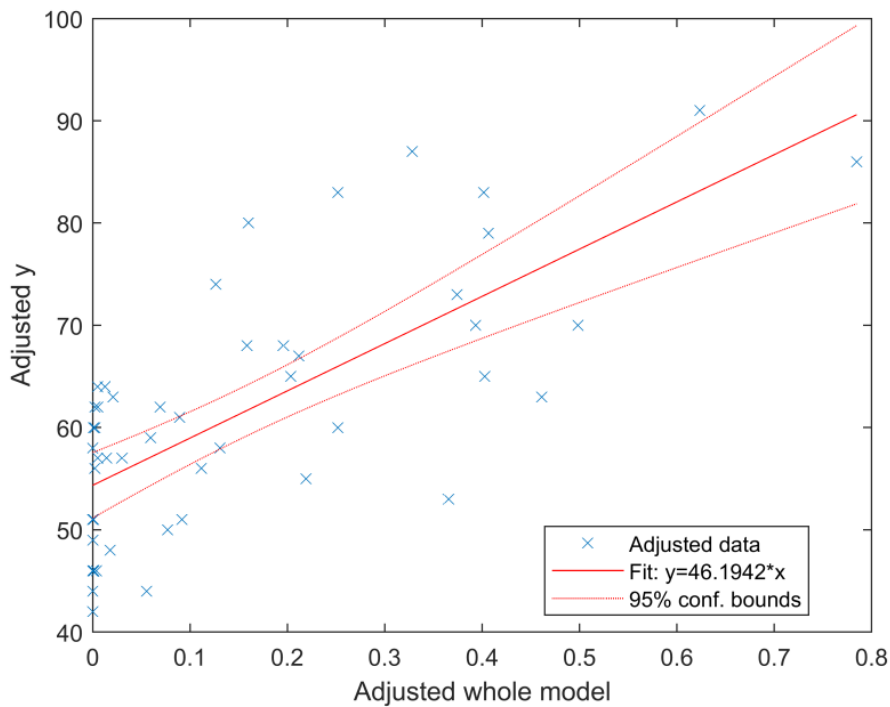


**Figure 4.3:** Adjusted multiple regression model where  $Wmax$  is plotted on the y axis, and  $X = x_1$  and  $x_2$ .  $N = 50$ .

Regression diagnostics when  $tLmax$  is plotted on the y axis resulted in residuals greater than 20 being removed to ensure normality and remove outliers. Outliers removed include experiments 6, 10, 12, 16 and 19. This reduces the number of points to 56.

Vegetation cover was removed from the multiple linear regression model due to being statistically insignificant ( $p = 0.541$ ).

Time to maximum runoff ( $tLmax$ ) increased by increasing both surface and embedded stone cover ( $x_1$  and  $x_2$  respectively); where an 83.2% increase in surface stone cover results in a 25 second increase to reach  $Lmax$ . Similarly, a higher percentage of embedded stone cover (93.5%) results in a predicted 19 second increase in  $tLmax$  (Figure 4.12).

The multiple linear regression produced the follow equation (7):

$$tLmax = 27.088 + 30.597 \times x_1 + 20.685 \times x_2 + 8.16 \quad (7)$$

to quantify  $tLmax$ . This model (Figure 4.4) produces a  $p$  value of  $1.34e-07$ ,  $r^2$  0.45 with 53 degrees of freedom. Correlation coefficients are listed in Table 4.3.

	Estimate	SE	tStat	pValue
<b>(Intercept)</b>	27.088	1.4362	18.861	<0.001
<b>Surface Stones (<math>x_1</math>)</b>	30.597	6.9467	4.4045	<0.001
<b>Embedded Stones (<math>x_2</math>)</b>	20.685	4.9189	4.2053	0.0001

**Table 4.3:** Linear regression model estimated coefficients for  $tLmax$ ,  $x_1$  and  $x_2$ .

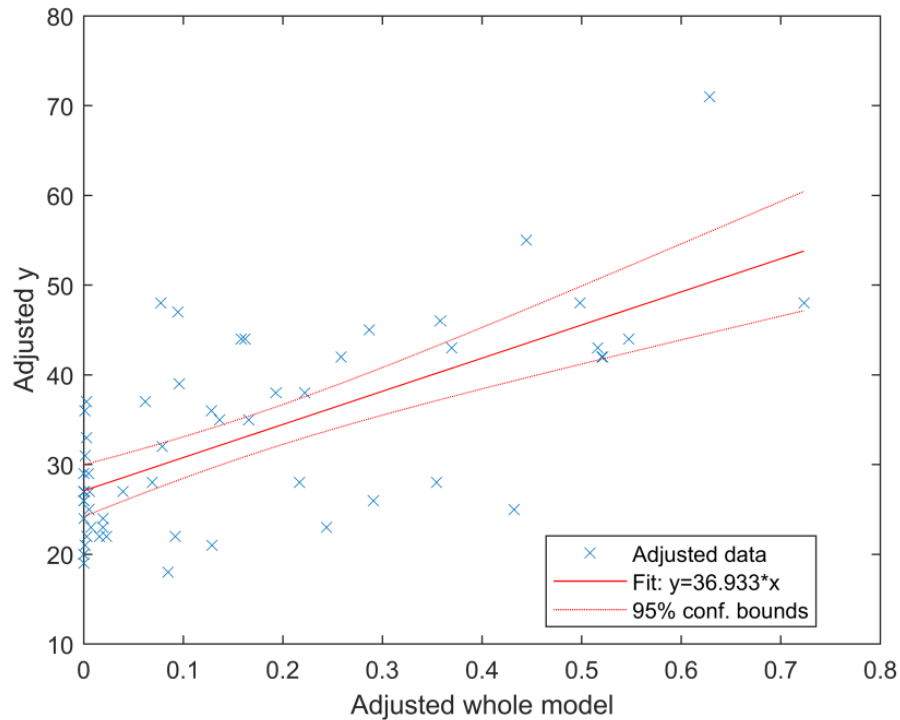


**Figure 4.4:** Multiple regression model where  $tLmax$  is plotted on the  $y$  axis,  $X$  is a combination of  $x_1$  and  $x_2$ .  $N = 56$ .

#### 4.3. Soil surface controls on flow concentration

Flow concentration is how concentrated overland flow becomes when applied to the surface. The degree of concentration has been quantified by establishing the minimum width of runoff and the maximum length of runoff. Runoff parameters have been statistically compared against cover (vegetation, surface stones and embedded stones), the average roughness of the slope (calculated in CloudCompare), the angle of the slope as well as the maximum and minimum grain size represented on the Phi scale (Wentworth, 1922).

$Wmin$  was investigated as a measure of flow concentration (Figure 4.5). Average roughness, slope angle and the upper particle size were statistically significant ( $p < 0.05$ ), indicating that the minimum concentration width is controlled by these variables. The percentage of embedded stone cover was significant to the 90% confidence limit ( $p < 0.1$ ), indicating that

this may be a minor control on concentration for  $Wmin$ . The following outliers are omitted from this regression model: Experiments 5, 7, 22, 23, 64, 74, 75 and 92 were removed due to residuals being greater than 5, ensuring regression assumptions were met.

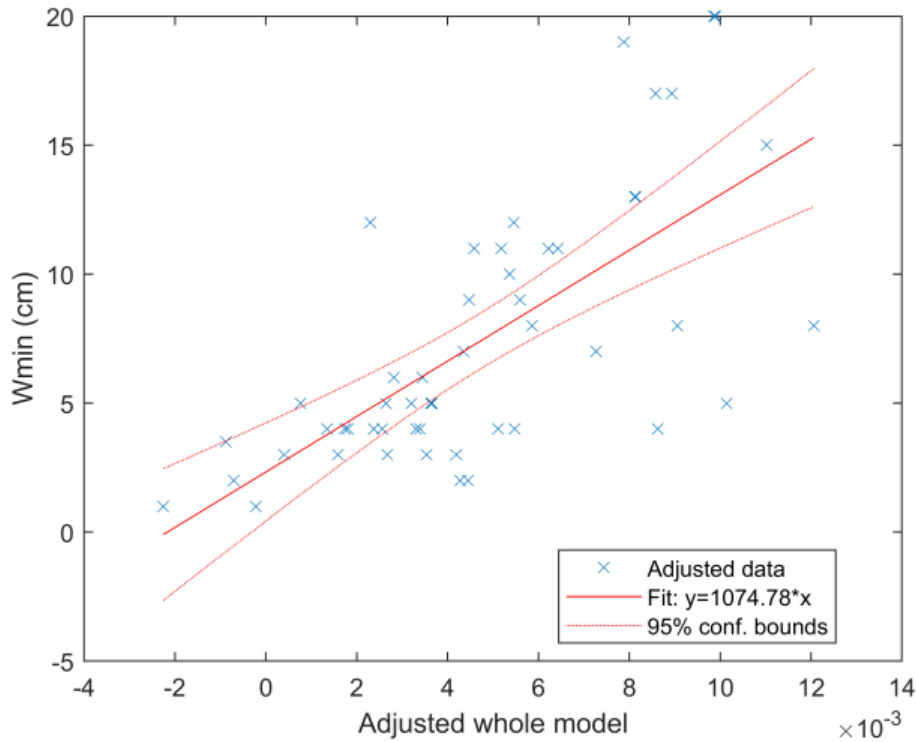


**Figure 4.5:** Multiple linear regression model for  $Wmin$ . Dashed line represents 95% confidence limits.  $N = 53$ .

The  $Wmin$  regression is quantified by the following equation (8):

$$Wmin = 2.332 - 4.6965 \times x_1 + 1074.8 \times x_2 - 0.27925 \times x_3 - 1.5843 \times x_4 + 3.84 \quad (8)$$

$Wmin$  regression has a  $p$  value of  $3.72e-06$ ,  $r^2$  0.479 with 46 degrees of freedom. Correlation coefficients are listed in Table 4.4.

	Estimate	SE	tStat	pValue
<b>(Intercept)</b>	2.332	2.7597	0.84502	0.402
<b>Embedded Stones (<math>x_1</math>)</b>	-4.6965	2.7513	-1.707	0.0946
<b>Average Roughness (<math>x_2</math>)</b>	1074.8	470.37	2.2849	0.0267
<b>Angle of Slope (<math>x_3</math>)</b>	-0.27925	0.095993	-2.9091	0.006
<b>Upper Particle Size (<math>x_4</math>)</b>	-1.5843	0.3678	-4.3076	<0.001

**Table 4.4:** Regression coefficients for Figure 4.5.

Increasing embedded stone cover by 93.5% results in a reduction of  $W_{min}$  by 4 cm, also by increasing slope angle there is a reduction of  $W_{min}$  by 8 cm. Decreasing the upper particle size (from boulder to gravel) has the most significant impact on  $W_{min}$ , decreasing the predicted minimum width by 11 cm. However, increasing average roughness results in a 7 cm increase in  $W_{min}$ .

The controls on flow concentration in relation to  $L_{max}$  are well constrained (Figure 4.2, Table 4.1), with vegetation and surface stone cover statistically significant ( $p < 0.05$ ), alongside average roughness (quantified in CloudCompare) and slope angle ( $p < 0.05$ ). The  $r^2$  value of this linear regression model is 0.571, with a  $p$  value of 2.19e-08. This suggests that although the stated variables don't fully account for  $L_{max}$ , they have a significant role in controlling the flow concentration down slope.

When vegetation increases (to 79%), and stone surface (to 53.5%) cover increases,  $L_{max}$  decreases by 3.4 m and 1.8 m respectively. Contrasting this, an increase in roughness and angle of slope results in a 2.1 m and 1.4 m increase in  $L_{max}$  (Figure 4.2).

Different runoff dimensions have varying controls.  $L_{max}$  is controlled mainly by vegetative cover, surface stone cover, roughness and the angle of slope. In comparison, the lateral dimensions ( $W_{min}$  and  $W_{max}$ ) are dictated by roughness, surface stone cover and the maximum particle size. Time to maximum runoff is mainly a function of stone cover, whether that be resting on the surface or embedded.

## 5. Discussion

### 5.1. The effectiveness of the infiltrator

As identified in Chapter 2 (section 2.8.2), the ideal properties of an instrument for measuring the factors affecting overland flow on dryland hillslopes should be capable of being deployed across a wide range of surface cover, soil, and slope types. The infiltrator does this whilst minimising water consumption, as well as remaining highly mobile. The infiltrator proved simple to use on slopes with varying levels of cover at steep angles; applying runoff to the surface was straightforward, with no user issues.

During the field trip, 100 experimental runs were conducted over a six-day period (Chapter 4, section 4.1). This illustrates the number of experiments that can be conducted in a finite duration, whilst considering equipment construction and data capture. The key issue experienced with experimentation was locating bare surfaces; 15% of runs had a total cover less than 5%, whilst only one surface (experiment 63) had a total amount of surface cover less than 1%. This, however, is a limitation of the field area and not of the infiltrator.

Use of the infiltrator was effective on a wide range of surfaces, as long as care was taken as not to disturb the soil beneath the device; something which the ring and tension infiltrometers require. Not disturbing the soil was an issue on slopes which were steep; loose soil made it difficult to navigate the wetted area without falling and damaging the runoff perimeter, resulting in an increase of time taken to complete the experimentation.

Ensuring the infiltrator runoff output was horizontal prior to experimentation became increasingly difficult due to the poor quality of the flexible tripods used. Following using the tripods for several runs, the plastic connector between the legs and the head of the tripod would shear making them unusable. To address this problem, stability was guaranteed by using locally sourced rocks beneath the four corners of the infiltrator, which although was more time consuming, provided a more solid platform.

Weather and surface morphology reduced the number of usable SfM models to 64 from the original 100. Bright sunlight created shadows across the experiment area, resulting in images not being able to display detail due to changes in exposure. This causes images to become unmatchable when undergoing the SfM workflow, as the SfM-MVS algorithm cannot identify matching points (Chapter 3, section 3.3.2). Ideally, overcast cloud is the optimum weather for SfM, with little to no wind. Deep and thin rills also caused problems, as the camera could

not capture enough data for pairwise matching and reconstruction; this resulted in a high level of occlusion in the base of the rills.

The scale of the experimental plots was an issue for georeferencing orthophotographs due to the accuracy of the GPS used; a consumer grade GPS system (Garmin eTrex 20; maximum accuracy of 3m in the field) rather than a more accurate dGPS. Due to the low accuracy, the Garmin device was only used to locate each experimental plot, and scaling was conducted in Agisoft PhotoScan using a visible scale bar. The more accurate dGPS would have enabled accurate georeferencing and mapping of the experimental runs in GIS; however this may have introduced more errors due to the small plot scale. This compromise was made to reduce cost, increase usability and decrease time required per experiment; resulting in orthophotographs being georeferenced within their own local reference system.

## 5.2. The relationship between surface cover and runoff

Upon interpretation of the multiple regression models presented in Chapter 4 (section 4.2), it is clear that cover, whether vegetative or stone, is an influential control of surface runoff. Surface stone cover is a significant control of all analysed dimensions of runoff ( $L_{max}$ ,  $W_{max}$  and  $tL_{max}$ ), presenting the largest impact to runoff (Chapter 4, section 4.2). Increasing surface stone cover results in a decrease in  $L_{max}$ , which is possibly caused by increased infiltration upslope. This is likely due to the stone 'protecting' underlying soil from sealing, resulting in the possibility for increased infiltration (Poesen, 1986). An increase in surface stone cover by 83.2% also increases  $W_{max}$  and  $tL_{max}$  at an average of 35 cm and 26 seconds respectively. Although runoff length is decreasing, stone cover causes the spreading and slowing of runoff, which indicates that higher infiltration rates reduce flow momentum downslope.

Experimentation has also revealed that increased embedded stone cover by 93.5% significantly increases  $W_{max}$  and  $tL_{max}$  by an average of 18 cm and 19 seconds. The permeability of stone typically is much lower than that of soil (Bear, 1972), resulting in little to no infiltration through the rock directly. This causes increased surface runoff and reduced infiltration. As well as this, sealing can occur around the perimeter of an embedded rock fragment via the deposition of finer particles during rainfall or overland flow, resulting in a lower overall permeability and increasing overland flow (Poesen and Ingelmo-Sanchez, 1992).  $W_{max}$  and  $tL_{max}$  are also affected by the hydraulics of the overland flow, which is in turn influenced by stone cover. To improve data surrounding stone cover, the classification

of different lithologies may influence runoff dimensions as suggested by Martínez-Hernández *et al.* (2017).

$L_{max}$  is also influenced by vegetation cover, with  $L_{max}$  on average increasing by 1.5 m with a 78% increase in vegetation cover. Similarly to surface stone cover, the vegetation intercepts rainfall, decreasing kinetic energy and reducing the likelihood of some surface seals forming (Peng *et al.*, 2004). However, vegetation type (annual or perennial) influences infiltration differently. Annual vegetation protects the soil surface from the kinetic energy of rainfall, reducing the probability of kinetic seals forming and increasing infiltration rates (Peng *et al.*, 2004). Increased infiltration however only occurs when the annual vegetation is beginning to form. As organic matter accumulates around the vegetation, the soil texture becomes tighter, and infiltration rates decrease (Pingping *et al.*, 2013). However, it has been noted that the stratification of organic matter can increase infiltration rates by up to 30% (Franzluebbers, 2002). Perennial vegetation decreases infiltration rates due to the formation of a micro biotic soil derived from high organic matter concentrations (Peng *et al.*, 2004). If the biotic layer is destroyed due to wildfires or exposure to the kinetic energy of rainfall, infiltration rates increase as the soil is now bare and unprotected (Pingping *et al.*, 2013).

To further develop knowledge into the influences of vegetation cover on runoff and infiltration, a more detailed study concerning vegetation patterns could be conducted and incorporated with existing data. This will allow for better understanding regarding how these patterns influence runoff dimensions, as the influence of patterns on erodibility well understood (Puigdefábregas, 2005). In addition to this, an assessment of vegetation type (whether it be annual or perennial, as well as plant physical structure) may enable a more detailed classification of dryland surfaces to again be incorporated into the regression model (Peng *et al.*, 2004; Pingping *et al.*, 2013).

### 5.3. Flow concentration and soil surface controls

To quantify concentration, the runoff dimensions  $L_{max}$  and  $W_{min}$  were used (Chapter 4, section 4.3). Vegetative and surface stone cover are two key controls for decreasing  $L_{max}$ , as identified in section 5.2. It is also found that an increase in average roughness (from 0.002 to 0.009) and slope angle by 27° results in increased  $L_{max}$  (2.1 m and 1.4 m respectively). When the surface is rougher, the likelihood of surface depressions being present is greater due to there being more variation across the surface profile. Surface depressions can detain overland flow and enable infiltration to occur, whilst increasing the connectivity of the surface as more overland flow is generated (Dunkerley, 2004b). If a surface is rougher, there

is a greater likelihood that flow will concentrate, represented by an increase in  $L_{max}$ . This enables flow to coalesce into a single, high velocity concentrated thread. Combined with a steeper slope angle, where less vertical infiltration can occur by up to 80% on bare soils (Morbidelli *et al.*, 2016), more erosive single flow threads can develop and flow becomes more concentrated. In comparison, flow becomes more spread out on flat, planar surfaces and is less concentrated.

$W_{min}$  is largely controlled by similar variables (average roughness and angle of slope) but also has other influences; the percentage of stone cover that is embedded, and the upper particle size of the soil. As expected, an increase in angle of slope by  $27^\circ$  results in a decrease in  $W_{min}$  by 8 cm. This is a result of the overland flow travelling further down the slope, and therefore flow is distributed less laterally. Similarly, when average roughness increases (from 0.002 to 0.009),  $W_{min}$  becomes larger by 7 cm. This is likely due to roughness partially controlling the connectivity of the slope, facilitating flow threading; a decrease in roughness enables the overland flow to concentrate more rapidly, resulting in greater channelization and decreasing slope connectivity. This occurs via the reduction of flow threads as the flow is less restricted by microtopography.

When embedded stone cover is greater, typically it is found that  $W_{min}$  decreases in both single and multi-threaded flows; experimentation shows a 93.5% increase in embedded cover results in a 4 cm decrease in  $W_{min}$ . This could be attributed to the movement of stone fragments within the soil; as plants, animals and humans may disrupt the surfaces, resulting in any existing surface characteristics, such as textural porosity and stone position, being altered (Poesen *et al.*, 1990; Poesen *et al.*, 1994). In response to the aforementioned factors, any change would alter the surface hydrological properties to no longer reflect natural conditions. Future research is required to better understand the influence of slope characteristics on  $W_{min}$ . The final identified control on  $W_{min}$  is upper particle size; when Phi size is decreased from -8 to -1,  $W_{min}$  responds by decreasing by an average of 11 cm. As flow is less constrained by particles that cannot be transported by the flow, it enables  $W_{min}$  to concentrate into a single flow thread and propagate further downslope.

#### 5.4. An aggregate measure for infiltration and overland flow conveyance

By using a non-direct approach, infiltration cannot be directly measured. However, by utilising data collected from induced overland flow and soil surface characteristics, an infiltration index can be developed through the relationship between  $L_{max}$  and  $W_{min}$ , an aggregate measure.

It is probable that there is greater infiltration on shallow slopes (Morbidelli *et al.*, 2016), with more vegetative cover and surface stone cover, indicated by  $L_{max}$  generally being shorter. It is also likely that on rougher slopes (those with a higher percentage of surface depressions in particular), infiltration is greater due to interim storage spaces for overland flow and precipitation. This further decreases overland flow resulting in the lower likelihood of flow coalescence and greater lateral distribution of runoff over the slope. Furthermore, slopes with less concentration (i.e. more disperse, shorter runoff) have a high probability of having greater rates of infiltration due to water exposure to a greater soil surface area. Equally, when the soil particles are larger, infiltration is likely to be greater as a result of more effective dispersal of overland flow, increasing the connectivity with other areas on the slope, whilst reducing concentration. With further study into the type of connectivity (structural or process based) witnessed on the slopes (Bracken *et al.*, 2013), the relationship between connectivity and flow concentration can be better understood and integrated with the findings from this study.

In comparison of the infiltrator to existing methods of infiltration measurement (direct or indirect), it is clear that for use on well-maintained land (e.g. agricultural) an infiltrometer, such as the ring or tension, produces data which is more accurate. However the infiltrator does more than measure infiltration and therefore the comparison between current measuring methods and the new one is not like for like. Using the infiltrator in rangelands enables a higher percentage of surfaces to be examined in a relatively quick and inexpensive manner, whilst remaining representative of the environment. Although further work is required to define and refine an infiltration overland flow index, the ratio of  $L_{max}:W_{max}$  can be used to directly compare surfaces.

### 5.5. Suggestions for further research

An investigation into improving the data collection in the field is required, mainly for capturing images for SfM for two reasons; firstly, to mitigate the impact of harsh shadows as a result of bright sunlight; and secondly, to improve the image capture process for the user on steep, unstable surfaces. Improving data capture would also enable further exploration of the relationship between roughness and flow concentration. Currently, this requires more data regarding flow concentration characteristics, especially the establishment of multi-threaded flows and how these vary over different surfaces. Combining with a more detailed study on embedded stone cover, such as differentiating between bedrock and their lithology as well as stone fragments would assist in advancing the understanding of the relationship

between cover and infiltration. In addition, the depth of the embedded stones and if there is any sealing as seen in Poesen *et al.* (1990), would further this research.

The classification of vegetation (e.g. annual or perennial, physical structure) would further the understanding of the influence of vegetative cover on runoff characteristics, concentration and using an infiltration index. Also, by using DEMs generated from SfM, numerical runoff modelling could be conducted to supplement the understanding of how runoff interacts with cover and other surface characteristics. This would also provide an assessment of the runoff which is generated from the infiltrator and assist in assessing the effectiveness of flood management methods in different locations by varying surface characteristics.

### 5.6. Wider Implications

The workflow presented throughout the thesis can be used to further inform research for example, by parameterising numerical models such as CRUM (Reaney *et al.*, 2007) or LAPSUS (Lesschen *et al.*, 2009), with data that is more representative of a given area. As well as this, a workflow that can be used globally enables the direct comparison of different localities to one another; rather than utilising a myriad of techniques. The characterisation of infiltration and overland flow presented uses a novel spatial data collection method, producing an aggregate measure of the two processes. This knowledge can be used to better inform both local and governmental land management policies including erosive and flood vulnerabilities; providing safety and conservation plans which can be tailored to specific areas based on similar case studies worldwide, improving upon methods which are currently available.

## 6. Conclusion

Methods for measuring infiltration are effective in drylands when the soil is well-maintained, shallow and free of stones and vegetation, however traditional methods typically don't always incorporate hydrological processes such as overland flow. As soils like this only represent 25% of the land use in drylands (Safriel, 2006), a new method was required to further understand infiltration. It was also noted in the introduction that, while infiltration affects overland flow in drylands, so does the microtopography of the soil surface because this can cause flow to become concentrated and more erosive or diffuse and less erosive. The novel infiltrator provides a solution for measuring infiltration and the degree to which overland flow can concentrate and diffuse, whilst remaining representative of surface cover without the requirement to alter it, nor any other surface properties. It performed well under a wide array of conditions, and successfully produced data from which further analysis could be conducted.

Relationships identified from the data analysis were generally expected; however, further field study is required to better understand the relationship between bare surfaces and hydrological process on steeper slopes; especially in relation to understanding flow concentration. The development of an infiltration index based on the combination of  $L_{max}$  and  $W_{min}$  would also enable the quantification of susceptibility of semi-arid hillslopes to overland flow and erosion; without the need to disturb the soil surface. In doing this, when combined with a quick and simple measurement process (i.e. capture slope characteristics, conduct experiment, capture runoff dimensions), the quantification of infiltration will enable better land use planning, alongside flood risk prediction and management in high risk areas.

The infiltrator has the potential for improvement with the use of higher-quality materials, although this would naturally increase production cost, as well as appropriate adjustments to the data capture workflow as suggested in Chapter 5 (section 5.5). In achieving this, an infiltration index can be established allowing drylands globally to be compared, and for flood prevention and management techniques to work more effectively.

The purpose of the new measurement method is the quantification of infiltration and overland flow on complex dryland hillslopes and low cost. This has been successfully achieved, whilst identifying an array of relationships between infiltration, surface runoff and surface characteristics. As well as this, the infiltrator method introduces a new technique for analysing infiltration and runoff on semi-arid hillslopes, whilst providing a ratio of overland flow and erosivity.

## 7. References

- Abrahams, A. D. and A. J. Parsons. 1994. Hydraulics of interrill overland flow on stone-covered desert surfaces. *Catena*, **23**(1-2), pp.111-140.
- Abrahams, A. D., A. J. Parsons and J. Wainwright. 1995. Effects of vegetation change on interrill runoff and erosion, Walnut Gulch, southern Arizona. *Biogeomorphology, Terrestrial and Freshwater Systems*. Elsevier, pp.37-48.
- Abrol, V., M. Ben-Hur, F. G. A. Verheijen, J. J. Keizer, M. a. S. Martins, H. Tenaw, L. Tchekansky and E. R. Graber. 2016. Biochar effects on soil water infiltration and erosion under seal formation conditions: rainfall simulation experiment. *Journal of Soils and Sediments*, **16**(12), pp.2709-2719.
- Abu-Taleb, M. F. 1999. The use of infiltration field tests for groundwater artificial recharge. *Environmental Geology*, **37**(1-2), pp.64-71.
- Administration, N. O. a. A. 2018. *Integrated Surface Database Station History, August 2018* [online]. [Accessed 05/08/2018]. Available from: <https://www.ncdc.noaa.gov/>.
- Al-Awadhi, J. M. 2013. A case assessment of the mechanisms involved in human-induced land degradation in north-eastern Kuwait. *Land Degradation & Development*, **24**(1), pp.2-11.
- Alemu, G., P. W. Unger and O. R. Jones. 1997. Tillage and cropping system effects on selected conditions of a soil cropped to grain sorghum for twelve years. *Communications in Soil Science and Plant Analysis*, **28**(1-2), pp.63-71.
- Amoozegar, A. and G. V. Wilson. 1999. Methods for measuring hydraulic conductivity and drainable porosity. *Agricultural drainage*, (agriculturaldra), pp.1149-1205.
- Angulo-Jaramillo, R., J.-P. Vandervaere, S. Roulier, J.-L. Thony, J.-P. Gaudet and M. Vauclin. 2000. Field measurement of soil surface hydraulic properties by disc and ring infiltrometers: A review and recent developments. *Soil and Tillage Research*, **55**(1), pp.1-29.
- Ankeny, M., T. C. Kaspar and R. Horton. 1988. Design for an automated tension infiltrometer. *Soil Science Society of America Journal*, **52**(3), pp.893-896.
- Arnau-Rosalen, E., A. Calvo-Cases, C. Boix-Fayos, H. Lavee and P. Sarah. 2008. Analysis of soil surface component patterns affecting runoff generation. An example of methods applied to Mediterranean hillslopes in Alicante (Spain). *Geomorphology*, **101**(4), pp.595-606.
- Bear, J. 1972. *Dynamics of Fluids in Porous Media*. Dover Publications.

- Bergkamp, G., A. Cerda and A. C. Imeson. 1999. Magnitude-frequency analysis of water redistribution along a climate gradient in Spain. *Catena*, **37**(1-2), pp.129-146.
- Borrelli, P., C. Ballabio, P. Panagos and L. Montanarella. 2014. Wind erosion susceptibility of European soils. *Geoderma*, **232-234**, pp.471-478.
- Bracken, L. J., J. Wainwright, G. A. Ali, D. Tetzlaff, M. W. Smith, S. M. Reaney and A. G. Roy. 2013. Concepts of hydrological connectivity: Research approaches, pathways and future agendas. *Earth-Science Reviews*, **119**, pp.17-34.
- Brady, N. and R. Weil. 2008. *The nature and properties of soils*.
- Bridge, B. J. and M. J. Bell. 1994. Effect of cropping on the physical fertility of Krasnozems. *Australian Journal of Soil Research*, **32**(6), pp.1253-1273.
- Bryan, R. B. and J. Deploty. 1983. Comparability of soil-erosion measurements with different laboratory rainfall simulators. *Catena*, pp.33-56.
- Carrivick, J. L., M. W. Smith and D. J. Quincey. 2016. *Structure from Motion in the Geosciences*. John Wiley & Sons.
- Chandler, J. H. and S. Buckley. 2016. Structure from motion (SfM) photogrammetry vs terrestrial laser scanning. In: M. B. CARPENTER and C. M. KEANE, eds. *Geoscience Handbook 2016: AGI Data Sheets*. 5th ed. Alexandria, VA: American Geosciences Institute, Section 20.1.
- Chen, L., S. Sela, T. Svoray and S. Assouline. 2013. The role of soil-surface sealing, microtopography, and vegetation patches in rainfall-runoff processes in semiarid areas. *Water Resources Research*, **49**(9), pp.5585-5599.
- Clark, M. P., Y. Fan, D. M. Lawrence, J. C. Adam, D. Bolster, D. J. Gochis, R. P. Hooper, M. Kumar, L. R. Leung, D. S. Mackay, R. M. Maxwell, C. Shen, S. C. Swenson and X. Zeng. 2015. Improving the representation of hydrologic processes in Earth System Models. **51**(8), pp.5929-5956.
- Clement, R., M. Desclotres, T. Gunther, O. Ribolzi and A. Legchenko. 2009. Influence of shallow infiltration on time-lapse ERT: Experience of advanced interpretation. *Comptes Rendus Geoscience*, **341**(10-11), pp.886-898.
- De Laat, P. J. M. and J. C. Nonner. 2012. Artificial recharge with surface water; a pilot project in Wadi Madoneh, Jordan. *Environmental Earth Sciences*, **65**(4), pp.1251-1263.
- Decagon Devices, I. 2016. *Mini Disk Infiltrometer*. Pullman, WA.
- Dimanche, P. H. and W. B. Hoogmoed. 2002. Soil tillage and water infiltration in semi-arid Morocco: the role of surface and sub-surface soil conditions. *Soil & Tillage Research*, **66**(1), pp.13-21.

- Dunkerley, D. 2004a. Flow threads in surface run-off: Implications for the assessment of flow properties and friction coefficients in soil erosion and hydraulics investigations. *Earth Surface Processes and Landforms*, **29**(8), pp.1011-1026.
- Dunkerley, D. 2004b. Flow threads in surface run-off: Implications for the assessment of flow properties and friction coefficients in soil erosion and hydraulics investigations. *Earth Surface Processes and Landforms: The Journal of the British Geomorphological Research Group*, **29**(8), pp.1011-1026.
- Fan, J., Q. J. Wang, S. B. Jones and M. G. Shao. 2016. Soil water depletion and recharge under different land cover in China's Loess Plateau. *Ecohydrology*, **9**(3), pp.396-406.
- Feki, M., G. Ravazzani, A. Ceppi, G. Milleo and M. Mancini. 2018. Impact of Infiltration Process Modeling on Soil Water Content Simulations for Irrigation Management. *Water*, **10**(7), p850.
- Franzuebbers, A. J. 2002. Water infiltration and soil structure related to organic matter and its stratification with depth. *Soil and Tillage Research*, **66**(2), pp.197-205.
- Gargouri-Ellouze, E. and Z. Bargaoui. 2009. Investigation with Kendall plots of infiltration index-maximum rainfall intensity relationship for regionalization. *Physics and Chemistry of the Earth*, **34**(10-12), pp.642-653.
- Guzha, A. C. 2004. Effects of tillage on soil microrelief, surface depression storage and soil water storage. *Soil & Tillage Research*, **76**(2), pp.105-114.
- Hanson, J. D., K. W. Rojas and M. J. Shaffer. 1999. Calibrating the root zone water quality model. *Agronomy Journal*, **91**(2), pp.171-177.
- Heilweil, V. M., T. S. Mckinney, M. S. Zhdanov and D. E. Watt. 2007. Controls on the variability of net infiltration to desert sandstone. *Water Resources Research*, **43**(7).
- Hikel, H., A. Yair, W. Schwanghart, U. Hoffmann, S. Straehl and N. J. Kuhn. 2013. Experimental investigation of soil ecohydrology on rocky desert slopes in the Negev Highlands, Israel. *Zeitschrift Fur Geomorphologie*, **57**, pp.39-58.
- Huang, J., Y. Li, C. Fu, F. Chen, Q. Fu, A. Dai, M. Shinoda, Z. Ma, W. Guo, Z. Li, L. Zhang, Y. Liu, H. Yu, Y. He, Y. Xie, X. Guan, M. Ji, L. Lin, S. Wang, H. Yan and G. Wang. 2017. Dryland climate change: Recent progress and challenges. *Reviews of Geophysics*, **55**(3), pp.719-778.
- Ibn Ali, Z., I. Triki, L. Lajili-Ghezal and M. Zairi. 2017. A method to estimate aquifer artificial recharge from a hill dam in Tunisia. *Journal of Arid Land*, **9**(2), pp.244-255.
- Instituto Nacional De, E. 2012. Resultados definitivos Algarve.

- Ismail, S. M. and H. Depeweg. 2005. Simulation of continuous and surge flow irrigation under short field conditions. *Irrigation and Drainage*, **54**(2), pp.217-230.
- Kelishadi, H., M. R. Mosaddeghi, M. A. Hajabbasi and S. Ayoubi. 2014. Near-saturated soil hydraulic properties as influenced by land use management systems in Koohrang region of central Zagros, Iran. *Geoderma*, **213**, pp.426-434.
- Kirkby, M., L. Bracken and S. Reaney. 2002. The influence of land use, soils and topography on the delivery of hillslope runoff to channels in SE Spain. *Earth Surface Processes and Landforms*, **27**(13), pp.1459-1473.
- Koob, T., M. E. Barber and W. E. Hathhorn. 1999. Hydrologic design considerations of constructed wetlands for urban stormwater runoff. *Journal of the American Water Resources Association*, **35**(2), pp.323-331.
- Kottek, M., J. Grieser, C. Beck, B. Rudolf and F. Rubel. 2006. World map of the Koppen-Geiger climate classification updated. *Meteorologische Zeitschrift*, **15**(3), pp.259-263.
- Lai, J. and L. Ren. 2007. Assessing the Size Dependency of Measured Hydraulic Conductivity Using Double-Ring Infiltrometers and Numerical Simulation. *Soil Science Society of America Journal*, **71**(6), pp.1667-1675.
- Langbein, W. B. and S. A. Schumm. 1958. Yield of sediment in relation to mean annual precipitation. *Eos, Transactions American Geophysical Union*, **39**(6), pp.1076-1084.
- Lavee, H. and J. W. A. Poesen. 1991. Overland-flow generation and continuity on stone-covered soil surfaces. *Hydrological Processes*, **5**(4), pp.345-360.
- Lesschen, J. P., J. M. Schoorl and L. J. G. Cammeraat. 2009. Modelling runoff and erosion for a semi-arid catchment using a multi-scale approach based on hydrological connectivity. **109**(3-4), pp.174-183.
- Lewis, B. 1992. *Digital Chart of the World (Countries)*.
- Lghoul, M., T. Teixido, J. A. Pena, R. Hakkou, A. Kchikach, R. Guerin, M. Jaffal and L. Zouhri. 2012. Electrical and Seismic Tomography Used to Image the Structure of a Tailings Pond at the Abandoned Kettara Mine, Morocco. *Mine Water and the Environment*, **31**(1), pp.53-61.
- Li, X. Y., A. Gonzalez and A. Sole-Benet. 2005. Laboratory methods for the estimation of infiltration rate of soil crusts in the Tabernas Desert badlands. *Catena*, **60**(3), pp.255-266.
- Li, Y. Z., K. Liang, C. M. Liu, W. B. Liu and P. Bai. 2016. Evaluation of different evapotranspiration products in the middle Yellow River Basin, China. *Hydrology Research*, **48**(2), pp.498-513.

- Liberati, A., D. G. Altman, J. Tetzlaff, C. Mulrow, P. C. Gøtzsche, J. P. A. Ioannidis, M. Clarke, P. J. Devereaux, J. Kleijnen and D. Moher. 2009. The PRISMA statement for reporting systematic reviews and meta-analyses of studies that evaluate healthcare interventions: explanation and elaboration. *BMJ*, **339**.
- Loch, R. J. 1994a. Effects of fallow management and cropping history on aggregate breakdown under rainfall wetting for a range of Queensland soils. *Australian Journal of Soil Research*, **32**(5), pp.1125-1139.
- Loch, R. J. 1994b. A method for measuring aggregate water stability of dryland soils with relevance to surface seal development. *Australian Journal of Soil Research*, **32**(4), pp.687-700.
- Maestre, F. T. and M. D. Puche. 2009. Indices based on surface indicators predict soil functioning in Mediterranean semi-arid steppes. *Applied Soil Ecology*, **41**(3), pp.342-350.
- Magnetic-Declination. 2018. *Magnetic Declination* [online]. [Accessed 04/03/2018]. Available from: <http://www.magnetic-declination.com/#>.
- March, S. 2018. *Canon EFS vs APS-C* [online]. [Accessed 02/03/2018].
- Martinez-Pagan, P., A. Faz and E. Aracil. 2009. The use of 2D electrical tomography to assess pollution in slurry ponds of the Murcia region, SE Spain. *Near Surface Geophysics*, **7**(1), pp.49-61.
- Martínez-Hernández, C., J. Rodrigo-Comino and A. Romero-Díaz. 2017. Impact of lithology and soil properties on abandoned dryland terraces during the early stages of soil erosion by water in south-east Spain. *Hydrological Processes*, **31**(17), pp.3095-3109.
- Masri, Z., M. Zöbisch, A. Bruggeman, P. Hayek and M. Kardous. 2003. Wind erosion in a marginal Mediterranean dryland area: a case study from the Khanasser Valley, Syria. *Earth Surface Processes and Landforms*, **28**(11), pp.1211-1222.
- Menon, M., Q. Yuan, X. Jia, A. J. Dougill, S. R. Hoon, A. D. Thomas and R. A. Williams. 2011. Assessment of physical and hydrological properties of biological soil crusts using X-ray microtomography and modeling. *Journal of Hydrology*, **397**(1-2), pp.47-54.
- Michaelides, K., R. Hollings, M. B. Singer, M. H. Nichols and M. A. Nearing. 2018. Spatial and temporal analysis of hillslope–channel coupling and implications for the longitudinal profile in a dryland basin. *Earth Surface Processes and Landforms*, **43**(8), pp.1608-1621.
- Michaelides, K. and M. D. Wilson. 2007. Uncertainty in predicted runoff due to patterns of spatially variable infiltration. *Water Resources Research*, **43**(2).

- Middleton, N. and D. Thomas. 1997. *World atlas of desertification*. 2nd ed.
- Moameni, A. and A. Farshad. 1998. Evaluation of prevailing irrigation practices and their relation to soil properties - A case study of Hamadan-Bahar Area of western Iran. *Annals of Arid Zone*, **37**(2), pp.119-131.
- Mohamed, A. S. 2012. *Geochemical and hydrodynamic approaches of Trarza groundwater recharge, South-Western Mauritania*. thesis, Université Paris Sud - Paris XI.
- Morbidelli, R., C. Saltalippi, A. Flammini, M. Cifrodelli, T. Picciafuoco, C. Corradini and R. S. Govindaraju. 2016. Laboratory investigation on the role of slope on infiltration over grassy soils. *Journal of Hydrology*, **543**, pp.542-547.
- Nicholson, S. E. 2011. *Dryland climatology*. Cambridge University Press.
- O'Connor, J., M. J. Smith and M. R. James. 2017. Cameras and settings for aerial surveys in the geosciences: optimising image data. *Progress in Physical Geography*, **41**(3), pp.325-344.
- Oster, J. L., K. Kitajima, J. W. Valley, B. Rogers and K. Maher. 2017. An evaluation of paired delta O-18 and (U-234/U-238)(0) in opal as a tool for paleoclimate reconstruction in semi-arid environments. *Chemical Geology*, **449**, pp.236-252.
- Peng, L., L. Zhanbin and L. Kexin. 2004. Effect of vegetation cover types on soil infiltration under simulating rainfall. In: *13th International Soil Conservation Organisation Conference*.
- Perroll, K. and K. Sandstrom. 1995. Correlating landscape characteristics and infiltration - A study of surface sealing and subsoil conditions in semi-arid Botswana and Tanzania. *Geografiska Annaler Series a-Physical Geography*, **77A**(3), pp.119-133.
- Perroux, K. and I. White. 1988. Designs for disc permeameters. *Soil Science Society of America Journal*, **52**(5), pp.1205-1215.
- Pierson, F. B., C. J. Williams, P. R. Kormos, S. P. Hardegree, P. E. Clark and B. M. Rau. 2010. Hydrologic Vulnerability of Sagebrush Steppe Following Pinyon and Juniper Encroachment. *Rangeland Ecology & Management*, **63**(6), pp.614-629.
- Pingping, H., S. Xue, P. Li and L. Zhanbin. 2013. Effect of Vegetation Cover Types on Soil Infiltration Under Simulating Rainfall. *Nature Environment and Pollution Technology*, **12**(2), p193.
- Poesen, J. 1986. Surface sealing as influenced by slope angle and position of simulated stones in the top layer of loose sediments. *Earth Surface Processes and Landforms*, **11**(1), pp.1-10.

- Poesen, J. 1990. Erosion process research in relation to soil erodibility and some implications for improving soil quality. *In: J. ALBALADEJO, M. A. STOCKING and E. DIAZ, eds. Soil Degradation and Rehabilitation in Mediterranean Environmental Conditions.* C.S.I.C., Mercia, pp.159-170.
- Poesen, J. and F. Ingelmo-Sanchez. 1992. Runoff and sediment yield from topsoils with different porosity as affected by rock fragment cover and position. *Catena*, **19**(5), pp.451-474.
- Poesen, J., F. Ingelmo-Sanchez and H. Mucher. 1990. The hydrological response of soil surfaces to rainfall as affected by cover and position of rock fragments in the top layer. *Earth surface processes and landforms*, **15**(7), pp.653-671.
- Poesen, J. and H. Lavee. 1994. Rock fragments in top soils: significance and processes. *Catena*, **23**(1-2), pp.1-28.
- Poesen, J., D. Torri and K. Bunte. 1994. Effects of rock fragments on soil erosion by water at different spatial scales: a review. *Catena*, **23**(1-2), pp.141-166.
- Puigdefábregas, J. 2005. The role of vegetation patterns in structuring runoff and sediment fluxes in drylands. *Earth Surface Processes and Landforms*, **30**(2), pp.133-147.
- Qiu, G. Y., F. Xie, Y. C. Feng and F. Tian. 2011. Experimental studies on the effects of the "Conversion of Cropland to Grassland Program" on the water budget and evapotranspiration in a semi-arid steppe in Inner Mongolia, China. *Journal of Hydrology*, **411**(1-2), pp.120-129.
- Reaney, S. M., L. J. Bracken and M. J. Kirkby. 2007. Use of the Connectivity of Runoff Model (CRUM) to investigate the influence of storm characteristics on runoff generation and connectivity in semi-arid areas. **21**(7), pp.894-906.
- Reaney, S. M., L. J. Bracken and M. J. Kirkby. 2014. The importance of surface controls on overland flow connectivity in semi-arid environments: results from a numerical experimental approach. *Hydrological Processes*, **28**(4), pp.2116-2128.
- Renard, K. G. 1979. Rainfall simulation as a research tool. *Proceedings of the Rainfall Simulator Workshop, Tucson, AZ*, **10**, pp.60-64.
- Reynolds, W. and D. Elrick. 2002. Pressure infiltrometer. *In: J. H. DANE and G. C. TOPP, eds. Methods of soil analysis, Part 4: Physial Methods.* pp.826-836.
- Reynolds, W. D., D. E. Elrick, E. G. Youngs and A. Amoozegar. 2002. 3.4.3.1 Introduction. *In: J. H. DANE and C. G. TOPP, eds. Methods of Soil Analysis: Part 4 Physical Methods.* Madison, WI: Soil Science Society of America, pp.817-843.

- Safriel, D., Z. Adeel, D. Niemeijer, J. Puigdefabregas, R. White, R. Lal, M. Winslow, J. Ziedler, S. Price, E. Archer, C. King, B. Shapiro, K. Wessels, T. Nielsen, B. Portnov, I. Reshef, J. Thornell, E. Lachman and D. McNab. 2005. Dryland Systems. *In: M. EL-KASSAS and E. EZCURRA, eds. Millenium Ecosystem Assessment.*
- Safriel, U., Adeel, Z., Niemeijer, D., Puigdefabregas, J., White, R., Lal, R., Winslow, M., Ziedler, J., Prince, S., Archer, E., King, C., Shapiro, B., Wessels, K., Nielsen, T., Portnov, B., Reshef, I., Thonell, J., Lachman, E., and McNab, D. 2006. Ecosystems and human well-being: Current state and trends vol 1. *Environment and Urbanization*. pp.623-662.
- Salmon, O. and A. Schick. 1980. Infiltration tests. *Arid Zone Geosystems. US Army Eur. Res. Office. Research Report, DA-JA-DAERO-78G-111. Physical Geography, Hebrew University of Jerusalem*, pp.55-115.
- Sanders, L. 1998. *A manual of field hydrogeology*. Upper Saddle River, N.J.
- Schwarz, M., F. Preti, F. Giadrossich, P. Lehmann and D. Or. 2010. Quantifying the role of vegetation in slope stability: A case study in Tuscany (Italy). *Ecological Engineering*, **36**(3), pp.285-291.
- Seeger, M. 2007. Uncertainty of factors determining runoff and erosion processes as quantified by rainfall simulations. *Catena*, **71**(1), pp.56-67.
- Shangguan, Z. P., M. A. Shao, T. W. Lei and T. L. Fan. 2002. Runoff water management technologies for dryland agriculture on the Loess. *International Journal of Sustainable Development & World Ecology*, **9**(4), pp.341-350.
- Sharma, P., V. Abrol, G. R. M. Sankar and B. Singh. 2009. Influence of tillage practices and mulching options on productivity, economics and soil physical properties of maize (*Zea mays*)-wheat (*Triticum aestivum*) system. *Indian Journal of Agricultural Sciences*, **79**(11), pp.865-870.
- Siddaway, A. 2014 *What is a systematic literature review and how do I do one?* Unpublished.
- Simonneaux, V., A. Cheggour, C. Deschamps, F. Mouillot, O. Cerdan and Y. Le Bissonnais. 2015. Land use and climate change effects on soil erosion in a semi-arid mountainous watershed (High Atlas, Morocco). *Journal of Arid Environments*, **122**, pp.64-75.
- Skierucha, W., A. Wilczek, A. Szyplowska, C. Sławiński and K. Lamorski. 2012. A TDR-based soil moisture monitoring system with simultaneous measurement of soil temperature and electrical conductivity. *Sensors*, **12**(10), pp.13545-13566.
- Smith, M. 2015. Direct acquisition of elevation data: Terrestrial Laser Scanning. *Geomorphological Techniques. British Society for Geomorphology.*

- Smith, M. W. 2009. *Overland flow resistance & flood generation in semi-arid environments: explaining the restrained draining of the rain in Spain*. thesis, Durham University.
- Smith, M. W. and D. Vericat. 2015. From experimental plots to experimental landscapes: topography, erosion and deposition in sub-humid badlands from structure-from-motion photogrammetry. *Earth Surface Processes and Landforms*, **40**(12), pp.1656-1671.
- Stone, J. and G. Paige. 2003. Variable rainfall intensity rainfall simulator experiments on semi-arid rangelands. *In: Proc. 1st Interagency Conf. on Research in the Watersheds*, pp.83-88.
- Sun, X., Y. Xu, N. Z. Jovanovic, E. Kapangaziwiri, L. Brendonck and R. D. H. Bugan. 2013. Application of the rainfall infiltration breakthrough (RIB) model for groundwater recharge estimation in west coastal South Africa. *Water Sa*, **39**(2), pp.221-230.
- Tabeni, S., F. A. Yannelli, N. Vezzani and L. E. Mastrantonio. 2016. Indicators of landscape organization and functionality in semi-arid former agricultural lands under a passive restoration management over two periods of abandonment. *Ecological Indicators*, **66**, pp.488-496.
- Tutiempo. 2018a. *Climate Data: Sagres 1973 - 2001* [online]. [Accessed 06/08/2018]. Available from: <https://en.tutiempo.net/climate/ws-85380.html>.
- Tutiempo. 2018b. *Climate Data: Sagres 2001 - 2018* [online]. [Accessed 06/08/2018]. Available from: <https://en.tutiempo.net/climate/ws-85330.html>.
- Van Hoorn, J. 1979. Determining hydraulic conductivity with the inversed auger hole and infiltrometer methods. *In: Proceedings of the International Drainage Workshop, 16-20 May 1978, Wageningen, The Netherlands/edited by Jans Wesseling*: Wageningen, International Institute for Land Reclamation and Improvement, 1979.
- Van Wie, J. B., J. C. Adam and J. L. Ullman. 2013. Conservation tillage in dryland agriculture impacts watershed hydrology. *Journal of Hydrology*, **483**, pp.26-38.
- Verbist, K., S. Torfs, W. M. Cornelis, R. Oyarzun, G. Soto and D. Gabriels. 2010. Comparison of Single- and Double-Ring Infiltrometer Methods on Stony Soils. *Vadose Zone Journal*, **9**(2), pp.462-475.
- Verbist, K. M. J., W. M. Cornelis, S. Torfs and D. Gabriels. 2013. Comparing Methods to Determine Hydraulic Conductivities on Stony Soils. *Soil Science Society of America Journal*, **77**(1), pp.25-42.
- Walker, W. R. 1989. *Guidelines for designing and evaluating surface irrigation systems*.

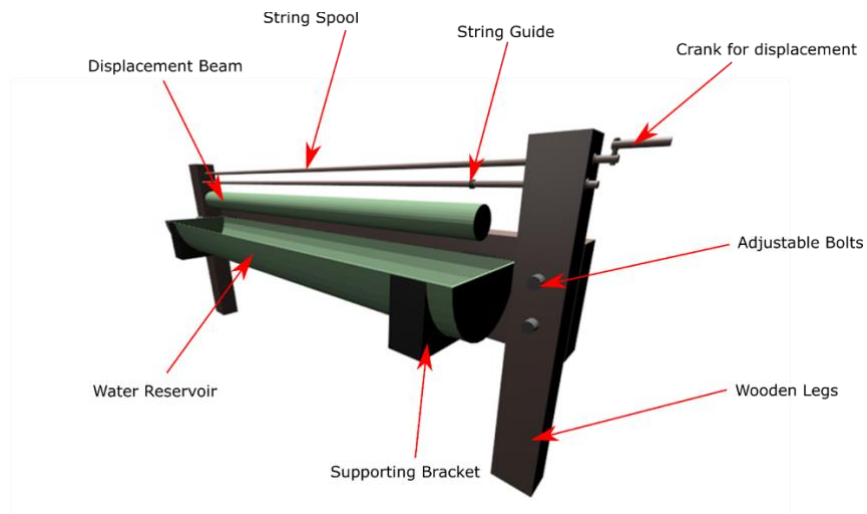
- Wentworth, C. K. 1922. A Scale of Grade and Class Terms for Clastic Sediments. *The Journal of Geology*, **30**(5), pp.377-392.
- Westoby, M., J. Brasington, N. Glasser, M. Hambrey and J. Reynolds. 2012. 'Structure-from-Motion' photogrammetry: A low-cost, effective tool for geoscience applications. *Geomorphology*, **179**, pp.300-314.
- Williams, C. J., F. B. Pierson, P. R. Kormos, O. Z. Al-Hamdan, S. P. Hardegree and P. E. Clark. 2016. Ecohydrologic response and recovery of a semi-arid shrubland over a five year period following burning. *Catena*, **144**, pp.163-176.
- Williams, J. D., S. B. Wuest, W. F. Schillinger and H. T. Gollany. 2006. Rotary subsoiling newly planted winter wheat fields to improve infiltration in frozen soil. *Soil & Tillage Research*, **86**(2), pp.141-151.
- Wu, L. and L. Pan. 1997. A generalized solution to infiltration from single-ring infiltrometers by scaling. *Soil Science Society of America Journal*, **61**(5), pp.1318-1322.
- Wubda, M., M. Descloitres, N. Yalo, O. Ribolzi, J. M. Vouillamoz, M. Boukari, B. Hector and L. Seguis. 2017. Time-lapse electrical surveys to locate infiltration zones in weathered hard rock tropical areas. *Journal of Applied Geophysics*, **142**, pp.23-37.
- Xu, X., C. Lewis, W. Liu, J. D. Albertson and G. Kiely. 2012. Analysis of single-ring infiltrometer data for soil hydraulic properties estimation: Comparison of BEST and Wu methods. *Agricultural Water Management*, **107**, pp.34-41.
- Yang, L., J. Smith, M. L. Baeck, E. Morin and D. C. Goodrich. 2017. Flash Flooding in Arid/Semiarid Regions: Dissecting the Hydrometeorology and Hydrology of the 19 August 2014 Storm and Flood Hydroclimatology in Arizona. *Journal of Hydrometeorology*, **18**(12), pp.3103-3123.
- Young, M. H., E. V. McDonald, T. G. Caldwell, S. G. Benner and D. G. Meadows. 2004. Hydraulic properties of a desert soil chronosequence in the Mojave desert, USA. *Vadose Zone Journal*, **3**(3), pp.956-963.
- Zema, D. A., A. Labate, D. Martino and S. M. Zimbone. 2017. Comparing Different Infiltration Methods of the HEC-HMS Model: The Case Study of the Mesima Torrent (Southern Italy). *Land Degradation & Development*, **28**(1), pp.294-308.
- Zhou, H., W. Z. Zhao and Q. Y. Yang. 2016. Root biomass distribution of planted Haloxylon ammodendron in a duplex soil in an oasis: desert boundary area. *Ecological Research*, **31**(5), pp.673-681.

Zhou, J., B. X. Hu, G. D. Cheng, G. X. Wang and X. Li. 2011. Development of a three-dimensional watershed modelling system for water cycle in the middle part of the Heihe rivershed, in the west of China. *Hydrological Processes*, **25**(12), pp.1964-1978.



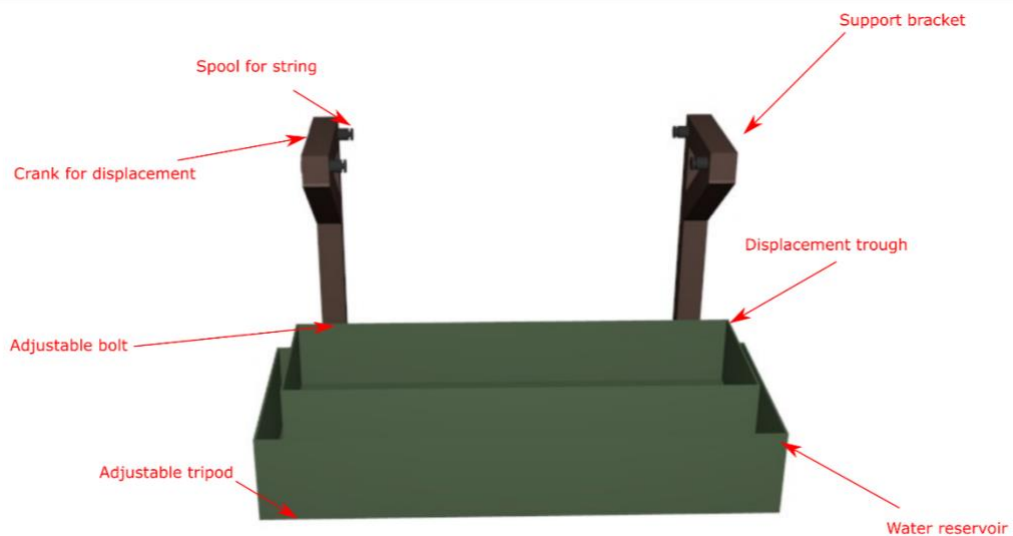
## Appendix

### Appendix i: Prototype One 3D model



3D model of prototype one created with Blender (note no scale due to warped perspective). 3D model available at <https://skfb.ly/6yp6P>

### Appendix ii: Prototype Two 3D model



3D model of prototype two created with Blender (note no scale due to warped perspective). 3D model available at <https://skfb.ly/6AJwI>

## Appendix iii: ArcPy Automation Script (Setup)

```

1. # This script will set up the arc environment for
2. # digitisation including creating a geodatabase and feature classes
3.
4. import arcpy, os, time
5.
6. # timer
7. tic = time.time()
8.
9. arcpy.env.overwriteOutput = True
10.
11. print('Has run been defined?')
12.
13. if run % 1 != 0:
14.     print('No, ending script. Define run before running script!')
15.     exit()
16. else:
17.     print 'Yes, Run Number:',run
18.
19. output_path = ("D:/Digitisation/%d/" % run)
20. working_path = ("D:/Digitisation/")
21. arcpy.env.workspace = output_path
22.
23. gdb = output_path + 'Database_%d.gdb' % run
24.
25. # Is there a file geodatabase?
26. if os.path.exists(gdb):
27.     print('Geodatabase exists, moving on...')
28. elif not os.path.exists(gdb):
29.     print("Geodatabase doesn't exist, creating now...")
30.
31.     arcpy.CreateFileGDB_management(output_path, "Database_%d" % run)
32.     print('File geodatabase created!')
33. else:
34.     print('There seems to be an issue, please investigate. The script will
now terminate.')
35.     exit()
36.
37. # Create feature classes (will overwrite the same name if it exists)
38. print('Creating feature classes...')
39.
40. Wetted_area = arcpy.CreateFeatureclass_management(gdb, 'Wetted_area')
41. print('1/5')
42. Veg = arcpy.CreateFeatureclass_management(gdb, 'Veg')
43. print('2/5')
44. Stone_ontop = arcpy.CreateFeatureclass_management(gdb, 'Stone_ontop')
45. print('3/5')
46. Stone_embedded = arcpy.CreateFeatureclass_management(gdb, 'Stone_embedded')
47. print('4/5')
48. Bare_soil = arcpy.CreateFeatureclass_management(gdb, 'Bare_soil')
49. print('5/5')
50.
51. print('Feature classes created!')
52.
53. # Set geodatabase path
54. gdb = output_path + 'Database_%d.gdb' % run
55.
56. # Set Coordinate System
57. spatial_ref = arcpy.SpatialReference("ETRS 1989 UTM Zone 29N")
58.
59. arcpy.env.cartographicCoordinateSystem = spatial_ref
60.
61. # Set mxd document

```

```

62. mxd = arcpy.mapping.MapDocument("CURRENT")
63. mxd.save()
64.
65. toc = time.time()
66. print(toc-tic, 'seconds elapsed')

```

#### Appendix iv: ArcPy Automation Script (Area Calculation)

```

1. # This script is to be run after digitisation of the area.
2.
3. import arcpy, time, os
4.
5. print('Has run been defined?')
6.
7. if run % 1 != 0:
8.     print('No, ending script. Define run before running script!')
9.     exit()
10. else:
11.     print 'Yes, Run Number:',run
12.
13. # Stopwatch
14. tic = time.time()
15.
16. arcpy.env.overwriteOutput = True
17.
18. output_path = ("D:/Digitisation/%d/" % run)
19. working_path = ("D:/Digitisation/")
20. arcpy.env.workspace = output_path
21.
22. gdb = output_path + 'Database_%d.gdb/' % run
23.
24. def identity(feat):
25.
26.     # Identity analysis on the feature
27.     arcpy.Identity_analysis("Wetted_area",feat,gdb + feat + "_identity")
28.
29.     # Identify feature class path:
30.     new_feat = feat + "_identity"
31.     fc = gdb + new_feat
32.
33.     # Remove the first attribute row (irrelevant to analysis)
34.     del_query = "OBJECTID < 2"
35.     with arcpy.da.UpdateCursor(new_feat,"OBJECTID",del_query) as delete_row
36.     :
37.         for row in delete_row:
38.             delete_row.deleteRow()
39.
40.     # Calculate total area within wetted perimeter (m^2)
41.     summed_total = 0
42.     with arcpy.da.SearchCursor(fc,"Shape_Area") as cursor:
43.         for row in cursor:
44.             summed_total = summed_total + row[0]
45.
46.     print(new_feat, 'total area is: ', summed_total, 'm^2')
47.
48. # Print the wetted area and wetted perimeter
49. path_to_wetted_area = gdb + "Wetted_area"
50.
51. wetted_area = 0
52. with arcpy.da.SearchCursor(path_to_wetted_area,"Shape_Area") as cursor:
53.     for row in cursor:

```

```
54.         wetted_area = wetted_area + row[0]
55.
56. wetted_per = 0
57. with arcpy.da.SearchCursor(path_to_wetted_area,"Shape_Length") as cursor:
58.     for row in cursor:
59.         wetted_per = wetted_per + row[0]
60.
61. print("Wetted area: ", wetted_area, "m^2")
62. print("Wetted perimeter: ", wetted_per, "m")
63.
64. identity('Veg')
65. identity('Stone_ontop')
66. identity('Stone_embedded')
67.
68. # Set mxd document and save
69. mxd = arcpy.mapping.MapDocument("CURRENT")
70. mxd.save()
71.
72. # End stopwatch
73. toc = time.time()
74. print('Seconds elapsed: ',toc-tic)
```

### Appendix v: CloudCompare Automation Script

```
for %i in (*.txt) DO (CloudCompare -SILENT -O %i -AUTO_SAVE OFF -C_EXPORT_FMT
ASC -SEP COMMA -EXT txt -SS OCTREE 8 -ROUGH 0.05 -SAVE_CLOUDS -CLEAR)
```